**AFRL-IF-RS-TR-2006-318**
**Final Technical Report**
**October 2006**


# SPATIAL MODELING TOOLS FOR CELL BIOLOGY

**CFD Research Corporation**

**Sponsored by**
**Defense Advanced Research Projects Agency**
**DARPA Order No. J058/U040**



**AIR FORCE RESEARCH LABORATORY**
**INFORMATION DIRECTORATE**
**ROME RESEARCH SITE**
**ROME, NEW YORK**

# NOTICE AND SIGNATURE PAGE

Using Government drawings, specifications, or other data included in this document for any purpose other than Government procurement does not in any way obligate the U.S. Government. The fact that the Government formulated or supplied the drawings, specifications, or other data does not license the holder or any other person or corporation; or convey any rights or permission to manufacture, use, or sell any patented invention that may relate to them.

This report was cleared for public release by the Air Force Research Laboratory Rome Research Site Public Affairs Office and is available to the general public, including foreign nationals. Copies may be obtained from the Defense Technical Information Center (DTIC) (http://www.dtic.mil).

AFRL-IF-RS-TR-2006-318 HAS BEEN REVIEWED AND IS APPROVED FOR PUBLICATION IN ACCORDANCE WITH ASSIGNED DISTRIBUTION STATEMENT.

FOR THE DIRECTOR:

/s/

CLARE THIEM
Work Unit Manager

/s/

JAMES A. COLLINS, Deputy Chief
Advanced Computing Division
Information Directorate

This report is published in the interest of scientific and technical information exchange, and its publication does not constitute the Government's approval or disapproval of its ideas or findings.

# REPORT DOCUMENTATION PAGE

*Form Approved*
**OMB No. 0704-0188**



| 1. REPORT DATE *(DD-MM-YYYY)* | 2. REPORT TYPE | 3. DATES COVERED *(From - To)* |
|---|---|---|
| OCT 2006 | Final | |

**4. TITLE AND SUBTITLE**

SPATIAL MODELING TOOLS FOR CELL BIOLOGY

**5a. CONTRACT NUMBER**
FA8750-04-C-0247

**5b. GRANT NUMBER**

**5c. PROGRAM ELEMENT NUMBER**

**6. AUTHOR(S)**

Andrzej Przekwas, Tom Friend, Rodrigo Teixeira, Z.J. Chen and Patrick Wilkerson

**5d. PROJECT NUMBER**
BIOC

**5e. TASK NUMBER**
FD

**5f. WORK UNIT NUMBER**
RC

**7. PERFORMING ORGANIZATION NAME(S) AND ADDRESS(ES)**
CFD Research Corporation
Cummings Research Park
215 Wynn Drive, Suite 501
Huntsville AL 35805

**8. PERFORMING ORGANIZATION REPORT NUMBER**

**9. SPONSORING/MONITORING AGENCY NAME(S) AND ADDRESS(ES)**

DARPA
3701 North Fairfax Drive
Arlington VA 22203-1714

AFRL/IFTC
525 Brooks Rd
Rome NY 13441-4505

**10. SPONSOR/MONITOR'S ACRONYM(S)**

**11. SPONSORING/MONITORING AGENCY REPORT NUMBER**
AFRL-IF-RS-TR-2006-318

**12. DISTRIBUTION AVAILABILITY STATEMENT**
*APPROVED FOR PUBLIC RELEASE; DISTRIBUTION UNLIMITED. PA# 06-733*

**13. SUPPLEMENTARY NOTES**

**14. ABSTRACT**
Rapid accumulation of genomic and proteomic data from novel high throughput experimental screening technologies demand novel mathematical approaches and models to process and interpret massive amounts of data. Scientific potentials and military relevance of computational biology and bioinformatics have inspired DARPA/IPTO's visionary BioSPICE project to develop computational framework and modeling tools for cell biology. The goal of this CFDRC project was to formulate fundamental mathematical models and their numerical solution procedures for solving spatiotemporal cell biology problems and to develop software tools for multi-dimensional modeling of cell and tissue biology. CFDRC has developed Computational Biology, CoBi, software tools to simulate complex cell and organ biology problems. The code has been successfully applied to a number of cell biology problems including: bacterial chemosensing and chemotaxis, bacterial sporulation, EGFR signal transduction, cellular and tissue calcium oscillations, cellular and tissue oxygen and energy metabolism, morphogenesis of the yeast cell, and perfusion of a cell in an organ.

**15. SUBJECT TERMS**

Computational biology, cell biology, mathematical modeling, signaling pathways, numerical methods

| 16. SECURITY CLASSIFICATION OF: | | | 17. LIMITATION OF ABSTRACT | 18. NUMBER OF PAGES | 19a. NAME OF RESPONSIBLE PERSON |
|---|---|---|---|---|---|
| a. REPORT | b. ABSTRACT | c. THIS PAGE | | | Clare D. Thiem |
| U | U | U | UL | 115 | 19b. TELEPHONE NUMBER (*Include area code*) |

# TABLE OF CONTENTS

**Page No.**

APPENDICIES

## LIST OF FIGURES

## LIST OF TABLES

## ACKNOWLEDGMENTS

This project would not be possible without the vision, and determination of Dr. Sri Kumar, DARPA/IPTO Project Manager of the Bio-Computation (BioCOMP) Program and the advocate of the Bio-SPICE simulation framework. We would like to express our sincere appreciation to Dr. Kumar for the inspiration, scientific guidance, and constructive feedback during the duration of this project. Mr. Clare Thiem of the Air Force Research Laboratory, AFRL/IFTC Rome NY, was the Technical Manager for this CFD Research Corporation (CFDRC) project providing both inspiration and motivation. Mr. Thiem's thrust and belief in the potential power of advanced mathematical modeling and patience during model development are greatly appreciated. We are also thankful to Dr. Thomas Renz of AFRL/IFTC for stimulating discussions in using Computational Biology (CoBi) software for exploring nano Bio-Computing problems.

We would also like to express our appreciation to the PIs of the DARPA BAA BioCOMP teams for their interest and technical suggestions (often critical) at the PI Meetings. This project is attracting significant attention from several individuals at DoD medical research laboratories. We are grateful for that interest and hope that the models developed in this project will be a springboard for several future projects.

We are also grateful to several colleagues at CFDRC who helped during this project, in particular to Dr. Ashok Singhal, President of CFDRC, Dr. Maciej Pindera, and Dr. Hui Ding. We also extend our thanks to Dr. Mahesh Athavale, Dr. Yu Jiang, and Dr. Michal Furmanczyk, former Computational Medicine and Biology (CMB) division team members. This report was skillfully assembled, proofread, and enhanced by Ms Silvia Harvey of CFDRC.

Some of the illustrations presented in this report have been obtained from National Institute of Health (NIH) and National Library of Medicine (NLM) public domain web sites. Current electronic links for these pictures are provided in the figure caption. The authors are grateful to NIH and NLM for permission to reproduce some of the images in this report.

## EXECUTIVE SUMMARY

There are more than $10^{14}$ cells in the human body, and every second, more than 10 million die and are replaced. The unity of an organism is coordinated by many levels of material, chemical, and electric communication between the cells. Until recently progress in cell biology was limited by human comprehension of complex cellular interactions observed from laboratory experiments. The large number of variables, complex functionality, and nonlinear interactions in cell biology events severely limit human's capability to directly comprehend cellular behavior. The only logical way to compactly describe and understand such complex systems is to use mathematics and computational modeling. Rapid accumulation of genomic and proteomic data from novel high throughput experimental screening technologies demand novel mathematical approaches and models to process and interpret massive amounts of data. These models will ultimately address a variety of dynamic intracellular processes ranging from interactions within a gene regulation network to intracellular and intercellular signal transduction. At present, however, compact elegant mathematical models of cellular biology are rare.

In the last two decades, computational technologies, such as Computational Fluid Dynamics (CFD) and Finite Element Method (FEM) based Computational Structures Dynamics (CSD), have revolutionized classical engineering disciplines including fluid dynamics and structures mechanics. We believe that emerging computational technologies are poised to produce a greater revolution in medicine and biology. Based on that belief, CFD Research Corporation (CFDRC) formed a new Computational Medicine and Biology (CMB) division in 2002 that is determined to spearhead that revolution.

Scientific potentials and military relevance of computational biology and bioinformatics have also attracted DARPA's interest. The DARPA IPTO ambitious and visionary Bio-Computation (BioCOMP) Program to develop open source computational framework, called Bio-SPICE, along with broad range of cell biology modeling tools was started in 2001. Bio-SPICE stands for the Simulation Program for Intra-Cellular Processes. The BioCOMP Program was tasked to develop novel modeling methods and simulation software for broad but complementary aspects of cell biology such as: metabolic pathways, cellular signaling, cell cycle and division, chemosensing, chemotaxis, cellular colonies, and microorganisms. The CFDRC role in the BioCOMP Program was to explore multidimensional, spatiotemporal mathematical modeling techniques in cellular biology.

Prior to this project CFDRC was involved in the DARPA BioCOMP subcontract to the Lawrence Berkeley Laboratory (LBL) working on mathematical formulation and computational exploration of spatiotemporal cell biology models. Summary of that project is presented in the Appendix A of this report. That effort provided a good starting point for the present project, whose objective was to develop spatiotemporal computational cell/organ biology tools.

The focus of the project described in this report, was to develop a self-contained software framework solving partial differential equations governing flow, diffusion, and biochemistry applicable for spatiotemporal modeling of cell and organ biology problems. During a two-year

period CFDRC developed **Co**mputational **Bi**ology (**CoBi**,) software tools to simulate complex cell and organ biology problems. The code was written in modern C++ programming language using state of the art numerical techniques for solving large systems of partial differential equations (PDEs) and CFDRC multiphysics modeling expertise. A graphical user interface (GUI) for CoBi, JCoBi, was written in Java and interactive 3D graphics. CoBi has been designed to interact with the other Bio-SPICE software tools using Systems Biology Markup Language (SBML, http://sbml.org/index.psp ) as a standard interface.

This report describes the mathematical formulation of cellular biophysics and biochemistry models used in the code development, numerical methods for solving large-scale systems of PDE equations, and CoBi software structure. The code has been successfully applied to a number of cell biology problems. This report describes the models in detail and presents simulation results for several cell biology problems including: bacterial chemosensing and chemotaxis, bacterial sporulation, epidermal growth factor receptor (EGFR) signal transduction, cellular and tissue calcium oscillations, cellular and tissue oxygen and energy metabolism, morphogenesis of the yeast cell, and perfusion of a cell in an organ. The CoBi code has been developed, validated, and demonstrated on several cell biology and organ physiology problems. The code has been used as the starting point for several DARPA and DoD projects related to military medicine, DNA based bio-computing, personnel protection, and biodefense.

This project has established excellent foundations for future computational medicine and biology projects (CMB) at CFDRC for military and civilian medical applications. After two years of this project, CoBi has matured to the point that it can be used for solving problems not only in cell biology but also organ biology and whole body (organism) physiology. CFDRC has invested significant IR&D resources in CoBi code development, integration, and testing. The code is being used as a starting point for several projects with DoD focused on biotechnology, nanotechnology, and military medicine.

# 1.0 INTRODUCTION

## 1.1 Background

CFD Research Corporation (CFDRC) has been involved in the DARPA/IPTO BAA 01-26 BioCOMP Program between January 2002 and April 2006. The objective of the DARPA BioCOMP Program, conceptualized and organized by Dr. Sri Kumar of DARPA/IPTO was to develop a computational framework that enables the construction of sophisticated models of intracellular processes that can be used to predict and control the behavior of living cells. One of the program tracks was to develop Bio-SPICE modeling framework, which stands for the Simulation Program for Intra-Cellular Processes. DARPA has initiated the project to develop computational models and open source software for modeling cell biology. Among several projects, typically lead by US academic teams, CFDRC's project task was first to formulate and explore a spatiotemporal (multidimensional) modeling approaches and then to implement and demonstrate it on cell and organ biology problems.

The project described in this report was conducted as a direct contract funded by DARPA and coordinated and technically directed by the Air Force Research Laboratory (AFRL/IFTC Rome NY). Mr. Clare Thiem of AFRL/IFTC was the DoD Technical Project Manager for the CFDRC BioCOMP Program. This project was conducted during June 2004 to May 2006. The overall objective of the CFDRC BioCOMP Program was to develop a self-contained software framework solving partial differential equations governing flow, diffusion, and biochemistry applicable for spatiotemporal modeling of cell and organ biology problems. The specific objective of this project was to develop **Co**mputational **Bi**ology (**CoBi**) software tools and a graphical user interface (GUI) using state-of the art numerical techniques and novel programming tools (C++ and Java) to simulate complex cell and organ biology problems. CoBi has been designed to interact with the other Bio-SPICE software tools using **Systems Biology Markup Language (SBML,** http://sbml.org/index.psp ) as a standard interface. The prototype CoBi software developed in this project was delivered in source to DARPA (SRI Bio-SPICE site) in February 2005 and the final code along with the code documentation has been delivered to AFRL/IFTC at the end of the project.

## 1.2 Project Objectives

The overall objective of the CFDRC BioCOMP Program was to develop a software toolkit and modeling framework for multidimensional, spatiotemporal comprehensive modeling of cell biology.

The objective of the present follow up project was to develop a self-contained software framework and computational cell and organ biology for applications in military medicine, bio-computation, biotechnology, and in civilian medical and biological sciences. The experience gained in CFDRC's earlier involvement in the BioCOMP Program, described in Appendix A, in modeling 3D cell biology problems and the established biomembrane model was a starting point for this project. CFDRC proposed to adapt the existing 3D model of cell biomembrane for complete simulation of cell biology including intracellular, extracellular and membrane bound

biophysical and biochemical events. The CoBi software tools should be able to solve generalized advection-diffusion-reaction equations governing cell biology and biophysics using state-of-the-art numerical methods. Thus, the objectives for this project were as follows:

1. Develop a 3D unstructured grid solver for volumetric diffusion-reaction processes,
2. Integrate the existing membrane model (developed in the previous DARPA BioCOMP Program ) with the volumetric model using the embedded boundary approach,
3. Develop a generalized biochemistry solver module for modeling complete cell biology problems including extracellular, intracellular, and membrane bound biochemical reactions,
4. Establish general computational biology software tools for modeling cell, colony, tissue, and organ biology. Provide a framework for 3D transient solution of any number of advection-diffusion-reaction partial differential equations in complex geometries of cellular and culture/tissue structures,
5. Develop interfaces between CoBi and other Bio-SPICE tools and community standard databases, modeling languages (e.g. SBML), and open source graphical post processing tools (e.g. VizIT),
6. Develop flexible Graphical User Interface (GUI) for CoBi, JCoBi, to enable easy model setup and simulation control,
7. Validate the software on several benchmark problems,
8. Demonstrate CoBi on several defense related cell and organ biology problems, and utilize it for other DoD projects,
9. Document CoBi and deliver it to DARPA and to DoD Laboratories.

It is felt that all of the major objectives of this project have been successfully accomplished. The CoBi code has been developed, validated, and demonstrated on several cell biology and organ physiology problems. The code has been used as the starting point for several DARPA and DoD projects. CFDRC is using CoBi as the enabling technology for projects related to military medicine, DNA based biocomputing, personnel protection, and biodefense. The code has been delivered to interested DoD Laboratories. The following sections describe the model, software, and examples from comprehensive simulation studies.

## 2.0 COMPUTATIONAL CELLULAR BIOLOGY

### 2.1 Relevant Introduction to Cellular Biology

Living systems, from simple organisms to the human body, contain organs. Organs are composed of tissues, tissues consist of cells, and cells are formed of organelles, and molecules. Figure 2.1 – the biological cell is the basic unit of all living organisms (for detailed discussions of cell biology see e.g. Lodish 2000). There are more than 300 trillion cells in the human body, and every second of every day, more than 10 million die and are replaced. The unity of an organism is coordinated by many levels of material, chemical, and electric compunctions. Specific organ tissues and individual cells are surrounded by molecular membranes produced by cells. The biological universe consists of two types of cells, shown schematically in Figure 2.1 ***prokaryotic cells***, and ***eukaryotic cells***.

**Prokaryotes**, such *Escherichia Coli* bacteria, are single cell organisms, which have simple internal organization lack a nucleus, and the genetic material (DNA) is directly suspended inside the cell cytoplasm. **Eukaryotes**, comprising plant and animal kingdoms, have complex internal structure with various **organelles** and membrane limited nucleus that is kept separate from the **cytoplasm** by a double membrane structure. The cytoplasm contains the rest of the organelles and the area of the cytoplasm outside of the individual organelles is called the **cytosol**. Each organelle, surrounded by a membrane, contains a collection of specific enzymes and plays a unique role in the growth and metabolism of the cell. The most important organelles are: **nucleus** – containing DNA and other replication molecules, **mitochondria** – in which most of he cell energy metabolism takes place, **endoplasmic reticula** – build of complex membranes within which glycoproteins and lipids are synthesized, **Golgi vesicles** – which direct membrane constituents to appropriate places in cells, **peroxisomes** – in which fatty acids and aminoacids are degraded, and **lysosomes** – which also degrade internal and foreign molecules.

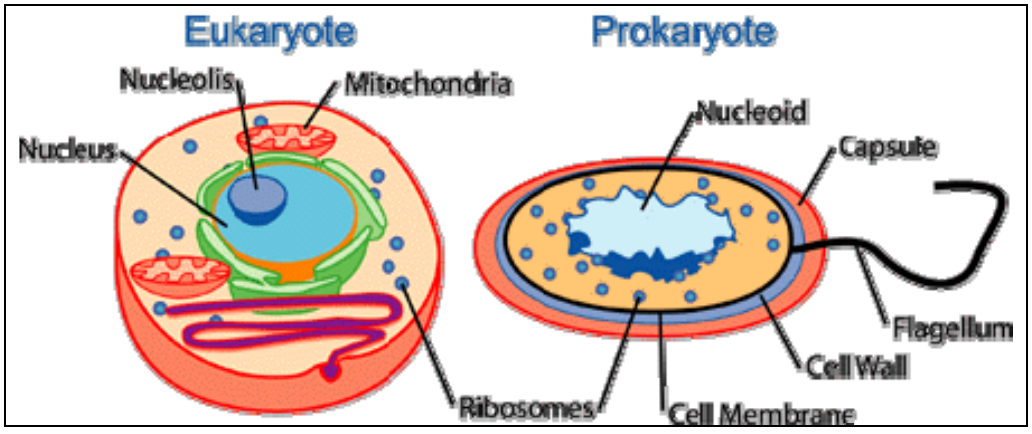


*Figure 2.1: Examples of mammalian (eukaryotic) and bacterial (prokaryotic) cells (with NIH permission), [http://www.ncbi.nlm.nih.gov/About/primer/genetics_cell.html](http://www.ncbi.nlm.nih.gov/About/primer/genetics_cell.html).*

Biological cells are surrounded by a membrane, phospholipid bilayer, designed to keep the cell interior together and protect the cell from the surrounding environment. The biochemical processes of cellular life takes place in the cytosol and cells communicate with the surrounding

and neighbor cells via reactions on the membrane and via the trans- membrane molecule exchange. The cytosol is the largest structure in the cell. It composes 54% of the cells total volume. The cytosol contains thousands of enzymes that are responsible for the catalyzation of glycolysis and gluconeogenesis and for the biosynthesis of sugars, fatty acids, and amino acids. The cytosol takes molecules and breaks them down, so that the individual organelles can use them.

The cytosol contains a skeletal structure, called the **cytoskeleton**. Cytoskeleton gives the cell its shape and allows it to organize many of the chemical reactions that occur in the cytoplasm. Additionally, the cytoskeleton can aid in the movement (motility) of the cell. It consists of protein filaments: actin filaments and the microtubules. The actin is responsible for contraction (like in muscles) and the microtubules are for structural strength of the cell. Cytoskeletal fibers also control movement of structures within the cell.

To survive cells have to carry out numerous functions ranging from replication and energy conversion to molecule transport and the various complicated cascades of biochemical reactions, **signaling**, used in cellular communication. Some of the most important functions are: Molecular transport, DNA replication, Reproduction, Protein synthesis, and Metabolism and Signaling.

One of the primary goals of all living organisms is to survive and reproduce – typically by **cell division**. Cell division occurs rapidly in living organisms. For example, in an adult human, millions of cells divide each second to maintain **homeostasis** (the proper balance in cells). Cells can reproduce in two ways, **mitosis,** and **meiosis**. In mitosis, the resulting daughter cell is an identical clone of the original cell. Mitosis is mostly used by somatic cells (cells of the body). Meiosis, however, is a form of sexual reproduction and only occurs in reproductive cells.

Mitotic **cell division** is an ordered set of events, **cell cycle**, culminating in cell growth and division into two daughter cells. It begins with **interphase**, when the cell replicates all of its genomic and cytoplasmic material and prepares for division. After preparation is complete, the cell enters the 4-phased mitosis. In mitosis, the cell sequentially goes through **prophase**, **metaphase**, **anaphase**, and **telophase**. Immediately after the completion of telophase, **cytokenesis** is initiated to end the cell division by literally separating the cell in two. Figure 2.2(a) schematically illustrates the cell division and cell cycle processes.

The cell cycle stages, Fig 2.2(b), are G1-S-G2-M. The G1 stage stands for "GAP 1". The S stage stands for "Synthesis". This is the stage in which DNA replication occurs. The G2 stage stands for "GAP 2". The M stage stands for "mitosis", and is when nuclear (chromosomes separate) and cytoplasmic (cytokinesis) divisions occur.

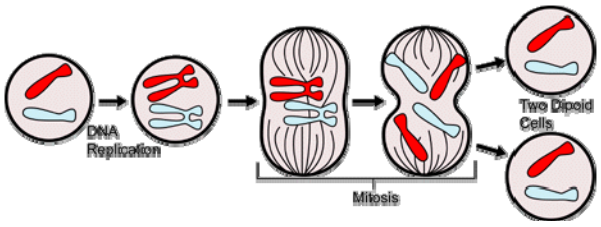


Figure 2.2(a)

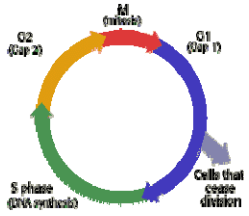


Figure 2.2(b)

*Figure 2.2: Schematics of events during cell division and cell cycle (with NIH permission, [http://www.ncbi.nlm.nih.gov/About/primer/genetics_cell.html](http://www.ncbi.nlm.nih.gov/About/primer/genetics_cell.html) .*

**Cytokinesis** is the final event of the cell cycle and is the process that divides one cell into two daughter cells. Figure 2.3 illustrates how different organisms conduct cytokinesis. In animal cells, the division site is first chosen, generally at the cell equator, and subsequently the cleavage furrow is assembled at the division site (Figure 2.3D). The furrow contains actin, myosin, and other proteins that are organized into a contractile ring called the actomyosin ring. The ring then ingresses or contracts, generating a membrane barrier between the cytoplasmic contents of each daughter cell. The ingressing furrow constricts components of the spindle midzone into a focused structure called the midbody. In the final cytokinetic event, called abscission, the furrow "seals", generating two completely separate cells.

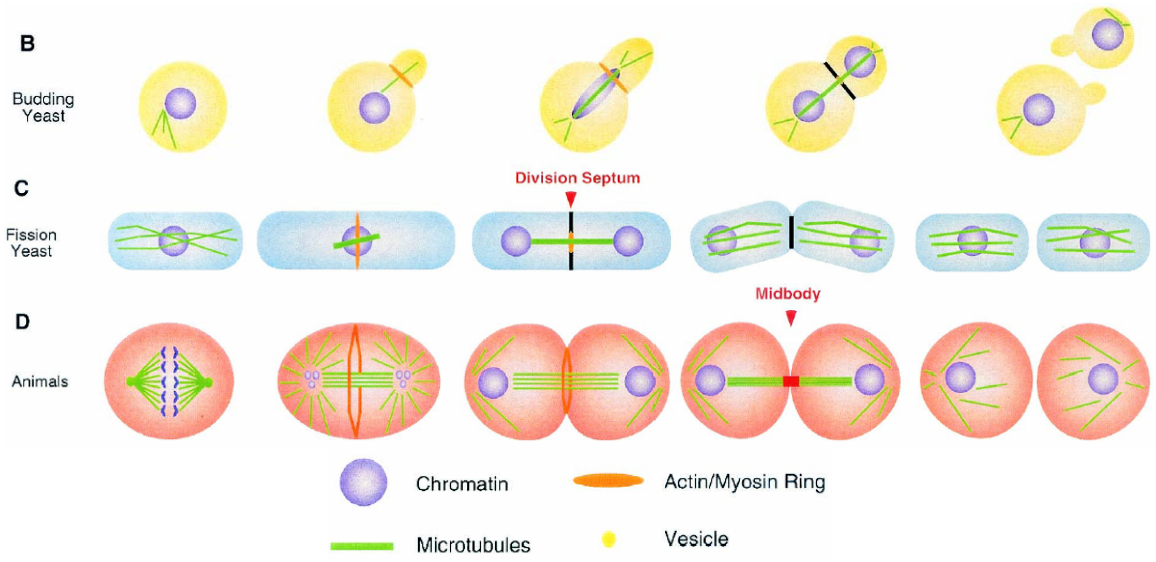


*Figure 2.3: General mechanisms of cytokinesis in eukaryotes. (B) In budding yeast cells, the ring is positioned at the interface between the mother cell and daughter bud, (C) In fission yeast and animal cells, the contractile ring is centrally placed, as both cell types divide by medial fission. Both budding and fission yeasts synthesize a division septum, which eventually degrades, resulting in physical cell separation. (D) In animals, the ingressing furrow constricts the spindle midzone components into a dense structure- midbody. Guertin2002. (with NIH permission), http://pubmedcentral.com/articlerender.fcgi?artid=120788 .*

Live biological cells exhibit an amazing capability to sense the surrounding environment and ability to respond to it. By rearranging their interior (cytoskeleton, organelles, membrane) mammalian cells grow, divide, move, expand/contract, and much more. Cell movement toward (or away) from an external stimulus, **cell taxis**, is induced by cell sensory organs, which activate cell asymmetry, deformation and motility mechanisms. Cell taxis stimulated by chemical agents – **chemotaxis** allows them to detect the direction (gradient) and proximity of an external chemical stimulus such as nutrient and energy, [Bray 2001].

Within a complex organism organs and individual cells communicate by exchanging **chemical messengers** traveling from one cell to another by direct contact or through the extracellular space (interstitium). The chemical signals received by target cells respond by activating **signaling pathways** involving intracellular proteins (metabolic enzymes, gene regulatory

proteins, ion channels, or cytoskeletal proteins). Signaling molecules, also called **ligands** (protein, small peptide, amino acid, nucleotide, steroid, hormone) are secreted from one cell in response to a specific stimulus travel to a target cell, where they bind to **specific receptors** on their membrane and elicit an intracellular response.

Within the cell the main method of **signal transduction** occurs through structural changes of pathway components. A given protein will affect the conformation of one or several other proteins, activating or inhibiting those proteins and thus propagating the signal down the pathway. The trigger for signal propagation often occurs with the binding of the signaling molecule to the receptor, which causes a conformational change in the receptor. Subsequently, cytosolic regions of the receptor are activated, making them active targets for intracellular and membrane associated proteins. The biochemical signal transduction in the cell is a complex and combinatorial process involving switches, integrating centers, feedback loops and crosstalk between pathways. Figure 2.4 presents example schematics of cell signaling pathways analyzed at CFDRC for modeling cellular neurotoxicity problems. Obtaining a detailed understanding of the dynamics of a biochemical reaction is a formidable challenge.

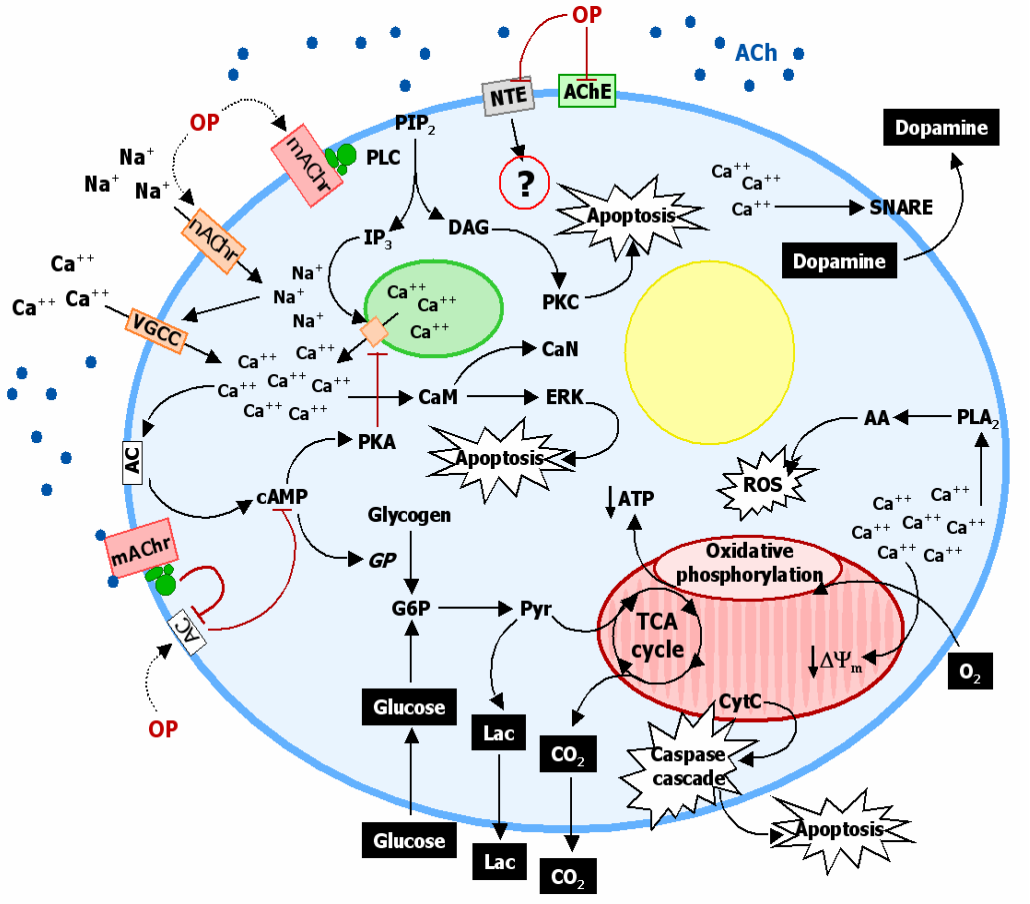


*Figure 2.4: Schematic of organophosphate neuron toxicity cellular signaling pathways, from CDFRC dose-dependent, analysis of signaling and activation, neurotransmitter release, and metabolic response in neurotypical PC12 cells, Jenkins J. and Hood J. 2006.*

## 2.2 Biological and Computational Challenges in Cellular Biology

Rapid progress in experimental biology and medicine, particularly at molecular and cellular levels, is generating an enormous amount of "bio-informatics" data. The raw data in digital or visual imaging form is analyzed and interpreted by highly skilled experts who formulate "models" of cellular events. These "models" are typically expressed in a long narrative form and described in biomedical journals. In molecular and cellular biology compact elegant mathematics based models are rare.

In the last few years it has been recognized that further understanding of biology will be possible only with a more comprehensive multidisciplinary approach involving: mathematics, informatics, computational biophysics, in addition to more traditional disciplines such as biochemistry, biology, physiology, and pathology, etc. Joel E. Cohen of the Rockefeller & Columbia Universities elegantly projected progress in biology as:

***"Mathematics Is Biology's Next Microscope, Only Better;***
***Biology Is Mathematics' Next Physics, Only Better"***

A Computational and bioinformatics approach to biology and medicine has enormous potential that has not yet been completely revealed. In the last two decades, computational technology (hardware and software) has been revolutionized and classical engineering disciplines such as fluid dynamics or structures mechanics evolved into Computational Fluid Dynamics (CFD) and Finite Element Method (FEM) based Computational Structures Dynamics (CSD). New industries have emerged and CFDRC is one of the best examples of US based commercial ingenuity and business successes. It is believed that similar scientific and business revolutions are approaching in Computational Medicine and Biology (CMB). In 2002 CFDRC formed a new CMB team determined to spearhead that revolution.

Scientific potentials and military relevance of computational biology and bioinformatics have also attracted the interest of DARPA. The DARPA IPTO ambitious and visionary BioCOMP Program to develop an open source computational framework and modeling tools for cell biology started in 2001. This framework is called Bio-SPICE which stands for the Simulation Program for Intra-Cellular Processes. The BioCOMP Program involves experts from a broad range of disciplines, including biology, biochemistry, biophysics, computer science, mathematics, and bioengineering. Several teams were tasked to develop novel modeling methods and simulation software for broad but complementary aspects of cell biology such as: metabolic pathways, cellular signaling, cell cycle and division, chemosensing, chemotaxis, cellular colonies, and microorganisms. New standards of model description languages (System Biology Modeling Language, SBML) were being pursued to enable model exchange, reuse and archiving.

In the current BioCOMP Program almost all Bio-SPICE development activities concentrate on the development of biochemistry (cell cycle, signaling, metabolism, genomics, etc) or bioinformatics (e.g. microarray data processing) use **Ordinary Differential Equations** (**ODEs**) and as a consequence describe cells as a "well stirred reactor". Spatial multidimensional cell modeling using **Partial Differential Equations** (**PDEs**) and accounting for cell morphology are

much more challenging and not well represented in the BioCOMP Program. Representing cells as "well stirred reactors", used in all Bio-SPICE biochemistry modeling tools, is clearly inadequate even for the simplest cells. The reaction mechanisms and rate constants in those models are "tuned" based on empirical data to fit experiments. Those rate constants are "contaminated" by other biophysics processes not accounted for explicitly in the models such as: diffusion, advection, directed transport (e.g. by molecular motors), cytoplasm cytoskeleton and membrane mechanics, electrostatics, and others. Such models are also not scalable, rate constants may be time dependent, or additional stochastic processes are added to cover for missed biophysics. It is likely that all the biochemistry reaction mechanisms rate constants will have to be recalibrated once used in more complete spatiotemporal cellular biology models.

Therefore there is an urgent need for prompt development of spatiotemporal cell biology models. The objective of the CFDRC project was to develop a software toolkit for multidimensional, spatiotemporal simulation of cell biology.

The BioCOMP Program will have enormous implications not only in basic scientific research but also more importantly in the US national commercial business and defense. Validated computational cell biology modeling tools will be used to assess novel drugs, novel therapies, safety, toxicity, and efficacy of drugs, drugs designed for individual patients, etc. From the military perspective, better biochemical sensors, better vaccines for bio-agents, better treatment of trauma of injured soldiers, etc. can be designed. Such tools may also influence paradigms of biocomputing.

### 2.3 Assessment of Cell Biology Spatial Modeling Methods

Most outstanding progress has been achieved in computational cellular biochemistry where cell biological pathway models are described by large systems of ODEs [Fall 2000]. Public domain software tools are being developed e.g. by Arkin (1998) (Bio-SPICE http://BioSPICE.lbl.gov/) in US and by Tomita (E-Cell, http://www.e-cell.org) see e.g. Tomita [2001], and Takahashi [2003] in Japan. Levchenko 2002 has recently presented a comprehensive example of an ODE based model of cellular chemotaxis. However they all lack spatial dimension and are at best "compartmentalized".

Multidimensional models of cells have been developed by Loew [Schaff 1999, Fink, 2000, Slepchenko 2003] and termed a Virtual Cell. 1D and 2D spatiotemporal computational models of chemotaxis have also been reported by: Bottino [2000, 2002], the Lauffenburger group at MIT [Narang 2001], Painter [2000], Mogilner [2002], and Othmer [2002]. The Virtual Cell model provides a formal framework for modeling biochemical and biophysical and transport phenomena in 2D and probably 3D (never published) cell geometries while considering the subcellular localization of the major cellular organelles (nucleus, endoplasmic reticulum). Cell geometry can be imported for microscopy images. Geometrical shapes of the cell have been represented with the Cartesian grid and curved shapes of the membrane have to be represented as "stair steps". Figure 2.5 presents an example of the Virtual Cell simulation results, the IP3-mediated calcium dynamics in differentiated N1E-115 mouse neuroblastoma cells with complex neuronal morphologies [Fink 2000]. The results point to an important role for cellular geometry in controlling the spatial and temporal patterns of intracellular signals.

Spatiotemporal models of biological cells have also been applied to cellular chemosensing and chemotaxis. Simulation results have been demonstrated for the 2D mechano-chemical cell motion model, quasi 2D chemical chemoattractant gradient sensing model, and detailed equations for nucleation, growth/capping by polymerization, and diffusion of actin filaments in cells. For physiological parameters the models show remarkable agreement with experimental observations. A 2D PDE "fluid based" chemotaxis model has been recently developed by Bottino 2000, 2002, where reaction, diffusion, advection equations were solved on triangular and Voronoi polyhedral (2D) meshes. Figure 2.5 illustrates the CFDRC simulation of in vitro cellular chemotaxis events. A cellular culture dish erythrocytes, a white blood cell, and a motile bacterium was setup to simulate the relative motion of the bacterium and the neutrophil which is stimulated by the chemokines released by the bacterium, A Lagrangian -Eulerian model has been used to solve movement of cells and diffusion of a chemokine in the culture.

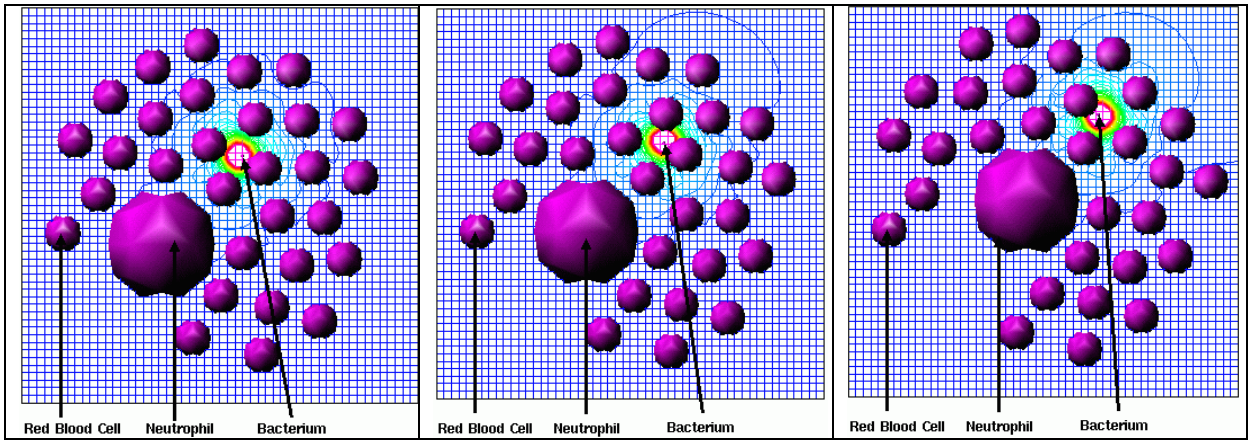


*Figure 2.5: CFDRC simulation of a bacterial and neutrophil chemotaxis in an in vitro cell culture.*

# 3.0 SPATIOTEMPORAL MODEL OF CELLULAR BIOLOGY

## 3.1 Computational Cell Biology

Substantial progresses over the past three decades in biochemistry and molecular cell biology, coupled with emerging high throughput techniques for detecting protein-protein interaction, have opened a new era in signal transduction research. At the same time however, recent analyses of cellular signaling pathways have revealed that they are extremely complex nonlinear molecular processes occurring throughout the cell volume and involve multiple species and signaling cascades. Because of their size and complexity, these networks are often too complicated for the human mind to organize and analyze. It has become necessary to develop mathematical models to understand the behavior of signaling networks controlling cellular biology.

The use of mathematical models and computer simulation has been successfully used in pharmacology and drug discovery to study ligand-receptor interactions, pharmacokinetics, and pharmacodynamics. Computational modeling of cellular metabolic and signaling pathways, the main focus of the BioCOMP Program, has been explored using four major modeling frameworks: chemical kinetics models, compartmental models, stochastic models, and diffusion-reaction models. The most familiar, simplest, and most commonly followed (in the BioCOMP Projects) modeling framework is the chemical kinetics approach. In this approach, the cell is treated as a "well-stirred reactor". The dynamics of a cellular signaling in that approach is described by a system of Ordinary Differential Equations (ODEs) in the form:

$$\frac{dC}{dt} = Generation - Consumption \tag{3.1}$$

Where C is the species concentration and the right hand side (RHS) typically involves several terms in which specie C participates arranged in two groups: generation of specie C and its consumption. The generation and consumption term can be a constant (e.g., synthesis), first order reactions (e.g., degradation), or nonlinear (e.g., second order reactions or Michelis-Menten kinetics for enzymes). For large signaling networks such as those shown in Figure 2.4 and Figure 2.5, in the preceding chapter, a large system of ODEs, each having large number of generation and consumption term on the RHS. In the last few years, advanced numerical techniques and robust software tools have been developed for solving large systems of ODEs such as those resulting from biochemical signaling pathways. Several of them have been developed and adapted for modeling cell biology problems during the DARPA Bio-SPICE program e.g. JigCELL software developed at Virginia Tech by Professor John Tyson group.

To understand the cellar biochemical dynamics that arises from variation in both space and time, either **compartmental or partial differential equation (PDE)-based models** are needed. Like chemical kinetics models, compartmental models are based on ODEs. However, instead of treating a cell as a single well stirred reactor, compartmental models divide the cell into compartments such as: membrane, cytoplasm, mitochondrion, nucleus, or extracellular space), collect the equation describing biochemical kinetics of species in individual compartments and allow species exchange between compartments.

Compartmental modeling has been used extensively in modeling the network involved in protein secretion and trafficking, and developmental biology. For the cases where explicit dependence on the spatial variables is needed, a partial differential equation (PDE)-based model is needed. The spatiotemporal dynamics of cell biochemical signaling can be described by the general advection-diffusion-reaction equation:

$$\underbrace{\frac{\partial C}{\partial t}}_{Transient} + \underbrace{\nabla \cdot (\mathbf{U}C)}_{Convection} = \underbrace{\nabla \cdot D\nabla C}_{\text{Diffusion}} + \underbrace{\dot{R}}_{\text{Reaction Source}} \tag{3.2}$$

where, C is the specie concentration, U is the fluid flow velocity, D is the diffusivity of the specie C in the cellular medium and R is the generalized source term. As in the simple kinetics, models the source term may consist of several generation and consumption terms. Note that equation (3.2) includes several terms for: transient, convection, diffusion, and source/sink term due to chemical reactions. Equation (3.2) is the PDE because the concentration depends on three spatial directions (x, y, z coordinates) and on time. Unlike in the ODE equations, PDEs are solved on a computational grid. Generation of 3D computational grid for a biological cells is a challenging problem in itself as the cell geometry may be changing in time and may be influenced by the cell biological events e.g. chemotaxis. In such cases, cell geometry and mesh need to be computed as part of the cell biology problem. Numerical solutions of even large scale ODE systems are very fast (seconds to minutes on powerful PCs). Numerical solutions of large scale time dependent 3D PDEs is much more computationally intensive. Depending on the problem, it may take only few minutes or as long as several days or weeks. There are very few spatiotemporal cell biology tools, one is the Virtual Cell (http://www.nrcam.uchc.edu/) and the other CoBi tool developed in this project.

## 3.2 Basic Transport Equations

Spatiotemporal computational modeling of flow, diffusion, and reaction processes in complex geometries requires several preparatory steps. The first and most important is to define the objective of the task and the expected result. A step-by-step approach is strongly recommended by first solving simplified but related problems and adding complexity after each successful step. A typical modeling procedure involves the following steps:

1. Create or import the model geometry and computational grid,
2. Select the models (e.g. flow, species transport, biochemistry pathways, etc),
3. Specify volume conditions, boundary conditions, initial conditions,
4. Specify material properties, and other physical constants,
5. Specify the solution control parameters e.g. number of times steps, under-relaxation,
6. Calculate a solution using CoBi.
7. Analyze the results using visualization tools e.g. VisIt tools from LBL,

After step 7, you may want to return to the previous steps refining mesh, models, or parameters.

All models in CoBi are formulated using an SI unit system which will be used in the description of the mathematical models. However using the appropriate model setup the user can change the

system and even use a nondimensional formulation – this requires a good understanding of all terms of the transport equations, models, and properties used. If you read an external grid file with X, Y, Z coordinates of grid vertices we assume it is setup in meters. If not, one will need to scale the grid using the preprocessor.

Throughout this section, for compactness, we will use the vectorial notation to describe partial differential equations. The reader will notice that most of them have a very similar form as shown below:

$$\underbrace{\frac{\partial C}{\partial t}}_{Transient} + \underbrace{\nabla \cdot (\vec{U} \cdot C)}_{Convection} = \underbrace{\nabla \cdot D \nabla C}_{\text{Diffusion}} + \underbrace{\dot{S}}_{\text{Source}} \tag{3.3}$$

where C is the transported property e.g., a concentration, U is the convective velocity vector, D is the diffusion coefficient, and S is the source term e.g. chemical reaction rate representing formation and consumption of species C. The nabla operator, $\nabla$, for a scalar variable C is called gradient for a vector variable U is called divergence:

$$\underbrace{\nabla C}_{Gradient} = \left(\frac{\partial \mathrm{C}}{\partial \mathrm{x}}, \frac{\partial \mathrm{C}}{\partial \mathrm{xy}}, \frac{\partial \mathrm{C}}{\partial \mathrm{z}}\right) \qquad \underbrace{\nabla \cdot U}_{Divergence} = \frac{\partial U_x}{\partial \mathrm{x}} + \frac{\partial \mathrm{U}_y}{\partial \mathrm{xy}} + \frac{\partial \mathrm{U}_z}{\partial \mathrm{z}} \tag{3.4}$$

CoBi has several unique modeling components related to cell and tissue biology. One of the most important is the membrane model. The membrane model and its interaction with the volume models of the cytoplasm and extracellular space will be described in a separate section in this chapter.

Spatiotemporal computational cell biology involves a coupled solution of cell biophysics and biochemistry. Cell biophysics may involve several disciplines including fluid flow, heat transfer, structural mechanics, electrostatics, and others. They are all mathematically described by complex PDEs. The biochemistry is described by a system of species transport equations, Equation 3.2.

The convective diffusive transport in cells and tissues occurs in a non-homogeneous porous media. The governing equations of fluid (e.g. water) flow in the biological cells and tissues are the Navier-Stokes equations, modified for a porous medium, and consist of the fluid continuity and momentum equations. Transport of multiple chemical species such as signaling molecules or drugs is described using convective-diffusive transport equations later in this document. The fluid transport equations are given below:

Continuity Equation

$$\frac{\partial}{\partial t}(\varepsilon\rho) + \nabla \bullet (\varepsilon\rho \mathbf{U}) = \mathbf{0} \tag{3.5}$$

In this equation, the first term is the mass change (density or volume) in the control volume. It is zero for incompressible flow and if the computational mesh, is not moving or deforming. The

flow of water under normal pressure and temperature is a good example of incompressible flow. The second term is the mass flux across surrounding surface of the same control volume.

Fluid Momentum Equations

$$\frac{\partial}{\partial t}\left(\varepsilon\rho\mathbf{U}\right)+\nabla\cdot\left(\varepsilon\rho\mathbf{U}\mathbf{U}\right)=-\varepsilon\nabla p+\nabla\cdot\left(\varepsilon\boldsymbol{\tau}\right)+\frac{\varepsilon^2\mu\mathbf{U}}{\kappa} \tag{3.6}$$

The first term on the left is the rate of change of momentum; the second term is the convection term. The first term on the right side is the pressure gradient term, the second term is viscous shear stress term, and the last term is the resistance term arising due to the porous medium. In above equations $\varepsilon$ is the porosity (1.0 open flow, 0.0 fully blocked volume), $\rho$ is the density, p is the pressure, U is the water perfusion velocity vector, $\tau$ is the shear stress, and $\kappa$ is permeability. A "**continuum approximation**" is assumed for the cellular space and organ tissue approximating the cells and intercellular space using the porosity concept.

Cellular biology involves complex interactions between the biophysical and biochemical processes occurring in the extracellular space, on cell membranes, and within intracellular space. Vast number of species (metabolic nutrients and product, signaling molecules, drugs) are created, transported, and processes in various regions. Computational modeling of these phenomena involves the solution of species transport/balance equations in extracellular, membranes and intracellular spaces within the tissue. The general transport equation for species in perfused tissue is described by a partial differential equation (PDE), Equation (3.7), and includes several terms for: transient, convection, diffusion, and source/sink term due to chemical reactions and can be written as follows:

$$\underbrace{\frac{\partial\varepsilon C}{\partial t}}_{\textit{Transient}}+\underbrace{\nabla\cdot(\varepsilon\mathbf{U}C)}_{\textit{Convection}}=\underbrace{\nabla\cdot\varepsilon D\nabla C}_{\text{Diffusion}}+\underbrace{\varepsilon\cdot\dot{\mathrm{R}}}_{\text{Reaction Source}} \tag{3.7}$$

where, **U** is the perfusion velocity, D is the diffusivity of drug in the medium and $\varepsilon$ is the porosity of the medium.

The species diffusion coefficient D in equation 3.7 represents "diffusivity in media". The experimentally measured total tissue effective diffusivity will need to be scaled by porosity D/ε. The species diffusivity value depends on several parameters representing intercellular space and the transported species.

Typically, the transport and biochemistry terms in the species balance PDE equations are solved using an operator splitting technique by:

1. First solving the system of ODE equations composed of transient-reaction terms for all species, and then
2. Solving all terms of the PDE equations with source terms computed from step 1.

An important part of the spatial cell modeling is the geometry definition and mesh generation. CoBi can handle a broad variety of grids including: simple Cartesian grids, curvilinear hexahedra, Octree grids, unstructured tetrahedral grids, and general polyhedral grids. Unlike in conventional engineering where the geometry is "man made" and defined by mathematical formulas (lines, surfaces, solids) cell biology is not well defined. It is very challenging to describe cell geometry in a mathematical form. The best way is probably to use a microscopy image of a cell and image processing software tools to generate the geometry and to generate mesh for that cell. Figure 3.1 presents an example approach developed at CFDRC to generate a Quadtree (in 2D) and Octree (in 3D) mesh on a biological cells.

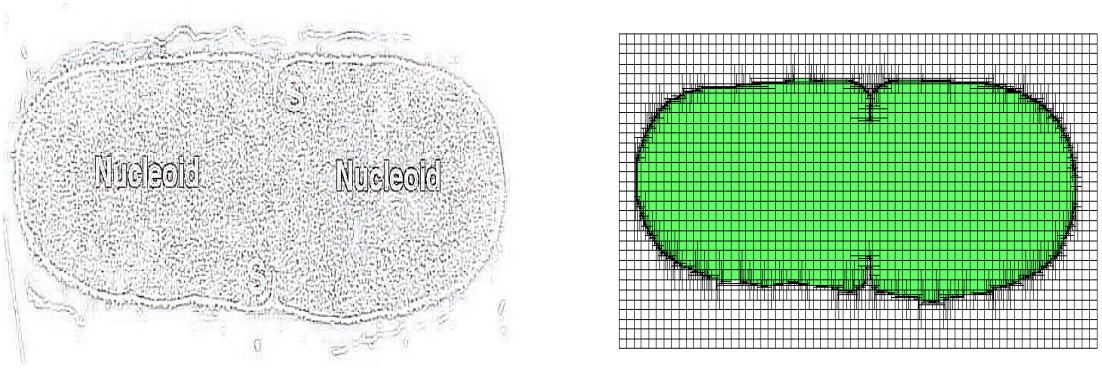


*Figure 3.1: Image based generated cell geometry and a quadtree mesh for a bacterial cell.*

## 3.3 Membrane Model

In cell biology, membranes play an extraordinary role protecting cells or organelles from the outside environment, controlling cell shape, enabling in-transport of nutrients and excretion of waste products. Membrane bound receptors (proteins and peptides) play the sensing, communications, and gate keeping roles. Despite the differences in membrane composition for different cell types we will treat them as very thin shells with embedded receptors, modeled as either bound or diffusible "species". The receptors can undergo chemical reactions with external, internal, and other membrane bound species. 3D transient (4D) surface diffusion-reaction equations on the membrane surface will be solved.

The membrane geometry can be time dependent, can move, and can undergo deformations. In the present version, local velocities (deformations) of the membranes will be prescribed or computed from other physiological models. In the computational model, it is assumed that the membrane surface can be defined as a set of interconnected triangles forming an "unstructured" 3D mesh.

### 3.3.1 ***Basic Equations and Assumptions***

Based on experience, the governing equations for membrane species are described in the integral form. It ensures strong conservation, easy formulation of moving/deforming geometry, and it provides intuitive framework for numerical approximation using Finite Volume Method (FVM) on arbitrary control volume shapes. The time-dependent scalar conservation law will be used in the following form:

$$\frac{\partial}{\partial t}\int_V \varphi_i dV + \oint_\sigma (\vec{v} - \vec{v}_g)\cdot \vec{n}\varphi_i d\sigma - \oint_\sigma D_i \vec{n}\nabla\varphi_i d\sigma = \int_V S_i dV \tag{3.8}$$

where $\varphi_i$ is the i-specie concentration, V is the control volume (function of time), $\sigma$ is the surface of the control volume, v, and $v_g$ are the advection velocity and grid velocity (e.g. due to the mesh deformation) vectors, n is the surface normal vector for control volume faces, $D_i$ is the diffusion coefficient for specie i, and $S_i$ is the source term e.g. due to reaction rate. The equation is solved in the inertial frame, so if the entire body of the membrane is moving v=0.

For moving/deforming grids, the volume conservation principle has to be ensured:

$$\frac{\partial}{\partial t}\int_V dV = \oint_\sigma \vec{v}_g \cdot \vec{n} d\sigma \tag{3.9}$$

This formulation is general enough to enable future extensions of the membrane model. Note that to represent surface bound (immobile or non-diffusive) receptors it is enough to set D=0.

### 3.3.2 ***Numerical Integration Method***

To numerically solve the governing equations FVM is used and integrate over an arbitrary control volume. Note that the surface integrals are replaced by flux terms across control volume faces. All dependent variables are stored at the cell centers, mesh coordinates at the mesh vertices, and all fluxes are calculated at the cell faces.

The transient term is integrated with a backward Euler method:

$$\frac{\partial}{\partial t}\int_V \varphi_i dV \approx \frac{V\varphi_i - V^o\varphi_i^o}{\Delta t} \tag{3.10}$$

The source term is a simple product of reaction rate times the cell volume. Note that the reaction rate is a nonlinear function of concentrations $\varphi_i$ and which needs to be linearized. In the current CoBi version, simple bimolecular as wells as Arrhenius, Michelis-Menten, and other more general expressions are used.

The diffusive fluxes are being calculated as surface integrals. Figure 3.2 illustrates the control volume notation used for flux evaluation.

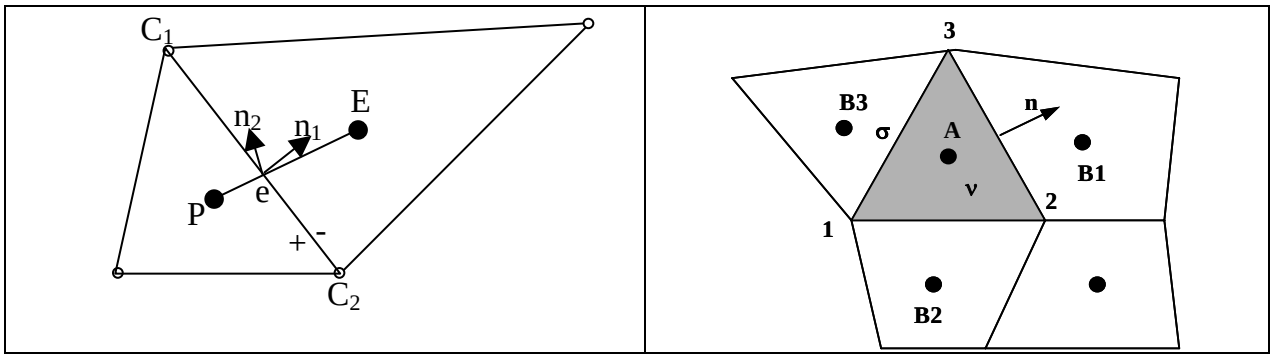


*Figure 3.2*: *Nomenclature used for Calculation of Cell Face Fluxes, and, Unstructured control volume notation.*

For convenience, the details of flux evaluation of a selected face denoted as e are presented. The same rules apply to all faces of the control volume. The diffusive flux of φ is comprised of two terms, main and cross terms as follows:

$$D_e = \int_\Gamma D_{\varphi,e} \nabla \varphi n_1 d\Gamma \approx (D_\varphi \nabla \varphi)_e \cdot \vec{n}_{1,e} A_e = D_e^m + D_e^c \tag{3.11}$$

where $A_e$ is the area of face e of the control volume, and $D^m$ and $D^c$ represent main and cross diffusion fluxes through face e. By discretizing the gradient of φ at the cell face center e with the central difference scheme, the following expressions are obtained:

$$D_e^m = D_{\varphi,e} \frac{A_e}{(\vec{r}_E - \vec{r}_P) \cdot \vec{n}_{1,e}} (\varphi_E - \varphi_P) \tag{3.12}$$

$$D_e^c = D_{\varphi,e} \frac{A_e (\vec{n}_1 \cdot \vec{n}_2)}{|\vec{r}_{c2} - \vec{r}_{c1}|} (\varphi_{c2} - \varphi_{c1}) \tag{3.13}$$

where $\varphi_{c1}$ and $\varphi_{c2}$ are the concentration values at the corners. The values at the corners are evaluated from the cell center values via interpolation (e.g. 1/r averaged).

The advective flux is evaluated as follows:

$$F_e = \int \varphi \vec{v} \cdot n_1 d\Gamma \approx (v_n A)_e \cdot \varphi_e \tag{3.14}$$

where $v_n$ is the face normal relative (transport-grid) velocity and $\varphi_e$ is the concentration vale at the center of the e face. For practical reasons we calculate cell face value based un the "upwind" value from the neighbor cell center i.e.:

$$\varphi_e \approx \begin{cases} \varphi_P \cdots v_n \geq 0 \\ \varphi_E \cdots v_n < 0 \end{cases} \tag{3.15}$$

All terms are computed fully implicitly. To minimize the computer storage requirements the cross diffusive fluxes are calculated semi-implicitly (previous iteration value).

The grid vertex velocity is specified from another (LBL main solver) software module but the cell face velocities are computed within the membrane module in CoBi based on the volumetric conservation law (shown above) as from either Backward Euler or Crank Nicholson approximation as follows:

$$v_g \approx \frac{\Delta V_F}{\Delta t} \qquad\qquad v_g \approx \frac{\Delta V_F}{2\Delta t} - v_g^o \tag{3.16}$$

where $v_g$ is the grid velocity normal to the face, $v_g^o$ is the old time step value, $\Delta V_F$ is the volume swept by the moving face of the deforming control volume, and $\Delta t$ is the time step.

After summing up all cell face fluxes and volume integral terms, the discretized equation can be expressed in the following algebraic form:

$$a_P \varphi_P = \sum_{nb} a_{nb} \varphi_{nb} + S_\varphi \tag{3.17}$$

Where $a_P$ is the main diagonal coefficient and $a_{nb}$ are the neighbor link coefficients, which involve contributions of advective and diffusive fluxes. This system of algebraic equations forms a matrix with a constant bandwidth of only four nonzero entries for the triangle cells. One of available sparse matrix solvers (e.g. Conjugate Gradient Squared, CGS, or GMRES) is used to solve the equation set. It is solved sequentially for each of the concentrations.

### 3.3.3 ***Model of Membrane Geometry***

The membrane surface is represented in the form of a graph of triangles, with coordinates defined at the vertices. Figure 3.3 illustrates example cell membrane triangulations. Each vertex also has the value of the cell membrane thickness. The flexibility to name surface patches is also provided to enable different volume and boundary condition specifications, and data post processing.

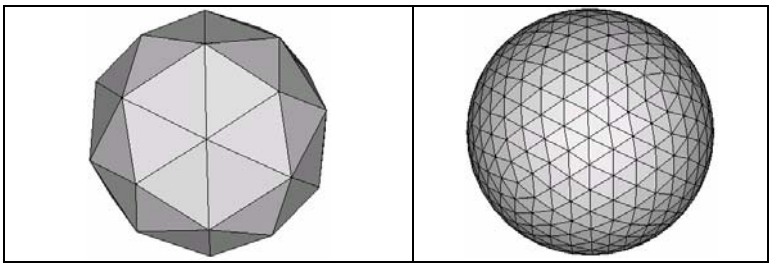

*Figure 3.3: Cell membrane triangulations.*

In the first CoBi release, uniform thickness is assumed. The membrane module automatically calculates all geometrical parameters of for each volume including, areas, volume, surface normals, distances etc.

### 3.4 Biochemistry Model

The source term $S_i$ (also marked as $R_i$) in the species transport equations (eq. 3.7) is computed based on the mechanism of reaction kinetics. The net source of chemical species *i* due to reaction $R_i$ is computed as the sum of the reaction sources over the $N_R$ reactions that the species participate in:

$$R_i = M_{w,i} \sum_{r=1}^{N_R} R_{i,r} \tag{3.18}$$

where $M_{w,i}$ is the molecular weight of species *i* and $R_{i,r}$ is the rate of reaction (creation or consumption) of species *i* in reaction *r*. The reaction mechanism can be written in the form of reversible reaction mass action law:

$$\sum_{i=1}^{N} \nu^{f}{}_{i,r}[C_i] \quad \underset{k^{b}{}_{r}}{\overset{k^{f}{}_{r}}{\rightleftharpoons}} \quad \sum_{i=1}^{N} \nu^{b}{}_{i,r}[C_i] \qquad \text{r=1, } N_R \tag{3.19}$$

where N is the number of species in the complete reaction mechanism and summation is over all species appearing in that reaction, $\nu^f$ and $\nu^b$ are the stoichiometric coefficients for reactants and products respectively and square brackets denote symbols of the species, $k^f$ and $k^b$ denote forward and backward (reverse) reaction rates constants for a giver reaction r. This formulation is valid for reversible or irreversible ($k^b$=0) reactions.

In CoBi, reaction may occur in the volume or on the surface e.g. cell membrane.

The individual reaction step rates for j-reaction step $\omega_j$ is

$$\omega_j = k_j^f \prod_{i=1}^{N_{species}} C_i^{\nu_{ij}^f} - k_j^b \prod_{i=1}^{N_{species}} C_i^{\nu_{ij}^r} \tag{3.20}$$

where $k^f j$ is the forward rate constant and $k^b j$ is the backward (reverse) rate constant and $C_i$ are the species concentrations (molar).

The molar rate of production (R>0 or destruction R<0) of species *i* in equation 3.18 can now be written as:

$$R_i^{production} = \sum_{j=1}^{N_R} \left( \nu_{ij}^r - \nu_{ij}^f \right) \cdot \omega_j \tag{3.21}$$

where $N_R$ is the number of reactions species in reaction r, $C_{j,r}$ are the molar concentrations of species (reactants and products respectively), and the symbol Π denotes multiplication. The forward and reverse reaction kinetics rates are supplied by the user. They can be functions of different varaibles (e.g. temperature). In some cases the forward rate and equilibrium constant $K_r$ are known allowing the reverse rate to be simply computed as:

$$k^b{}_r = \frac{k^f{}_r}{K_r} \tag{3.22}$$

Another type of biochemical reactions in CoBi are the enzyme-catalyzed reactions in which the enzyme E, a catalyst, and substrate S participate in a reversible reaction forming enzyme-substrate complex ES followed by an irreversible reaction of forming the product P and recycling the enzyme. The reaction mechanism can be expressed as:

$$S + E \underset{k_{-1}}{\overset{k_1}{\Longleftrightarrow}} ES \overset{k_2}{\Rightarrow} E + P \tag{3.23}$$

The above enzyme catalyzed kinetics reaction system can be expressed as either multi step mass action kinetics or Michaelis-Menten kinetics. For enzymatic reactions in closed systems, kinetic scheme (3.23) implies the following conservation relations:

$$E_T = \mathrm{E} + \mathrm{ES}, \tag{3.24}$$

and

$$S_T = \mathrm{S} + \mathrm{ES} \tag{3.25}$$

where $E_T$ and $S_T$ are, respectively, the total concentrations of the enzyme and the substrate in the system. Applying the law of mass action to kinetic scheme (3.23), and using equation (3.24-3.25) to eliminate, yields the following set of differential equations:

$$\frac{dS}{dt} = -k_1 \cdot (E_T - ES) \cdot S + k_{-1} \cdot ES \tag{3.26}$$

$$\frac{dES}{dt} = k_1 \cdot ((E_T - ES) \cdot S - K_M \cdot ES \tag{3.27}$$

$$\frac{dP}{dt} = k_2 \cdot ES \tag{3.28}$$

where the Michaelis constant $K_M$ is defined as

$$K_M = \frac{k_{-1} + k_2}{k_1} \tag{3.29}$$

This reaction scheme (3.23) is mathematically described by a set of coupled non-linear second-order algebraic (3.24-3.25) and differential equations (3.26-3.29) that could be numerically stiff. Stiff ODE solvers are then needed. When a quasi-steady-state assumption is made the initial rate of product formation can be expressed as a function of initial substrate concentration, and then obtaining kinetic parameters by solving the Michaelis–Menten (MM) equation:

$$\frac{dP}{dt} = v_0 = \frac{v_{\max} \cdot S_0}{K_M + S_0} \tag{3.30}$$

where $v_{max}$ is the maximum velocity (product formation rate) and $S_0$ initial substrate concentration.

Michaelis Menten law is also known as saturable or capacity-limited reactions and can be simplified for limiting conditions for the substrate concentration S. If $S>>K_M$ then it reduces to $v_{max}$ ( i.e. zero order reaction). The enzyme catalyzed kinetics reaction system, Eq. 3.23, has been extended to more complex biochemical reaction systems involving multiple substrates, multiple products, enzyme inhibitors and activators. Table 3.1 presents examples of such reactions.

*Table 3.1: Examples of enzyme catalyzed kinetics reactions and reaction rate expressions, $C_S$ and $C_I$ are the substrate and enzyme concentrations while $\omega$ is the reaction rate.*

| Type | Simplified Kinetics | Stepwise Rate Expression |
|---|---|---|
| Michaelis-Menten - MM | $S \underset{V_{\max}}{\overset{K_m}{\Rightarrow}} P$ | $\omega = \frac{V_{\max} C_S}{C_S + K_m}$ |
| MM plus inhibition and activation | $S \underset{K_1, K_2}{\overset{ke_o}{\Rightarrow}} P$ | $\omega = \frac{ke_o}{1 + \frac{K_1}{C_S} + \frac{C_S}{K_2}}$ |
| Competitive Inhibition | $S + I \underset{K_S, K_I}{\overset{ke_o}{\Rightarrow}} P + I$ | $\omega = \frac{ke_o C_S}{C_S + K_S\left(1 + \frac{C_I}{K_I}\right)}$ |
| Non-Competitive Inhibition | $S + I \underset{K_S, K_I}{\overset{ke_o}{\Rightarrow}} P + I$ | $\omega = \frac{ke_o C_S}{\left(C_S + K_S\right)\left(1 + \frac{C_I}{K_I}\right)}$ |
| Multiple Substrate/One Enzyme | $S_1 + S_2 \underset{K_1, K_2}{\overset{k_1, k_2, e_o}{\Rightarrow}} P_1 + P_2$ | $\omega^1 = \frac{k_1 e_o C_{S_1}}{K_1\left(1 + \frac{C_{S_1}}{K_1} + \frac{C_{S_2}}{K_2}\right)}$ |

| | | |
|---|---|---|
| | | $\omega^2 = \dfrac{k_2 e_o C_{S_2}}{K_2\left(1 + \dfrac{C_{S_1}}{K_1} + \dfrac{C_{S_2}}{K_2}\right)}$ |

In several cases one needs to model ligand L and receptor R binding e.g. on cell membranes. A simple L-R binding can be described as a reversible reaction:

$$R + L \underset{k_r}{\overset{k_f}{\Leftrightarrow}} C \tag{3.31}$$

Where, R is the membrane receptor available to bind with free ligand (e.g. drug) L and C is the bound ligand-receptor complex drug, and $k_f$, and $k_r$ are forward and backward rate constants. The rate of change in concentration of bound drug and fee drug is defined as:

$$\frac{dC}{dt} = k_f \cdot R \cdot L - k_r C \tag{3.32a}$$

$$\frac{dL}{dt} = -k_f \cdot R \cdot L + k_r C \tag{3.32b}$$

$$\frac{dR}{dt} = -k_f \cdot R \cdot L + k_r C \tag{3.32c}$$

Assuming $k_f$ and $k_r$ are known, the three equations for R, L, and C can be solved. Assuming that there is a finite number of receptor binding sites and introducing the maximum cell binding receptors, $B_{max,c}$ so that

$$B_{\max} = R + C \tag{3.33}$$

Substituting equation (3.33) into (3.32a) to remove the receptor R, there are only two equations for free and bound drug. For example, the equation for L is:

$$\frac{dC}{dt} = k_f \cdot (B_{\max} - C) \cdot L - k_r C \tag{3.34}$$

The biochemistry module in CoBi solves systems of Ordinary Differential Equations (ODEs) individually for each control volume in the 3D and membrane surface computational domain. The solution of ODE equations provides species concentrations for the PDE solver module. They are used to compute reaction kinetics source terms in the PDE equations.

### 3.5 Boundary, Initial, and Volume Conditions

The mesh imported to CoBi has to have following data:

- Number of nodes, faces, and volumes,
- X,Y,Z coordinates for all nodes,
- Node link lists to cells,
- Boundary condition path names and face link lists,
- Volume condition zone names and cell lists.

The names (tags) of boundary and volume conditions are used to impose Boundary Conditions (BCs) and Volume Conditions (VCs) on these surface/volume meshes. BCs specify the dependent variables at the domain boundaries whereas VCs specify material types and models to be used in different parts of the computational domain. At present CoBi users can specify them in the *.SIM file (a text file used as input to run CoBi) or interactively via JCoBi GUI (as described in JCoBi User's Manual). Note that JCoBi creates the *.SIM file so the user can verify or modify the BC and VC types and property values using any text editor. There may be different VCs for cell cytoplasm, for extracellular space and for the membrane.

The boundary types available in CoBi are as follows:

- Fluid flow inlet and exit: with specified pressure, velocity, or mass flow
- Wall
- Symmetry
- Periodic boundary,
- Internal faces e.g. membranes

### 3.6 Material Properties

CoBi simulation requires specification of models (e.g. flow, mixing, reaction, etc.) and the setup of the physical properties of the material. The user needs to input all material properties. Material properties are associated with volume conditions (VCs) which are "tagged" by names in the grid file. CoBi user inserts the values of specific properties in the *.SIM file (a text file used as input to run CoBi) or interactively via JCoBi GUI (as described in JCoBi User's Manual). Note that JCoBi creates the *.SIM file so the user can verify or modify the BC and VC types and property values using any text editor

Typical properties needed for CoBi simulations are:

- Density and/or molecular weights
- Viscosity
- Diffusion coefficients

Properties may be temperature and/or composition-dependent. The material properties are setup based on volume condition (VC) name tags associated with the grid.

# 4.0 DESCRIPTION OF COBI CODE FRAMEWORK

## 4.1 Overall Software Framework

CFDRC has developed core solver modules and the integrated software framework for computational biology. It has evolved from an initial membrane only solver to the coupled volume-membrane convection-reaction-diffusion equations coupled to the ODE biochemistry module. The integrated solver module, CoBi, has been tested on several problems related to cell biology and was delivered to DARPA (SRI) in February 2005. This section briefly presents the technical capabilities and software structure of CoBi tools.

The CoBi solver can solve flow and diffusion-reaction problems in any geometry ranging from single 0D compartment, to 1D plug reactor, to network of compartments connected by channels, to 1D, 2D, or 3D geometries of a single cell or multi-cellular tissues. The unique capability of CoBi is that in addition to volumetric equations, it can simultaneously solve PDE reaction-diffusion equations on thin membranes (surfaces) surrounding biological cells or subcellular organelles, endothelial or epithelial walls of vessels. The geometry may change in time, may deform, as part of the solution process. For example, the cell can grow during the cell division process. The code has the following modeling capabilities:

- Steady-state or transient analysis
- Incompressible Newtonian flows
- Heat transfer,
- Chemical species mixing and reaction in volume and on membranes
- Arbitrary volumetric sources of mass, momentum, and chemical species
- Flow and species diffusion-reaction in porous media

CoBi solver internally uses unstructured meshes but can impart structured, multilink structured, curvilinear body fitted, tetrahedral, octree, and any finite element mesh.

### 4.1.1 ***Preprocessing, Geometry, Meshing, and Model Setup***

At present CoBi reads two main files:

a) Mesh data with named volumetric regions that are used to set boundary and initial conditions as well as volumetric properties (diffusivity, density, porosity, etc.), and

b) Text file, *.SIM, providing problem definition specification including values for boundary conditions, material properties, numerical control parameters, etc.

A prototype simple geometric modeler and mesh generator have also been developed, and implemented it in the CoBi GUI module, JCoBi, for problem setup. To enable an efficient setup of biochemistry equations, direct interfaces to the open source cell biochemistry modeling languages, System Biology Modeling Language (SBML), was developed. It allows the user to import cell biology models setup with other Bio-SPICE tools such as JDesigner, Jarnac, and Jigcell.

### 4.1.2 *CoBi Software Programming*

A general and modular C++ software framework, CoBi, for solving advection-diffusion-reaction partial differential equations (PDEs) on unstructured grids was developed. The CoBi software has been written in C++ using object-oriented programming with very powerful database for handling geometry, mesh, solution fields, properties, and boundary/volume conditions. It combines the full Navier Stokes equation flow solver for incompressible flows, and a comprehensive model of volume and membrane surface constrained convection-diffusion-reaction model. It has database interfaces to geometry meshing tools and a direct interface to 3D visualization/animation tool VisIt (www.llnl.gov/**visit**/). Figure 4.1 presents the complete CoBi toolkit environment for modeling cell and tissue biology.

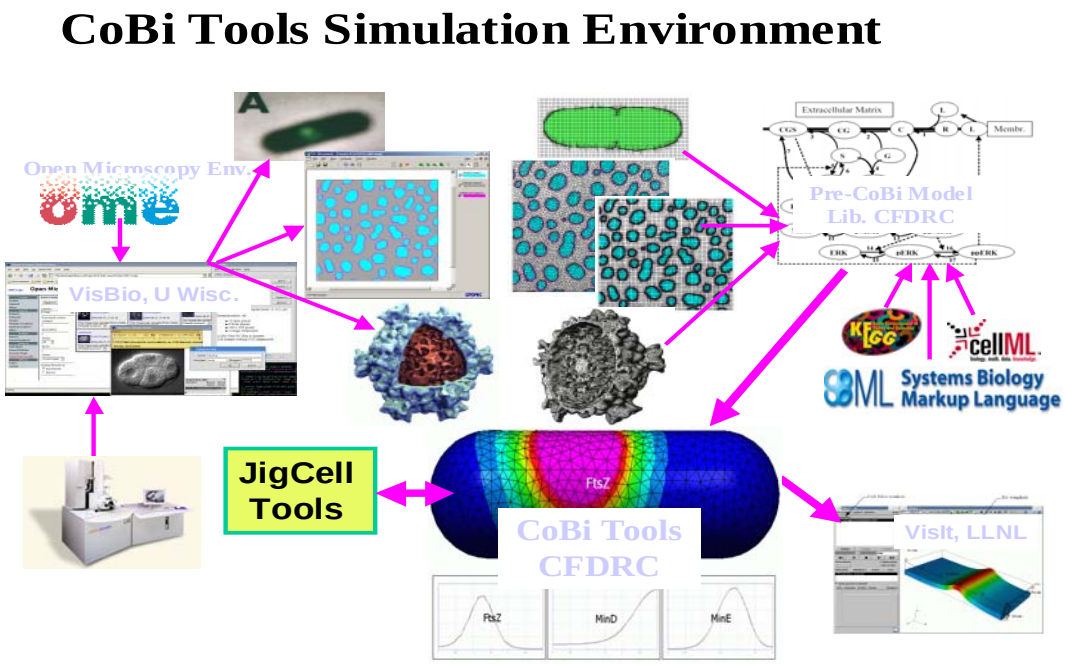


*Figure 4.1: Cell biology simulation environment and the CoBi modeling toolkit.*

### 4.1.3 *Visualization with VisIt Tools*

VisIt is a **free** (http://www.llnl.gov/visit/about.html) interactive parallel visualization and graphical analysis tool for viewing scientific data on UNIX and PC platforms. VisIt was developed by the Lawrence Livermore National Laboratory (LLNL), Department of Energy (DOE) Advanced Simulation and Computing Initiative (ASCI) to visualize and analyze the results of terascale simulations. Users can quickly generate visualizations from their data, animate them through time, manipulate them, and save the resulting images for presentations. It can be used to visualize scalar and vector fields defined on two- and three-dimensional (2D and 3D) structured and unstructured meshes. VisIt was designed to handle very large data set sizes in the terascale range and yet can also handle small data sets in the kilobyte range.

VisIt development at LLNL began in the summer of 2000, and the initial version of VisIt was released in the fall of 2002. VisIt supports C++, Python and Java interfaces. The C++ and Java interfaces make it possible to provide alternate user interfaces for VisIt or allow existing C++ or Java applications to add visualization support. This feature will allow CFDRC to adapt VisIT as a Cell Biology Visualizer. Figure 4.2 presents an example GUI window from the VisIT package.

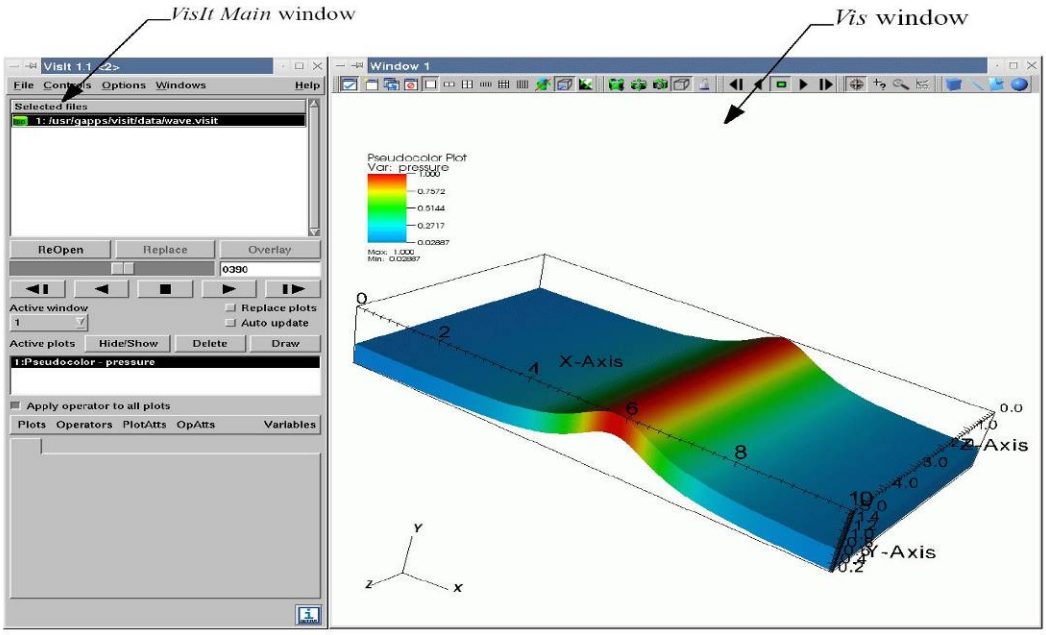


*Figure 4.2: GUI Window of the VisIT visualization toolkit used for modeling cell biology in CoBi.*

## 4.2 CoBi Solver Structure

The CoBi solver is written in model object oriented C++ software compiled on Linux and Windows. It is written in the form to enable future addition of new modules for physics and biology disciplines such as electrokinetics for neuronal cells, stress/deformation for modeling cell biomechanics, and other modules. The CoBi code consists of the following modules:

- In-core database with all variables, properties, mesh, solution
- I/O routines to input files, to mesh, and to visualization tools
- Main driver
- Mesh and geometry initialization module
- Physical data initialization
- Mesh movement module
- Flux calculation module (diffusive, advective)
- Flow module
- Reaction diffusion module
- Thermal module
- Simple chemical kinetics source terms evaluation module (including linearization)
- Matrix assembly

- Linear equation solvers

CoBi software framework consists of

- JCoBi a preprocessor graphical user's interface (GUI) for interactive setup of problem biophysics, boundary and volume conditionings setup, specification of material properties and solution control parameters. An interface to biochemical pathway tools such as JDesigner is enabled via the SBML interface,
- CoBi solver, the main computational engine solving all the equations, and
- VisIt – a graphical post processing for 3D results visualization and animation.

At present, the geometry modeling and grid generation module has limited capabilities. JCoBi can setup 2D and 3D geometries for typical cell shapes such as sphere, ellipsoid, box, etc. However, the code allows the user to import an externally generated grid file with annotated boundary and volume conditions. One potential approach to generate 2D cell biology meshes is to use the CFDRC Micromesh tool. The next section describes this approach.

JCoBI is written in Java while the CoBi solver is written in the C++ language. CoBi tools can be used on computers with either Windows or Linux operation systems.

Figure 4.3 shows the organizational structure of CoBi modeling framework.

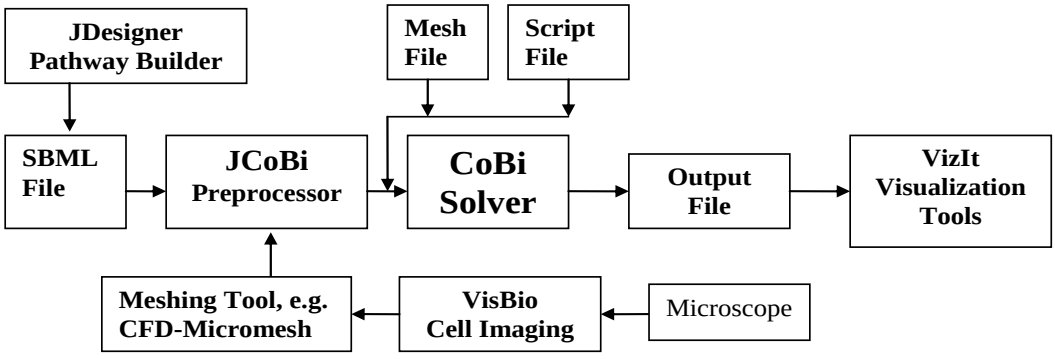


*Figure 4.3: Schematics of CoBi Program Structure.*

## 4.3 Automated Geometry and Meshing of Evolving Biological Cells

During this project, CFDRC has adapted the CFD-Micromesh software tool for the application in automated image processing, geometry construction, and mesh generation for 2D and quasi 3D simulation of cellular biophysics and biochemistry. Figure 4.4 presents example results in terms of original image, unstructured triangular mesh, adaptive binary tree mesh, and multi block structure mesh for the *Bacillus Subtilis* cell during germination process. Note the cell membrane capturing capability and formation of septum.

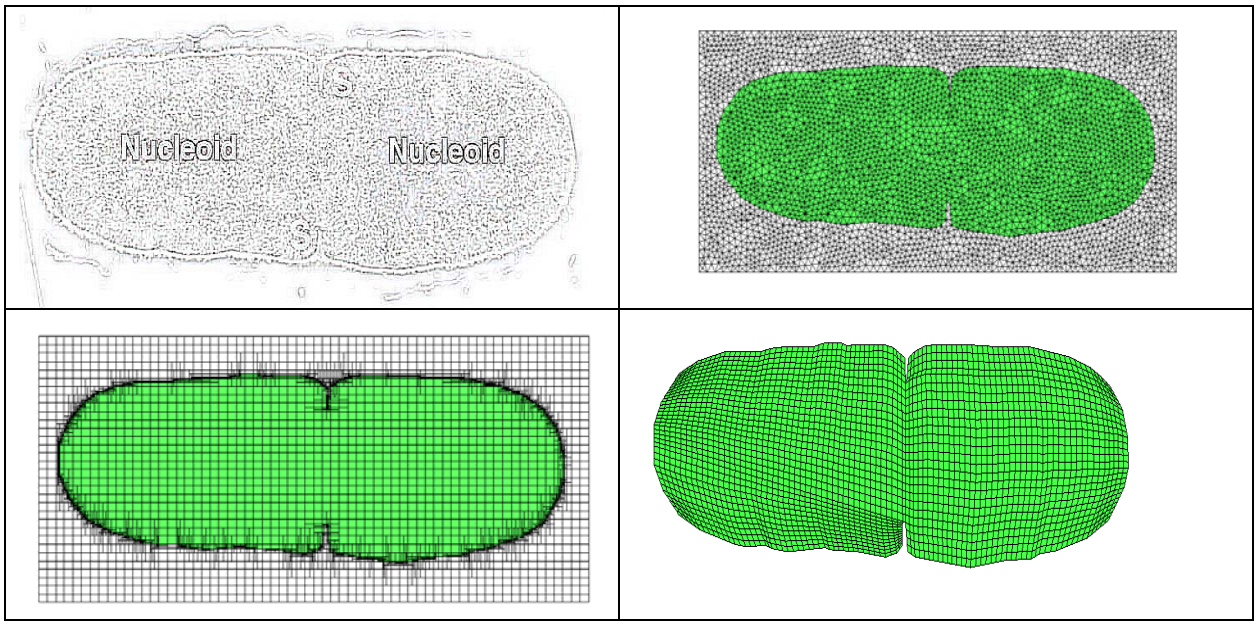


*Figure 4.4*: *Bacillus Subtilis during germination cell cycle division. Image and mesh examples obtained with CFD-Micromesh.*

## 4.4 Preprocessing and Geometry/Mesh Generation

At present, the geometrical model preprocessing is achieved by either using JCoBi for pre set parametric geometries of selected cell shapes, or reading an external text file (*.SIM) for the model setup and a DTF file for the computational mesh. In the second case, the mesh has to be generated by other software tools. JCoBi provides simple but complete capability to generate typical geometries representing cell shapes such as a sphere, rod, ellipsoid, cube, and their parametric variations. For block shapes, the user can selected structured mesh while the spherical and rod shape geometers are meshed with an unstructured 3D tetrahedral mesh. The Figure 4.5 presents a Geometry/Mesh Generation window in JCoBi.

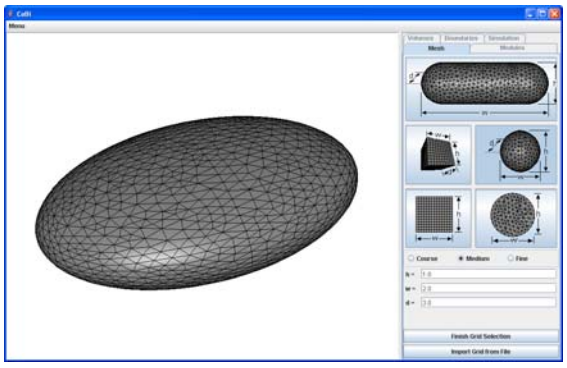

*Figure 4.5: JCoBi GUI Interface for generating 3D cell biology geometry.*

JCoBi provides graphical capability to set boundary and volume conditions. An imported mesh should have name tags attached to boundary condition mesh patches and volume conditions name tags to specific volumes. By “clicking” a boundary condition name tag in the GUI

window JCoBI will highlight that boundary and user can set the boundary condition values. Similar capability is available for setting volume condition values such as material properties and for activation of physical models. Figure 4.6 presents a JCoBi GUI snapshot from a window for setting boundary and volume conditions.

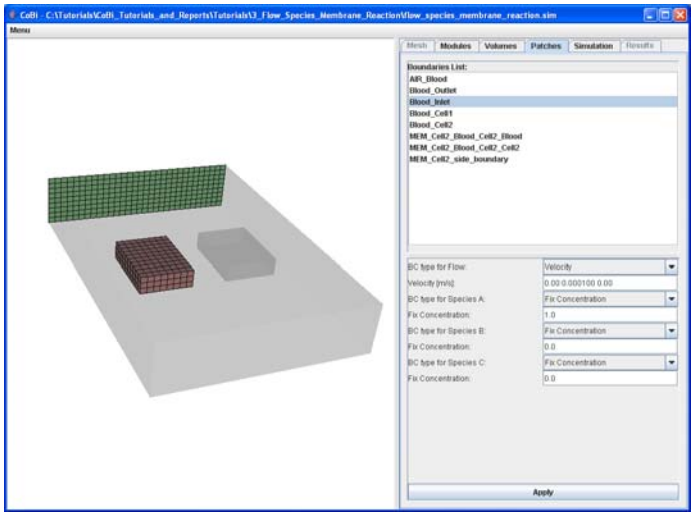


*Figure 4.6*: *JCoBi GUI window for setting boundary and volume conditions.*

To simulate a cell biology problem with CoBi the user needs to setup a "simulation file" containing information about mesh, boundary conditions, material properties, numerical solution controls, etc. The model setup file (filename.SIM) may be generated manually through a text editor, or generated through the newly developed JCoBi GUI module, for a user friendly graphical problem setup. Also from the GUI, the simulation may be run and monitored for convergence as described in the next section.

## 4.5 Post-processing

The computational results obtained with CoBi can be stored in two formats:
- DTF developed by CFDRC and freely available form CFDRC web site, and
- VTK an open source database format used for imaging.

For advanced 3D visualization and animation of simulation results we recommend using VisIt tools for the visualization of computational results. For more details see Section 4.1.3.

For the preliminary analysis of simulation results the user can use JCoBi tools. JCoBi provides capabilities to see 3D surfaces with color mapped solution variables e.g. specie concentration or temperature. During the execution of a CoBi "job" the user can monitor the progress of the job using the JCoBi line plotting capability. It allows the user to display (plot) the convergence characteristics and values of dependent variables at a monitoring point. Figure 4.7 presents example JCoBi windows with a 3D surface mapping of a specie concentration of bacterial rod geometry and an x-y plot of a time course of a dependent variable (specie concentration) at a monitoring point. The detailed capability of the JCoBi tool can be found in the CoBi User's Manual.

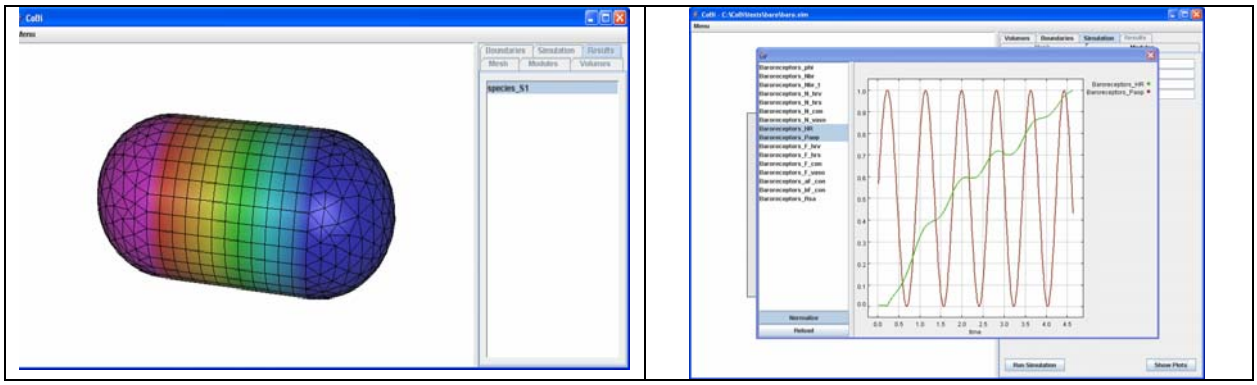

*Figure 4.7*: *JCoBi GUI interface for 3D graphical post processing of a species concentration of a bacterial surface and an x-y plot of a time course of a dependent variable (specie concentration) at a monitoring point.*

## 4.6 Example Problems Setup in JCoBi and Execution in CoBi

This section presents a brief description of the simulation process in the CoBi framework. An example problem of a three dimensional simulation of blood flow through a channel with two square cells located in the flow field, forcing flow around the two cells is demonstrated.

GEOMETRY: A three dimensional geometry and grid is generated for the simulation. After importing the mesh into JCoBi the user can setup the associated volume and boundary conditions as shown in Figure 4.8.

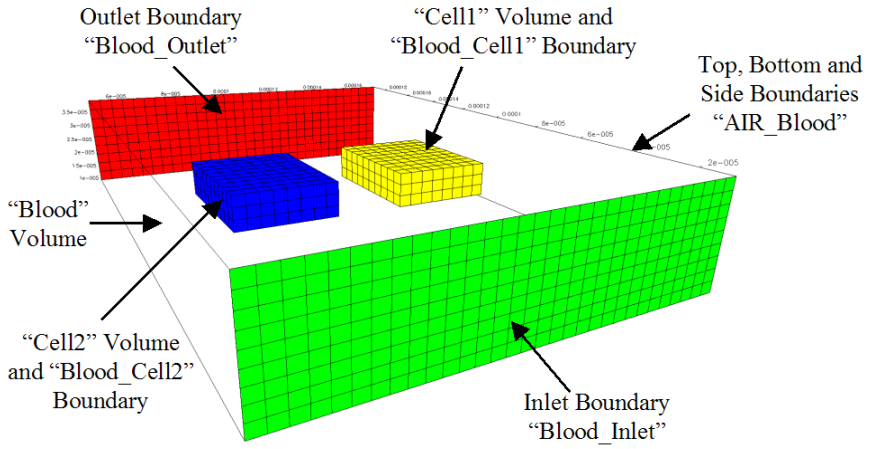


*Figure 4.8*: *JCoBi GUI interface for setting boundary and volume conditions.*

PROBLEM SETUP:

JCoBi, the graphical user interface for CoBi, may be used to setup the simulation. The main window upon opening the JCoBi is shown in Figure 4.9. If a simulation file (*.SIM) already exists, it may be opened through the "Menu" pull-down menu, or a new problem may be setup and saved.

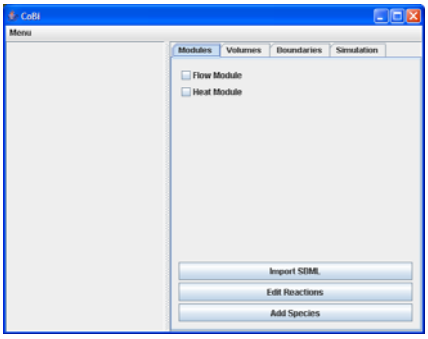


*Figure 4.9*: Main *JCoBi window.*

Flow Setup:

Under the "Modules" tab (Figure 4.10), activate the flow module by checking the box next to the "Flow Module".

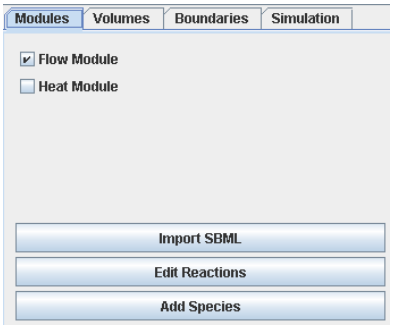


*Figure 4.10*: *Module selection.*

Volume Conditions:

The volumes presented in the simulation are listed under the "Volumes" tab (Figure 4.11). By selecting each volume in the list, the necessary settings may be entered for each volume. After completing the settings for each volume, click the "Apply" button to accept the settings. The following table summarizes the required settings for this simulation, and the image illustrates the settings for one of the volumes. Note that since there is to be no flow in the two cells, a viscosity value of zero is applied to these volumes.

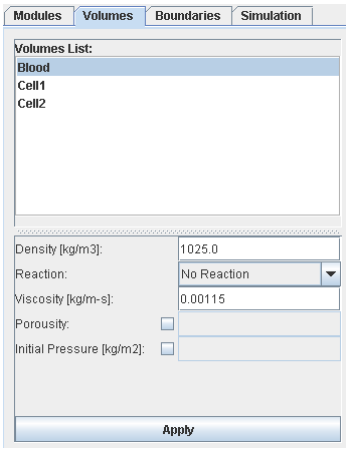


*Figure 4.11*: *Volume selection.*

*Table 4.1: Volume conditions.*

| Volume | Density | Reaction | Viscosity |
|---|---|---|---|
| Blood | 1025.0 | None | 0.00115 |
| Cell1 | 1125.0 | None | 0 |
| Cell2 | 1125.0 | None | 0 |

Boundary Conditions:

The boundary conditions presented in the simulation are listed under the "Boundaries" tab (Figure 4.12). By selecting each boundary in the list, the necessary settings may be entered for each boundary. After completing the settings for each boundary, click the "Apply" button to accept the settings. The following table summarizes the required settings for this simulation, and the image illustrates the settings for one of the boundaries. Note that for boundaries where there is to be no flow, velocity values of zero are used (u, v, w velocity components are required).

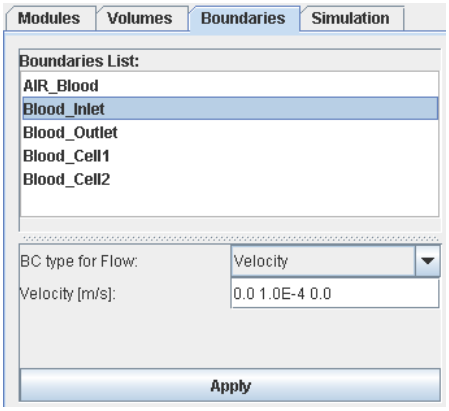


*Figure 4.12*: *Boundary selection.*

*Table 4.2: Boundary conditions.*

| Boundary | BC Type for Flow | Value |
|---|---|---|
| AIR_Blood | Velocity | 0 0 0 |
| Blood_Inlet | Velocity | 0 1.0E-4 0 |
| Blood_Outlet | Pressure | 0 |
| Blood_Cell1 | Velocity | 0 0 0 |
| Blood_Cell2 | Velocity | 0 0 0 |

Simulation Settings:

The simulation control settings can be set under the "Simulation" tab (Figure 4.13). The simulation control settings for this simulation are illustrated below. By default, DTF output files will be generated unless VTK output files are selected.

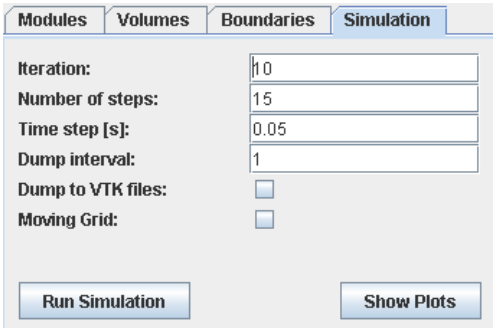


*Figure 4.13: Simulation control settings.*

Run Simulation:
Before running the simulation, save the simulation under the pull-down “Menu” button in JCoBi. Once the file is saved, click the “Run Simulation” button under the “Simulation” tab in JCoBi. Convergence of the simulation may be monitored by clicking the “Show Plots” button.

RESULTS:
The simulation results generated by CoBi are stored in either DTF or VTK format. The user can import them to any graphical post processing tools such as VisIt. Figure 4.14 presents example flow distribution from this demonstration simulation.

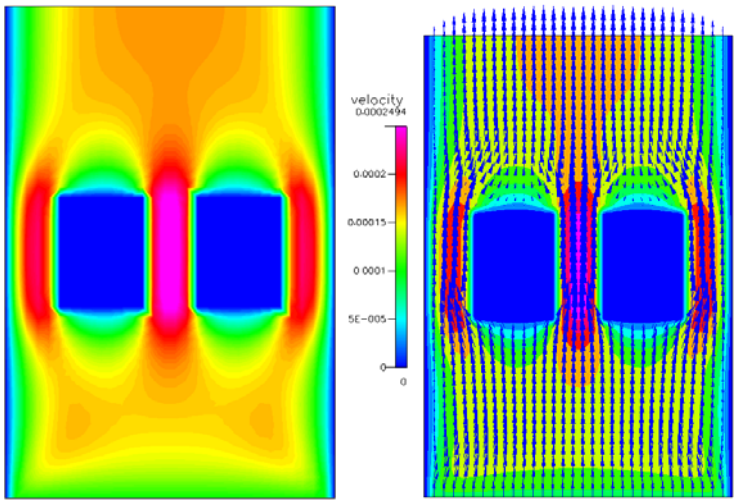


*Figure 4.14: CoBi Simulation results displayed in an independent graphics visualization tool such as VisIT.*

## 5.0 RESULTS OF CELL/TISSUE BIOLOGY SIMULATIONS WITH CoBi

In CFDRC's previous BioCOMP Program, a subcontract project with LBL, CFDRC has developed stand alone software for spatio-temporal modeling of biological membranes. A 3D cell biology Membrane Model has been developed and delivered in source form to LBL and SRI. Summary of that project and example simulation results are presented in the Appendix A to this report. In this project the Membrane Model has been used as the starting point for the development of the CoBi code. This section presents results obtained with the CoBi code for biological cell problems ranging from 2D and 3D membrane transport, to compartmental and spatiotemporal model of cellular signaling, to 3D tissue biology including perfusion and metabolism.

All the test cases presented in this section have been obtained with the CoBi code. The input data, in the form of *.SIM text files, used to run these cases along with technical comments and explanations are provided in Appendix B to this report. For an illustrative purpose, the input data for the first test case, membrane diffusion problem, is provided chapter 5.1.

After completed simulations, CoBi creates an output file for visualization of the solution results. The output file is created in the **vtk** format (www.**vtk**.org/pdf/file-**format**s.pdf ). The vtk file can be viewed using **VisIt** visualization tools developed by the Lawrence Livermore National Laboratory (www.llnl.gov/**visit**/), or other visualization software.

### 5.1 Diffusion on a Planar Membrane

***Diffusion Problem on Planar Square Thin Film*** -
Several 1D, 2D, and 3D species diffusion problems have been tested in CoBi to test code accuracy, robustness, and consistency. For example 1D problems have been setup as 2D or 3D to test solution uniformity, or comparison between 2D/3D structured grid and unstructured grid results have been made to check code mesh independence. A simple one dimensional specie diffusion problem was chosen to validate the accuracy of CoBi membrane model. The geometry, grid, and problem definition are shown in the Figure 5.1. It is a square box with unit length and its thickness is set to .01 and the mesh is an unstructured triangular grid. The exact solution to this problem is a linear distribution of specie concentration from zero to one in the horizontal direction. As expected and shown in Figure 5.1 CoBi membrane model gives an exact solution in this case. Exactly the same results were obtained with the structured mesh.

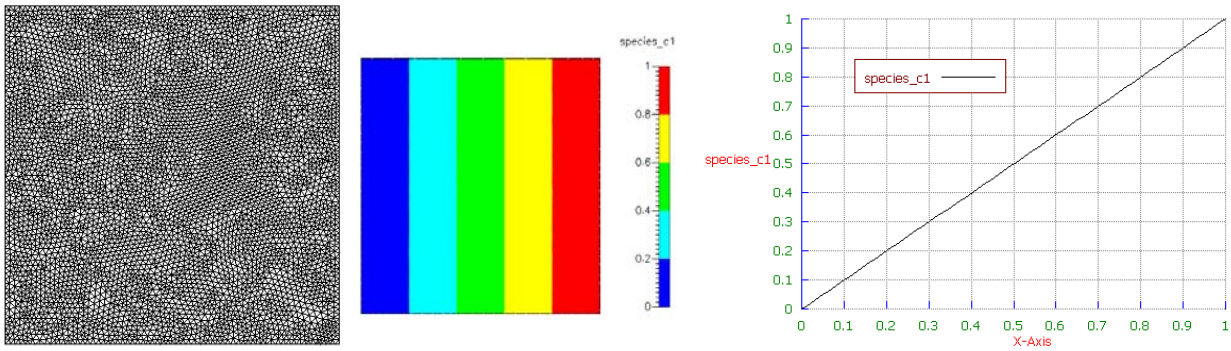


**Geometry/Mesh** **Species Distribution** **Species as spatial function**

*Figure 5.1: Computational results for a specie diffusion problem on planar square membrane.*

*Input File*

Two text based input files are needed to run the model:
- Membrane2D.MFG and,
- Membrane2D.SIM.

The MFG is a mixed element format used by CFDRC. It contains grid, volume condition, and boundary condition information. The detailed description of the format is available from CFDRC. The *.SIM file is an input text file created by the user. It can be created by any test editor (including Microsoft Word) and contains information about control parameters, values of volume conditions and boundary conditions. The line numbers, 01, 02, … (shown below) not needed in the *.SIM file read by CoBi. Here they are used to explain individual commands of the *.SIM file. The *.SIM file for this problem is as follows:

```
01      thickness 0.01
02      iteration 10

03      module share
04        vc Membrane const_dens 1

05      module species f1
06        sweeps 500
07        relaxation 0.1
08        vc Membrane const_diff 0.1
09        bc Left fix_value 0.0
10        bc Right fix_value 1.0
11        bc Top fix_flux 0.0
12        bc Bottom fix_flux 0.0
13        bc Membrane_outside fix_flux 0
14        bc Membrane_inside fix_flux 0
```

In the input file keyword *thickness* is the membrane thickness. Keyword *iteration* is the number of iterations for the steady state case or each time step. Keyword *module* is used to specify input data for the module. Keyword *share* means that input for shared data, such as density.

Keyword *vc* is used to specify a volume condition followed by a volume name, constant density, and the value. Keyword *species* is used for input of species module. Keyword *sweeps* is used to specify the maximum number of sweeps for the species. Keyword *relaxation* is used to input linear relaxation between a previous value and a new value. The next line *vc* sets the constant diffusivity for volume Membrane. Keyword *bc* means the input for boundary condition followed by boundary name, boundary condition type (fixed value/fixed flux).

Line 01 sets membrane thickness to 0.01;
Line 02 sets number of sub-iteration to 10;
Line 03 declares the start of share module;
Line 04 sets density to 1 for membrane;
Line 05 declares the start of species f1 equation;
Line 06 sets number of iterations for linear equation solver;
Line 07 sets relaxation factor for f1 to 0.1;
Line 08 sets the volume condition (vc) of species diffusivity to 0.1 for membrane;
Line 09-10 set fix concentration 0 on the Left and 1on the Right Boundaries;
Line 11-12 set zero gradient concentration on bottom/bottom surfaces;
Line 13-14 set no flux boundary condition to membrane inside/outside surfaces;

**Output File**
For visualization, the solution is output to files in the **vtk** format.

## 5.2 Diffusion on a Spherical Cell Membrane

This test problem is designed to validate and demonstrate the capability of the CoBi membrane model to simulate the diffusion of a species constrained on a curved surface. It is a challenging problem of solving 3D convection-diffusion-reaction transport equation on a general surface 3D mesh. Figure 5.2-a shows the spherical surface unstructured triangulated grid and three-dimensional species concentration distribution. At the boundary conditions we set the concentration of the species equal to 1 on a circular patch on the top of the sphere, while the concentration at the bottom circular patch is set to 0. The sphere has a radius of unity and the membrane thickness is 0.01.

The front view of the sphere with species concentration contour map is shown Figure 5.2-b. One can see that the species has high concentration gradient near the top and bottom regions due to smaller diffusion areas. The contour lines are straight, which means the numerical method preserves top-bottom symmetry and horizontal uniformity while the mesh is unsymmetrical.
The annotated CoBi input file for this test case is provided in Appendix B.

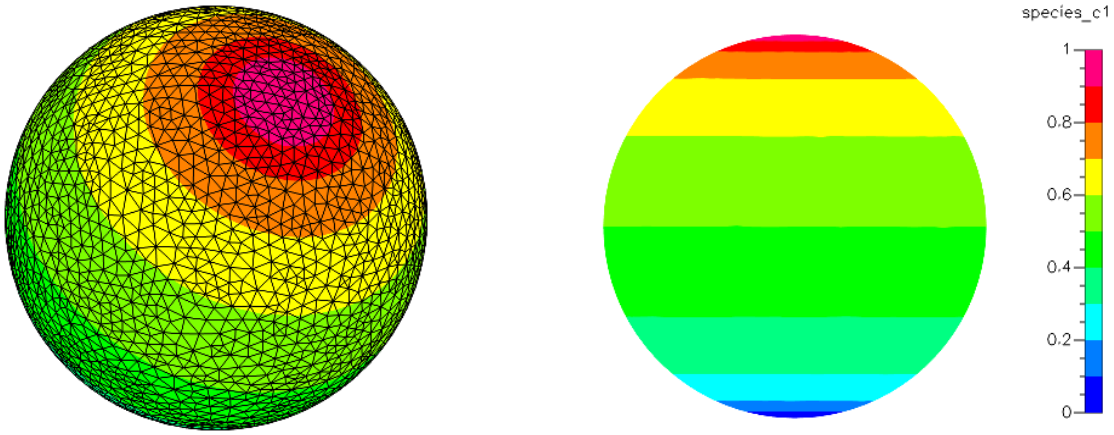


**a. Geometry and Grid** **b. Species Distribution**

*Figure 5.2: CoBi membrane model for specie diffusion on a thin spherical surface.*

## 5.3 Diffusion-Reaction of a Flat Membrane

This test case is designed to test the transient interaction between diffusion and chemical reaction between two species on a 2D surface. The geometry of this case is the same as test case 1 presented in section 5.1 above. An unstructured mesh has been used. Two species, A and B, are solved in transient mode with a simple one step chemical reaction as follows:

$$A + B \Rightarrow 2B + B$$

Both A and B species concentrations are initialized to zero on the surface (in this case volume condition). Specie A =1 is set on the right side boundary and B =1 is set on left side boundary and zero on the opposite sides respectively. Figure 5.3a shows time color contour map of specie A at a t=0.6s. Figure 5.3b shows a sequence of profiles of species concentration distributions along the x coordinate at t= 0.5s to t=1s. Note that until t=0.7s both species interdiffuse and there is little reaction (production of specie B). At t=1s specie B, being produced from A, dominates. The results match our expected trends. The annotated CoBi input file for this test case is provided in Appendix B.

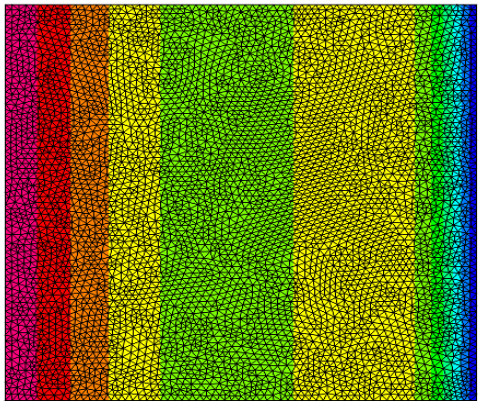

*Figure 5.3A*: *Color contour map of specie A.*

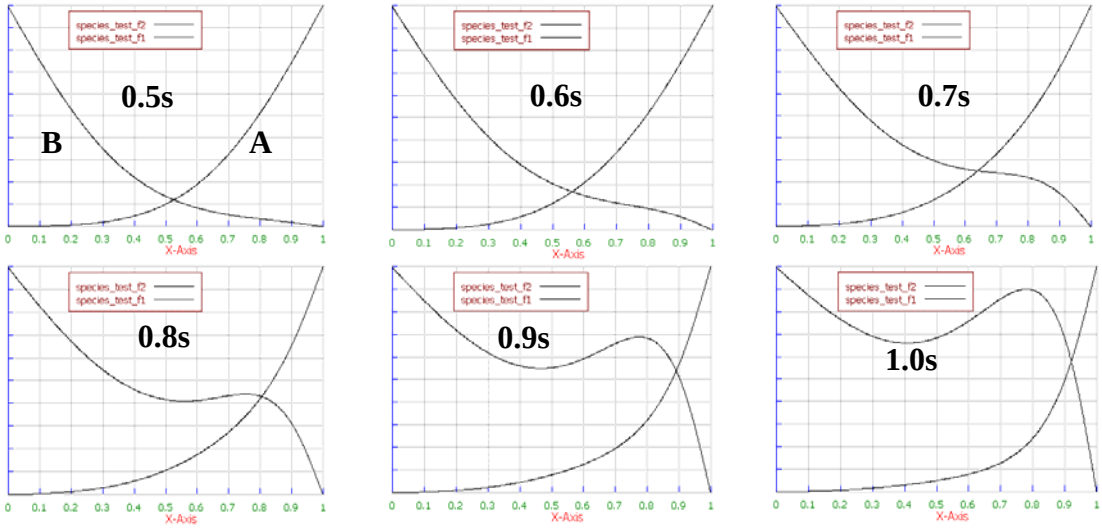


*Figure 5.3B: Species A and B concentration distributions as a function of time.*

## 5.4 Diffusion-Reaction on a Bacterial Membrane

We use this case to demonstrate the membrane model on a surface diffusion-reaction problem on the geometry typical to the *Bacillus* type of bacteria. As discussed in Section 4.4 above the JCoBi software can generate parametric geometric shape of a *Bacillus* type, cigar-like shape, of a bacterial membrane. The unstructured surface triangular mesh is also automatically generated in JCoBi by simple geometrical scaling based on user specified geometrical parameters of the bacterium (length and radius).

This test case is setup as a 3D unsteady diffusion-reaction problem for two species, A and B, solved on the bacterial surface shown in Figure 5.4. The boundary conditions and the reaction mechanism are similar to the test case presented in Section 5.3 above. A simple one step chemical reaction as follows:

$$A + B \Rightarrow 2B + B$$

Note that the Specie B is both a catalyst for specie A and a final product of the reaction.

On the left side of the bacterium the concentration of the species B is set to one while the species A is set to one on the right side. The concentrations for both species A and B on the whole membrane are initialized to zero. The geometry, grid and the concentration of specie B on the bacterial surface at time .9 sec. is shown in Figure 5.4. The contours of species B on the bacterium membrane as a function of time are plotted in Figure 5.5. As before the computational results match our expected trends.

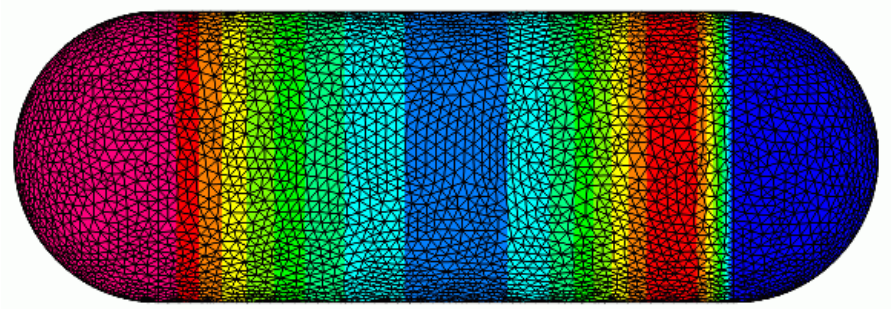

*Figure 5.4: Geometry of a typical cigar-like shape of a bacterial membrane and the concentration profile of specie B at t=0.9 sec .*

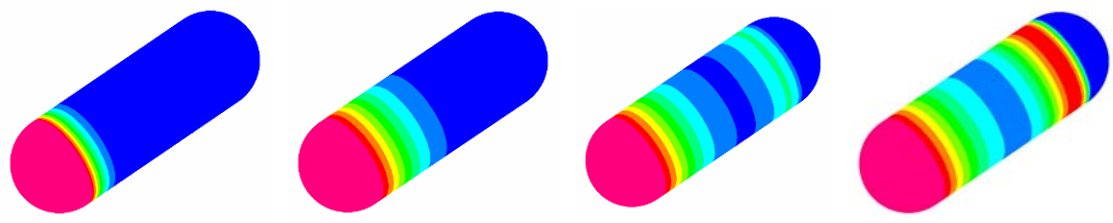


*Figure 5.5: Transient distributions of specie B concentration.*

## 5.5 EGFR Signal Transduction Pathway

The epidermal growth factor receptor (EGFR) has been found to be altered in a variety of human cancers. A number of agents targeting these receptors are currently in clinical trials or are already approved for clinical treatment [Personal communication with Dr Lance Liotta and Dr Gabriela Araujo of FDA-NCI Clinical Proteomics Program, Laboratory of Pathology, Center for Cancer Research, NCI/NIH, also Araujo et all 2005]. It is generally accepted that better understanding of EGFR signaling pathways will be very helpful in cancer diagnostics, designing genetic screening, co-targeting additional proteins upstream/downstream of EGFR to improve cancer therapy, and to optimize caner treatment.

EGFR signaling pathways have been recently computationally analyzed by several investigators [Araujo 2005]. We use this test case to validate CoBi against benchmark results of Araujo 2005 and to compare our results to similar calculations performed with J-Designer software available at CDRC. J-Designer is a biochemistry simulation software developed under DARPA BioCOMP Program http://sbw.kgi.edu/software/jdesigner.htm

CoBi has been used to reproduce the modeling results for the time dependent concentrations of several species (RP, RGS, RShGS, and RPLP) involved in the EGFR signal transduction cascade reported by Araujo et al. 2005 (Figure 5.6). Unlike other tools, CoBi can be used for detailed analysis of EGFR signaling pathway combined with transient flow/diffusion models and spatial models of signal transduction in tissues.

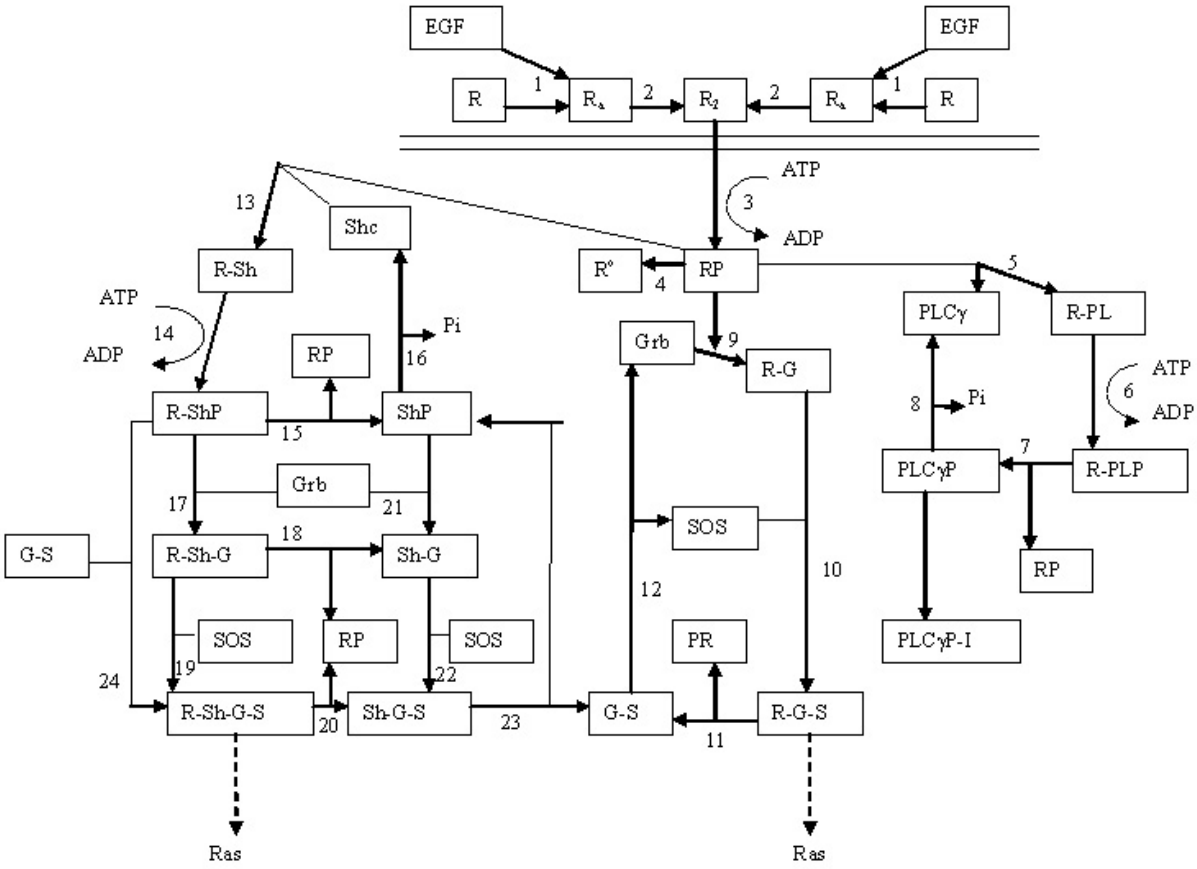


*Figure 5.6: Diagram of EGFR signal transduction pathway.*

The EGFR signaling pathway simulations, reported by Araujo et al. 2005, were repeated at CFDRC using both JDesigner and CoBi codes and results of time variations of several species concentrations including RP, RGS, RShGS, and RPLP were compared. Both JDesigner and CoBi simulations reproduced the results reported by Araujo [2005] very well. Similar computational times for CoBi and JDesigner have been observed. The simulation results of all three methods for species PRLP are shown in Figure 5.7.

| | |
|---|---|
| **A-**<br>**Araujo et al. 2005** | 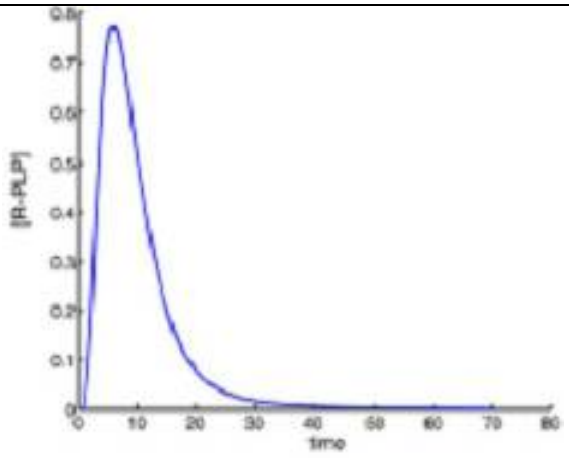 |
| **B-**<br>**FDRC Simulation Results Using J-Designer Software** | 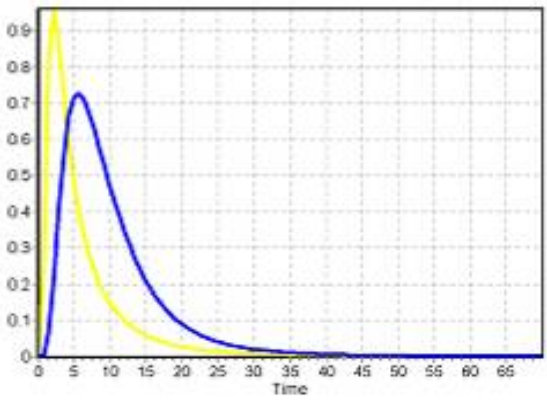 |
| **C-**<br>**CFDRC Simulations Using CoBi Software** | 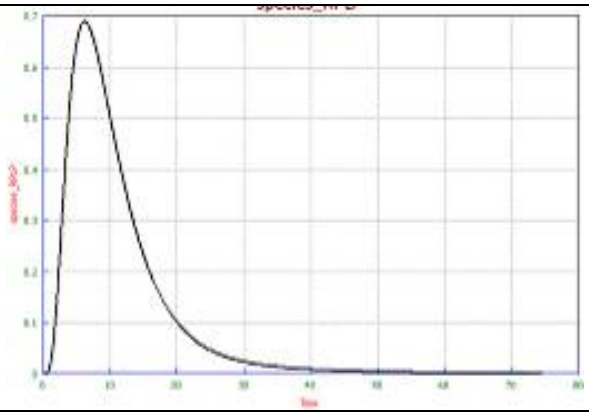 |

*Figure 5.7: Time course for specie PRLP during the EGFR signaling pathway simulations - A. Araujo et al.[2005];B. Using J Designer; C. Using CoBi.*

## 5.6 Multicellular Perfused Tissue EGF Signaling

In this case we demonstrate 3D modeling of species transport in the multicellular tissue with specific models of convection, diffusion, and reaction in perfused inter-cellular space (extracellular matrix), membrane, and intracellular space (cytosol). 3D time dependent partial differential equations (PDEs) were solved for all species within the intracellular space of the cytosol, in extracellular matrix (ECM) and on the cell membrane surface. The species conservation is expressed in the form:

$$\frac{\partial(C)}{\partial t} + \mathrm{u} \cdot \nabla \mathrm{C} - D\nabla^2 C = R \tag{5.1}$$

Where C is the drug concentration, u is the convective velocity, D is the drug diffusivity (can be anisotropic based on the cellular morphology and different in ECM, cytosol and on the membrane), R is the generalized reaction rate for specie C as shown in the reaction rate expressions table below. The reaction kinetics is similar to Lauffenburger EGFR model of endocytosis, Lauffenburher 1999, Maly 2004, 2004, and Wiley 2003. The cell-level model simulates the time-progression of following species:

- Extracellular ligand concentration *L*,
- Surface receptors *Rs and ligand-receptor* complexes *Cs*,
- Intracellular ligand *Li*, receptors *Ri*, and their complexes *Ci*, and
- Degraded ligands *Ld*

We use this kinetic model to simulate ligand depletion and endosomal sorting after an initial bolus of ligand into the extracellular medium. Figure 5.8 presents the schematics of the cellular endocytosis and receptor recovery process and the signaling pathway used for this model, Sarkar 2003. Figure 5.9 presents the kinetic and rate equations for EGF signaling model used in our simulations. In most of the previous simulations the process was modeled as a well stirred reactor model. In this project we simulate the problem in a 3D model of the perfused tissue.

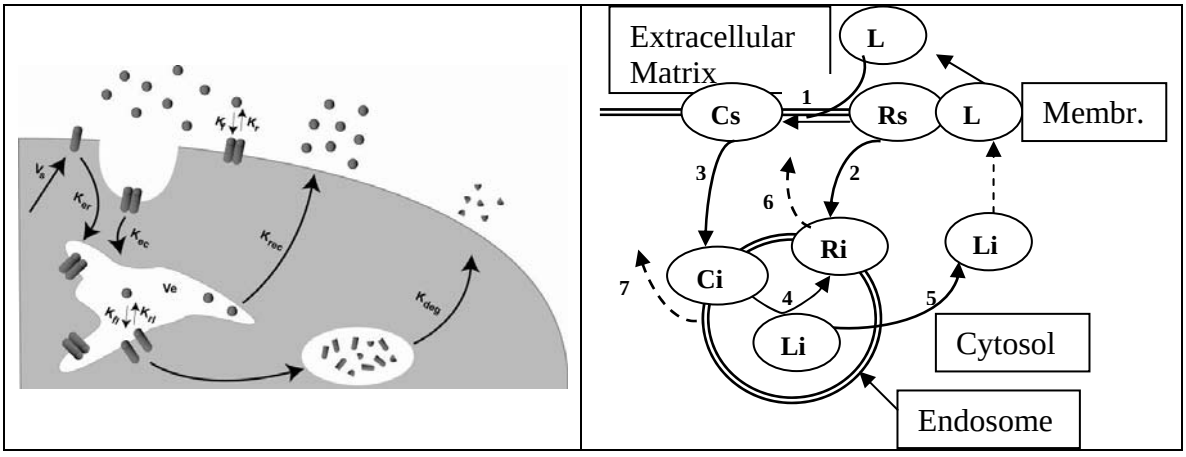


*Figure 5.8: Endocytic Trafficking – Multi cellular tissue model implemented in CoBi.*

| **Kinetic Equations** | | | **Rate Equations** |
|---|---|---|---|
| Extracellular Ligand | L | $\partial_t L = -v_1 + v_5$ | $v_1 = k_1 L \cdot R_s - k_{-1} C_s$ |
| Surface Receptor | $R_s$ | | $v_2 = k_2 R_s$ |
| $\partial_t R_s = -v_1 - v_2 + v_8$ | | | $v_3 = k_3 C_s$ |
| Surface Complex | $C_s$ | $\partial_t C_s = v_1 - v_3$ | $v_4 = k_4 L_i \cdot R_i - k_{-4} C_i$ |
| Intracellular Ligand | $L_i$ | | $v_5 = k_5 L_i$ |
| $\partial_t L_i = -v_4 - v_5$ | | | $v_6 = k_6 R_i$ |
| Intracellular Receptor | $R_i$ | | $v_7 = k_7 C_i$ |
| $\partial_t R_i = v_2 - v_4 - v_6$ | | | $v_8 = \dot{V}$ |
| Intracellular Complex | $C_i$ | | |
| $\partial_t C_i = v_3 + v_4 - v_7$ | | | |

*Figure 5.9: Kinetic and rate equations for EGF signaling model.*

The 3D tissue geometry was generated based on microscopy image of the cellular structure shown in Figure 5.10a below. To generate the computational mesh we have used CFD-Micromesh software developed at CFDRC. CFD-Micromesh imports the gif image of he cellular tissue, and identifies he cell volumes. The remaining part is treated as the interstitial space. A membrane model is specified at the outer boundaries of all cells. Finally an unstructured 3D triangle-based prismatic mesh is generated, Figure 5.10b. Figure 5.10b also presents the color map of drug ligand concentration in the extracellular space. Note that the ligand does not enter the intracellular space.

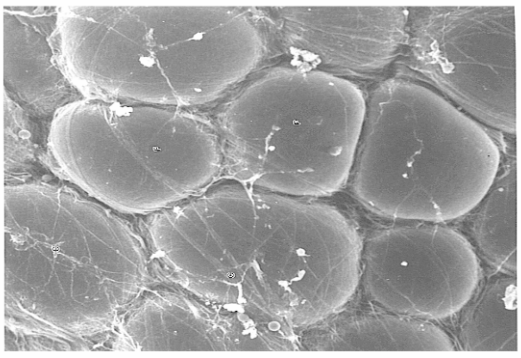

**a) Microscopy Image of Multicellular Tissue**

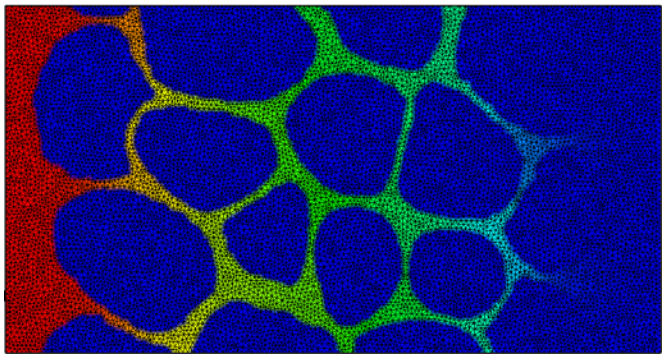

**b) CoBi Computational Mesh with Boundary and Volume Conditions**

*Figure 5.10: Microscopy image of the tissue, 3D unstructured mesh with CoBi predicted ligand concentration in the intercellular space of the tissue.*

Figure 5.11 presents transient simulation results for two time instances t1 and t2 > t1 for the drug ligand absorption in the perfused tissue. We present results for three species: extracellular ligand, membrane bound complex, and intracellular complex. Note that free ligand exists only in

the extracellular matrix (Fig. 5.11 top), membrane bound complexes Cs appear only on the membrane (Fig. 5.11 middle), and the intracellular complex Ci, is present only in the cytosol (Fig 5.11 bottom). As observed in typical laboratory experiments the intracellular complexes appear after certain time delay we also predict the membrane and intracellular complexes with time delay. Note that Ci is absent at t1 but is present inside the cell cytosol in the proximal cells at t2 > t1.

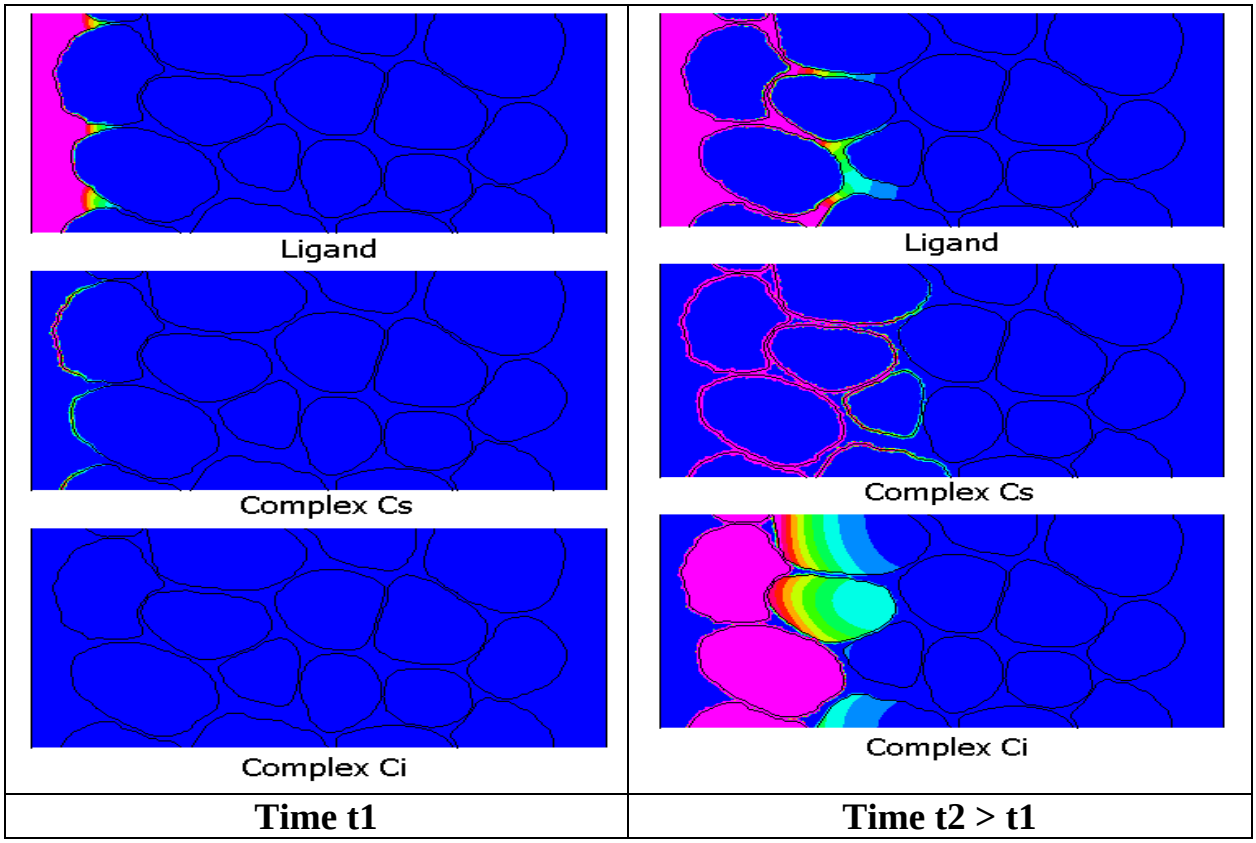


*Figure 5.11: Computational results for modeling EGF signaling and ligand drug delivery to a 3D tissue structure with CoBi.*

## 5.7 Cellular Calcium Oscillations

A published, single cell calcium wave model was used as a test case for CoBi [McKenzie 1998]. This model was selected because calcium waves have been observed in single cells and it is believed that they may play important roles in signal transduction in several human cell types in both physiological and pathological conditions. The results reported for the McKenzie model were reproduced using the CoBi solver.

Figure 5.12 shows a schematic of the McKenzie calcium wave model. The model uses a non-physiological 2-D square cell that is 1 mm on a side. No species are allowed to move into or out of the cell, which comprises a mesh of 40,000 grid cells. Calcium is normally stored in the endoplasmic reticulum (ER) and is released into the cytosol when $IP_3$ (inositol triphosphate) binds to calcium channels in the ER membrane. $IP_3$ is generated at the cytosolic side of the

plasma membrane when certain types of cell surface receptors are activated. This model simulates the activation of receptors by using initial conditions in which 3 separate areas of the membrane have high $IP_3$ concentrations (A, B, and C). This model also assumes that the ER is uniformly distributed within the cell and ignores intracellular compartmentalization.

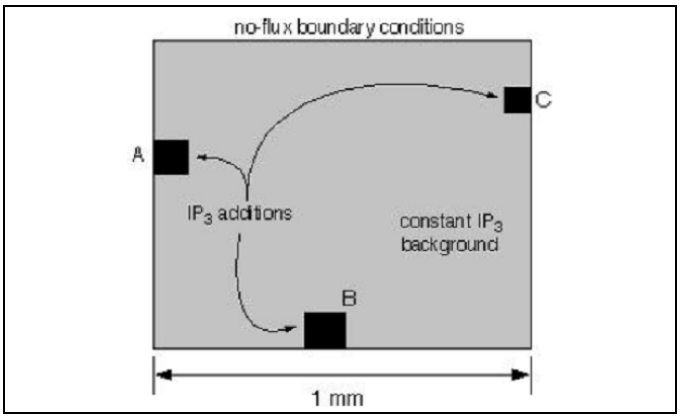


*Figure 5.12: Schematic of cellular calcium wave model.*

Figure 5.13 shows the results for various time points during a calcium wave simulation. These results are in qualitative agreement with the results published for McKenzie 1998 calcium wave model. Quantitative agreement was not possible because the publication did not specify the sizes and locations of A, B, and C in Figure 5.13 and the published figure was not drawn to scale.

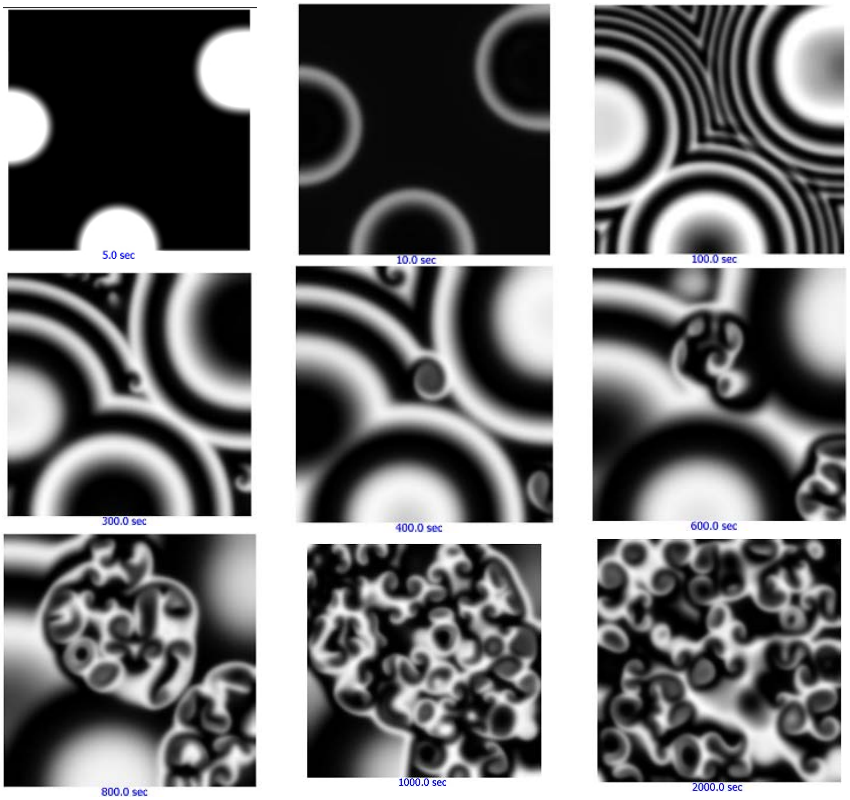


*Figure 5.13: Cellular calcium wave simulation.*

## 5.8 Tissue Calcium Waves

A model of calcium wave propagation between adjacent cells in a tissue was reproduced in CoBi [Sneyd 1998]. This model was selected because it is believed that calcium waves may play an important role in cell-to-cell communication within several organs in humans. Figure 5.14A and Figure 5.14B show schematics of the cell-to-cell calcium wave pathway and geometric mesh for the model. The model mesh includes 49 squares, each representing a biological cell, including the plasma membrane. Each cell square contains a mesh of 16*16 smaller squares that is used to model reactions and species transport within each cell. Figure 5.14C shows a representative result of the CoBi simulation.

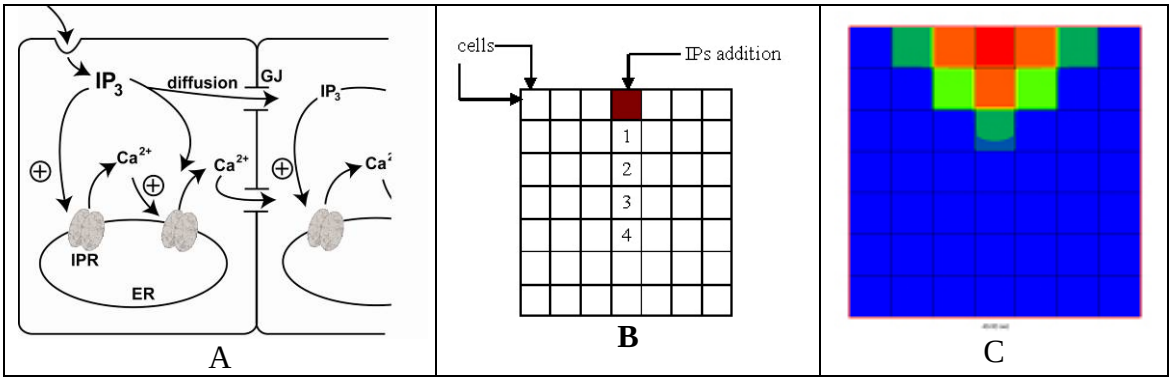


*Figure 5.14: Tissue calcium wave model - A. Schematic of pathway (Sneyd 1998) B. Model schematic (Sneyd 1998) and C. Calcium concentrations during CoBi simulation.*

The results reported for the Sneyd model were reproduced with CoBi except that the fluctuations in cytosolic calcium ion concentration decayed more rapidly in our simulation and did not decay to baseline levels (Figure 5.15). This result appears to derive from differences in initial conditions and rate constants for calcium ATPases that return calcium into the ER, which were not completely disclosed in the Sneyd 1998 published model. Our results do show the damped oscillatory patterns of calcium ion concentrations reported by Sneyd 1998.

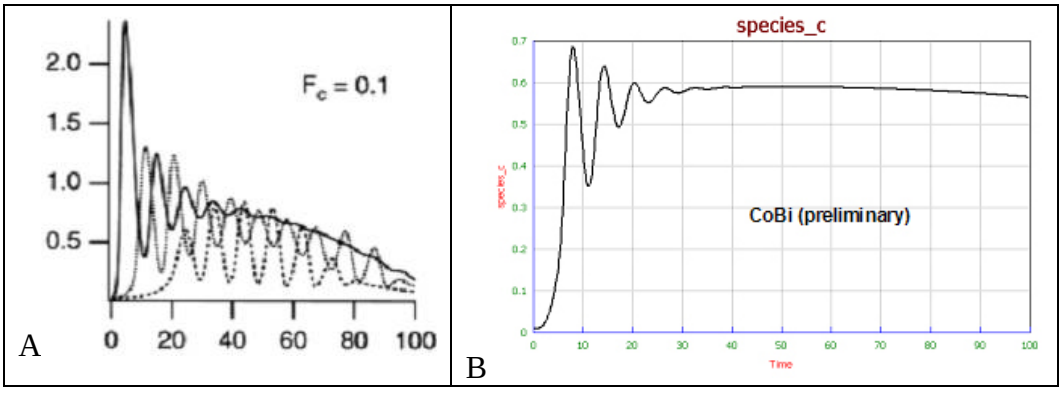


*Figure 5.15: Comparison of published and CoBi simulation results for calcium wave transmission between cells. A. $Ca^{2+}$ concentrations (solid line) from Sneyd and B. CoBi.*

## 5.9 Morphogenesis of Yeast Cell

Actin polymerization networks in yeast cells were simulated in CoBi using a model of fission yeast cell division developed by Dr. John Tyson at Virginia Polytechnic University. The CoBi solver was used to reproduce the time dependent changes in cell morphology for wild type and mutant strains of yeast during cell growth and division. Figure 5.16 shows a schematic of actin network formation and breakdown in yeast cells.

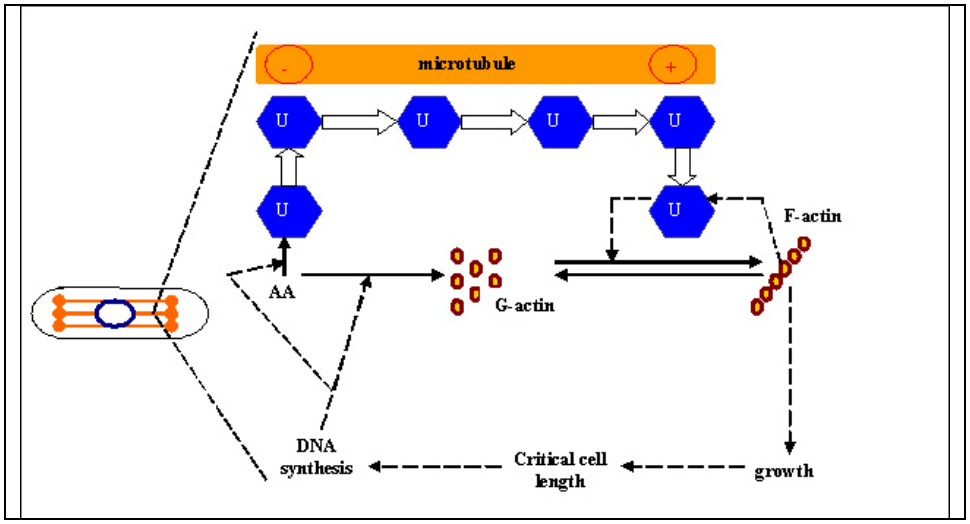


*Figure 5.16: Actin filament network dynamics [Csikasz-Nagy 2005].*

Protein U binds to microtubules and is transported to the ends of the cell where it is released to promote the autocatalytic feedback loop for actin polymerization. The delivery of U to cell ends by microtubules plays an important role in localizing actin polymerization to the ends of the cell. If the microtubules are disrupted, the convection mechanism is stopped and U distributes homogeneously throughout the cell. Figure 5.17 shows the results of a simulation in CoBi that reproduces the bending of a growing yeast cell having a mutation that causes a bent morphology. The input data for this test case is presented in Appendix B to this report.

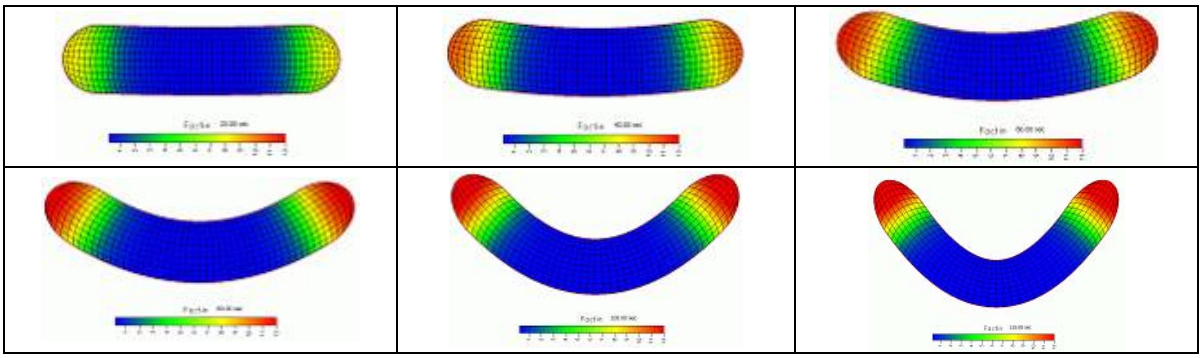

*Figure 5.17: CoBi simulation results for yeast mutants showing F-actin concentrations.*

## 5.10 Cellular Oxygen and Energy Metabolism

### Oxygen Metabolism Model

A cell hypoxia/ischemia simulation has been tested using CoBi for its potential applications in trauma injury modeling for military medicine. A cell metabolic model based on the cardiac myocyte model of Salem *et. al* [Salem, 2002] that includes responses to hypoxic and ischemic conditions was implemented in CoBi. It models the transport of glucose, lactate, fatty acids, oxygen ($O_2$) and carbon dioxide ($CO_2$) between the blood and the cytosolic compartments. ATP is produced from multiple, interdependent pathways including glycolysis, lactate oxidation, the TCA cycle, and oxidative phosphorylation.

The cellular oxygen metabolism model comprises two compartments, blood and tissue, with passive gas diffusion across the compartment boundaries. The diffusive flux, *J*, of oxygen, across the blood-tissue barrier is given by:

$$J_{b\to t,O2} = \lambda_{b\to t,O2}(C_{a,O2} - \sigma_{b\to t,O2}C_{t,O2}) \tag{5.2}$$

where $\lambda_{b\to t}$ is a diffusivity constant and $\sigma_{b\to t}$ is the partition coefficient. In general for $O_2$ and $CO_2$ we set $\sigma_{b\to t} = 1$. For other species such as free fatty acids and other substrates $\sigma_{b\to t} \neq 1$.

The ordinary differential equations evolving $O_2$ concentrations over time in both blood, $C_{b,O2}$, and tissue, $C_{t,O2}$, compartments are then:

$$\frac{dC_{b,O2}}{dt} = \frac{1}{V_b}\left(Q\left(C_{a,O2} - C_{b,O2}\right) - J_{b\to t,O2}\right) \tag{5.2}$$

$$\frac{dC_{t,O2}}{dt} = \frac{1}{V_t}\left(J_{b\to t,O2} - MR_{O2}\right). \tag{5.3}$$

Equations for $CO_2$ have a similar form. Q is the blood flow rate; $C_{a,O2}$ is the arterial or input concentration; $V_b$ and $V_t$ are the relative compartmental volumes in blood and tissue, respectively. In this form, relative volumes are tuning parameters to calibrate the sensitivity of each compartment to perturbations around the steady state. The oxygen consumption rate, $MR_{O2}$, is given by:

$$MR_{O2} = \alpha\left(C_{t,O2}/\left(k_m + C_{t,O2}\right)\right) RMR \tag{5.4}$$

Here, RMR is the relative metabolic rate, so at the basal metabolic rate, $RMR = 1$. The parameters $\alpha$ and $k_m$ are tuning parameters and contain no biological significance. The aim was to introduce an upper bound, $\alpha$; to the turnover rate of oxygen because cellular oxygen turnovers are saturable. After the complete oxidation of one mol of glucose, about 6 mol of $O_2$

and $CO_2$ are consumed and produced, respectively. Therefore, it was decided to set $MR_{O2} \approx MR_{CO2}$ here for simplicity. In the real cell glucose will be accompanied by fatty acids, lactate, phosphocreatine and ketone bodies as sources of energy. Hence we expect this simple model to capture the rough qualitative features $O_2$ and $CO_2$ fluctuations under varying work output (*RMR*) levels.

To calibrate the model all equations were entered into optimization software. The tuning parameters $\alpha$, $k_m$, $\lambda_{b\to t,O2}$ and $\lambda_{b\to t,CO2}$ were solved for by setting $dC_b/dt = 0$ and $dC_t/dt = 0$ for both species at rest (*RMR* = 1). The four concentration initial conditions, Q, $V_b$ and $V_t$ were set by organ-specific experimental data [Zhou, 2005].

The reduced model is able to capture qualitative trends of a normal response (Figure 5.18). In response to a doubling of the relative metabolic rate (RMR), a new steady state is reached in which $CO_2$ output is increased and blood and tissue oxygenation is decreased slightly.

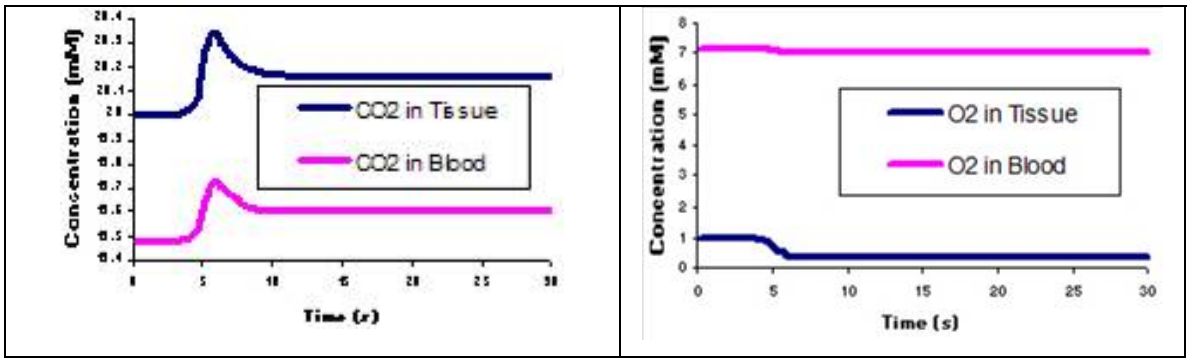


*Figure 5.18: Simple metabolic model response to a doubling of RMR from the rest state.*

**Energy Metabolism Model**

The present model built in CoBi is an adaptation and improvement over a published model for cardiac myocyte metabolism [Salem, 2002]. Cardiac myocytes are muscle cells and constantly require large amounts of energy to contract and pump blood. Our model consists of three separate compartments: blood, cytoplasm and mitochondria. This separation into functionally separate compartments adds flexibility and facilitates integration into the full human model. Communication between the three compartments occurs via passive or active transport depending on the species. The blood carries, oxygen, lactate, fatty acids and glucose to the cell compartment for ATP synthesis to fuel the cell and carries carbon dioxide and other byproducts away from the cell. The energy liberated from the conversion of ATP into ADP and AMP serves a multitude of vital functions in the cell including active transport across membranes and protein synthesis. Here, while some ATP will be used in other parts of the metabolic web (like glycogenesis) the vast majority will be converted into mechanical work for pumping blood against a blood pressure differential.

The metabolic scheme describes 18 key substrates located strategically in the major nodes (end points and branching points) of the full, known metabolic network (Figure 5.19).

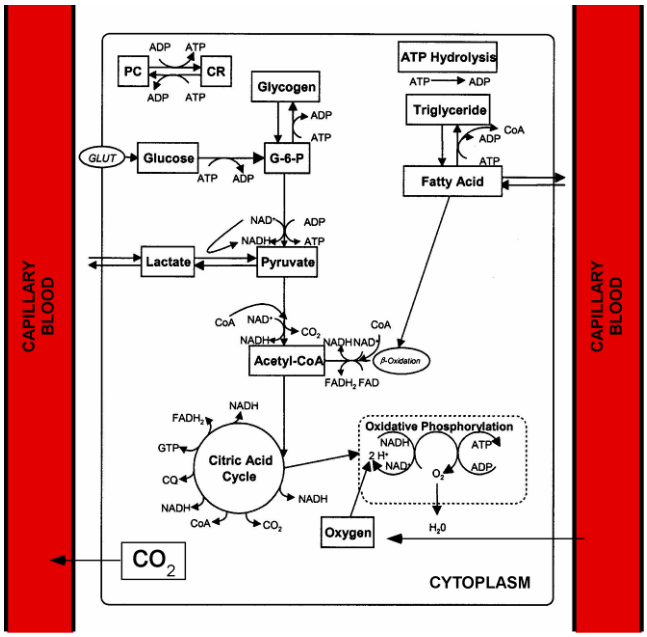


*Figure 5.19: Metabolic network diagram of the model developed at CFDRC (based on model of Salem et. al. 2002).*

The model represents the aerobic and anaerobic catabolism of glycogen, fatty acids and lactate coming from the blood. It also represents storage of energy reserves as phosphocreatine, glycogen and triglycerides. Interconversion rates between substrates are quantified by Michaelis-Menten-type (MM) kinetics without explicit consideration of enzyme concentration, activation, inhibition or other effects that modulate enzymatic activity. Instead, the MM mathematical form is used with the ratios of key regulatory factors in place of substrate concentration. The regulatory factors present in the model are: PS = [ADP]/[ATP]; RS = [NADH]/[NAD]; CS = [CR]/[PC]; and AF = [AC]/[FC]. Our concentrations always refer to the average concentration except when explicitly referred to as blood compartment concentrations. These regulatory factor ratios are known to exert major regulatory functions in the cell. For instance, the presence of high levels of [ATP] inhibits the turnover rate of oxidative phosphorylation while the presence of [ADP] stimulates it. This and other similar effects are captured in an approximate, but robust manner. For instance, the rate of conversion of phosphocreatine to creatine is represented by

$$\phi_{PC\to CR} = \lambda_{MAX,PC\to CR}\frac{PS}{PS_o + PS}C_{PC} \tag{5.5}$$

where $\phi_{PC\to CR}$ is the flux or turnover rate (μmol/g-min, as all units are on a per gram of wet tissue basis), $\lambda_{MAX,PC\to CR}$ is the maximum flux and PSo is the MM constant which we set equal to PS at rest. $C_{PC}$ is the concentration of phosphocreatine in the cytoplasm (the 'c' subscript was dropped here for simplicity). All metabolites and their abbreviations are found in Table 5.1.

*Table 5.1: Metabolite species and their abbreviations.*

| Species | Abbreviation | Compartment | Transport |
|---|---|---|---|
| Glucose | GL | Blood and Cytoplasm | Active (b to c) |
| Lactate | LA | Blood and Cytoplasm | Active both ways |
| Fatty Acids | FA | Blood and Cytoplasm | Passive |
| Oxygen | O2 | Blood and Cytoplasm | Passive |
| Carbon Dioxide | CO2 | Blood and Cytoplasm | Passive |
| Glucose-6-Phosphate | GP | Cytoplasm | None |
| Glycogen | GY | Cytoplasm | None |
| Triglyceride | TG | Cytoplasm | None |
| Pyruvate | PY | Cytoplasm | None |
| Acetyl-CoA | AC | Cytop. and Mitoch. | None |
| Free CoA | FC | Cytop. and Mitoch. | None |
| CoA in "pool" | CoApool | Cytoplasm | None |
| Nicotinamide Adenine Dinucleotide (oxidized) | NAD | Cytop. and Mitoch. | None |
| Nicotinamide Adenine Dinucleotide (reduced) | NADH | Cytop. and Mitoch. | None |
| Adenosine Diphosphate | ADP | Cytop. and Mitoch. | None |
| Adenosine Triphosphate | ATP | Cytop. and Mitoch. | None |
| Phosphocreatine | PC | Cytoplasm | None |
| Creatine | CR | Cytoplasm | None |

When more than one regulatory factor influences the rate a "ping-pong"-type kinetic formula is used. For instance, the conversion of pyruvate to acetyl-CoA is

$$\phi_{PY\to AC} = \lambda_{MAX,PY\to AC}\frac{1}{1+\dfrac{1/AF_o}{1/AF}+\dfrac{1/RS_o}{1/RS}}C_{PY} \tag{5.6}$$

The use of these forms correctly reduce reaction rates to zero as the concentrations of reactants reach zero. This is an improvement over previous models, which suffered from non-physiological results such as negative concentrations under all but a very narrow set of physiological input parameters for which the model was designed to mimic. The application of these robust and simple rates allows this model to be used in a much wider range of physiological states without retuning the rate constants. The full compliment of reaction rate equations can be found in *Appendix B.*

All metabolite concentrations are evolved in time by integration of ordinary differential equations (ODEs) expressing mass conservation. All ODEs have the general form:

$$volume\ x\ \frac{d}{dt}(concentration) = production - utilization + flux\ in - flux\ out.$$

In the cytoplasm, this is written as:

$$V_c\frac{dC_j}{dt} = \sum_{k=1}^{n}\alpha_{kj}\phi_{kj}^{p} - \sum_{k=1}^{m}\alpha_{jk}\phi_{jk}^{p} + J_{b\to c,j}^{F\ or\ P} - J_{c\to b,j}^{F\ or\ P} \tag{5.7}$$

and similarly to the mitochondrial compartment, *m*. The above equation is expressed in the symbols that will be used in the remainder of this text. Here, the volume, $V_j$, is the effective compartmental volume and a tuning parameter for adjusting the sensitivity of the metabolite to perturbations to the independent variables. In essence, it adjusts the timescale ($1/V_j$) of the

model. The production and utilization terms, the two summations, respectively, are just the algebraic sum of the rates of conversion of species 'j' to species 'k', or $\phi_{jk}$, multiplied by their corresponding stoichiometric coefficients, $\alpha_{kj}$ (all stoichiometric equations are given below in Table 5.2). The fluxes in and out of the cytoplasm of species 'j' are the mass transport rates $J^{F\,or\,P}_{b\to c,j}$ and $J^{F\,or\,P}_{c\to b,j}$, respectively. These fluxes may be passive (superscript-P), or active (superscript-F), depending on the species. In the blood compartment there are no production or utilization terms. The general form is written:

$$V_b \frac{dC_j}{dt} = Q(C_{aj} - C_{vj}) - J^{F\,or\,P}_{b\to c,j} \tag{5.8}$$

here, $Q$ represents the coronary blood flow rate, which is set to 1.0 mL/min at rest. The concentrations of arterial and mixed venous blood are $C_{aj}$ and $C_{vj}$, respectively. When calculating the transport rates, the relevant quantities are not the arterial or venous blood concentrations, but a mixture of the two. To remedy this, an *average blood concentration*, is written which assumes a linear combination of arterial and venous bloods at a proportion set by the mixing fraction, $F = 0.33$:

$$C_{bj} = FC_{vj} + (1-F)C_{aj}\,. \tag{5.9}$$

*Table 5.2: Summarized stoichiometric reactions.*

| Reaction | Equation |
|---|---|
| *CYTOSOL* | |
| Glycolysis 1 | Glucose + ATP→ Glucose-6-phosphate + ADP + $H^+$ |
| Glycolysis 2 | Glucose-6-phosphate + 2 Pi + 3 ADP + 2 $NAD^+$→2 Pyruvate + 3 ATP + 2 NADH + $H^+$ + 2 $H_2O$ |
| Glycogenesis | Glucose-6-phosphate + ATP + Glycogen (n) + $H_2O$ → Glycogen (n+1) + ADP + 2 Pi |
| Glycogenolysis | Glycogen (n+1) + Pi → Glycogen (n) + Glucose-6-phosphate |
| Pyruvate Oxidation | Pyruvate + CoA + $NAD^+$ → Acetyl-CoA + $CO_2$ + NADH |
| Pyruvate Reduction | Pyruvate + NADH + $H^+$ → Lactate + $NAD^+$ |
| ATP hydrolysis | ATP → ADP + Pi + Energy |
| Palmitate Oxidation | Palmitate + 8 CoA + 35/3 $NAD^+$ + 2 ATP + 7 $H_2O$ → 8 acetyl-CoA + 35/3 NADH + 7 $H^+$ + 2 ADP + Pi |
| Triglyceride Production | 3 Palmitate + Glycerol + 2 ATP → Triglyceride + 2 ADP + 2 Pi |
| Triglyceride Oxidation | Triglyceride → 3 Palmitate + Glycerol |
| Phosphocreatine Synthesis | Creatine + ATP → Phosphocreatine + ADP + $H^+$ |
| Phosphocreatine Breakdown | Phosphocreatine + ADP + $H^+$ → Creatine + ATP |
| *MITOCHONDRIA* | |
| Oxidative Phosphorylation | NADH + $H^+$ + 3 ADP + 3 Pi + ½ $O_2$ → $NAD^+$+ 4 $H_2O$ + 3 ATP |
| Citric Acid Cycle | Acetyl-CoA + 11/3 $NAD^+$ + ADP + Pi + 2 $H_2O$ → 11/3 NADH + 2 $H^+$ + CoA + ATP + 2 $CO_2$ |

As mentioned previously, the mass transport rates can be either passive or active. The passive rate is set by

$$J^{P}_{b\to c,j} = \lambda_{b\to c,j}(C_{b,j} - \sigma_{b\to c,j}C_{c,j}) \tag{5.10}$$

where $\sigma_{b\to c,j}$ and $\lambda_{b\to c,j}$ are adjustable parameters controlling the equilibrium set point and gain of the flux. Notice also that $\lambda_{b\to c,j}$ is similar to a diffusivity constant. Blood gasses and fatty acids are transported passively. In the case of active transport, the active sites available to carry molecules across membrane barriers are finite and therefore saturable. Hence, we employ an approximate rate of saturable form, which resembles a MM rate:

$$J^{F}_{b\to c,j} = \frac{T_{b\to c,j}C_{b,j}}{M_{b\to c,j} + C_{b,j}}. \tag{5.11}$$

Like in the case of the reaction rate equations, we set the constant in the denominator, $M_{b\to c,j}$, equal to the value for $C_{bj}$ at rest.

**Coupling to Work Rate**

Oxidations of fuels is controlled such that the ATP requirements for a variety of vital process within the cell are met. Therefore, even though energy conversion processes within the cell are typically efficient ($\eta \approx 0.5$), not all of the free energy not converted into heat goes into mechanical work production. Here we assume that only a small fraction $\beta = 0.1$ contributes to the mechanical pumping of blood throughout the body. Also, in calculating how much energy is available from the hydrolysis of ATP to ADP we have neglected AMP forms and written

$$\Delta G_{ATP\to ADP} = \Delta G^{o}_{ATP\to ADP} + RT\ln\left(C_{Pi}\cdot PS\right). \tag{5.12}$$

This expression also neglects other factors, such as pH and [$Mg^{2+}$], which also influence the available free energy. Furthermore, because our model does not treat free phosphate (Pi) fluctuations, we fix $C_{Pi}$ to the concentration at rest, letting only *PS* vary over time. The standard free energy of ATP hydrolysis is set to $\Delta G^{o}_{ATP\to ADP} = -31.5$ kJ/mol.

The rate of ATP hydrolysis is

$$\phi_{ATP\to ADP} = \frac{\dot{W}}{-\beta\Delta G_{ATP\to ADP}\cdot M}\,\frac{1/PS}{K_{ATP\to ADP} + 1/PS} \tag{5.13}$$

where $\dot{W}$ is the work rate (power) demand for pumping blood, which is equal to the product $Q\Delta P$, or the cardiac output times the pressure load across the heart. *M* is the mass of wet heart tissue since all expressions are written on this basis. The second factor in the equation was added *ad hoc* to force the conversion rate to vanish as ATP is depleted. In this sense, the first term represents the maximum work rate demands by the heart (similar to *V*max), while the second term modulates the actual energy delivery according to the availability of ATP. Setting $K_{ATP\to ADP} << 1/PS_o$, at conditions near the rest state, allows the model to supply almost the full

amount of energy demand. As the heart works harder, the supply-to-demand ratio will drop as ATP becomes depleted.

**Model Optimization**

Because the general topology of the metabolic network is conserved among many different cell types, the current model could be calibrated, or optimized, to represent different tissues with perhaps only minor modifications. Where other metabolic processes are important, these extra pathways could be added to the basic model and recalibrated accordingly.

Here the rate constants were optimized at steady state rest conditions to mimic the heart muscle (myocytes). The strategy was to obtain a constant concentration of all metabolites for rest levels of arterial, blood, cytoplasm and mitochondria concentrations by tuning the reaction and transport rate constants. The steady state constraint is simply:

$$\frac{dC_j}{dt} = 0 \tag{5.14}$$

for all concentrations in the blood, cytoplasm and mitochondria compartments. The initial conditions at rest are also known (or estimated) and fixed. In addition, the MM constants (*Km*'s) were set to their rest values as mentioned previously. With this, the only variables in the optimization were: all $\lambda_{MAX}$, $M$, $K_{ATP\to ADP}$, and the transport coefficients $\lambda_{b\to c,j}$ and $T_{b\to c,j}$. Finally, in the heart, about 60 to 90% of the acetyl-CoA comes from the breakdown of fatty acids. This was added as an extra constraint during the fine-tuning of model parameters:

$$\frac{\phi_{FA\to AC}}{\phi_{FA\to AC} + \phi_{PY\to AC}} = 0.67 \text{ at rest.} \tag{5.15}$$

Optimization was accomplished by a Newton search algorithm with an initial guess estimated from [8]. There were 26 variables and 24 equations in the final optimization. The two degrees of freedom in the model were used to perform a limited amount of manual fine-tuning on the sensitivity of the response to better match available experimental data (see *Model Validations*). The timescale of the responses (the time to reach steady state following a perturbation) were adjusted by varying the effective compartmental volumes ($V_j$) until it approximately matched experimental data on the evolution of several metabolites. The relative values of the volumes, however, were fixed according to published heart data [1] to 87% for heart and 13% for blood.

**Model Validations**

The predictive power of our model was tested against available experimental data on dog, swine and pig models [Pantely, 1990, 1991; Stanley 1992]. In these studies, blood flow through the left anterior descending (LAD) coronary artery was reduced to prescribed fractions of the control subject for 1-hour in anesthetized animals. These ischemia levels were set to 30% in [Pantely, 1990]; 50% in [Pantely, 1991]; and 60% in [Stanley 1992].

Simulations lasted 65 minutes. After 5 minutes of evolution at rest levels, a step change was applied to the coronary blood flow parameter $Q$ to the desired level of ischemia. The width of the step change was 1 minute but alterations of width did not affect the resulting fluctuations significantly. In general, simulations yielded well-behaved functions except, in a few cases, for very early abrupt fluctuations following immediately after the change in $Q$. The product of heart rate and left ventricular systolic pressure remained unchanged during several ischemia experiments of varying intensities. In general, while the heart rate increased slightly, the blood pressure decreased accordingly to keep the product nearly constant. From this it is speculated that the mechanical power output from the heart does not vary appreciably during ischemic conditions. In our model we reflect this by letting the mechanical power demand remain constant throughout the entire simulation.

All 1-hour ischemia simulations ran in a matter of just a few seconds using a stiff integral method with relative and absolute tolerances of $10^{-3}$.

According to Stanley *et. al.* [Stanley 1992], even moderate ischemia produces little to no change in glucose uptake even though it increases glucose extraction. Uptake is measured as the product of flow and arterial-to-venous concentration difference:

$$U_j = Q\left(C_{aj} - C_{vj}\right). \tag{5.16}$$

Also, FA uptake decreases while the heart switches from a net consumer to a net producer of LA. Our model was able to reproduce all of these uptake patterns (Figure 5.20).

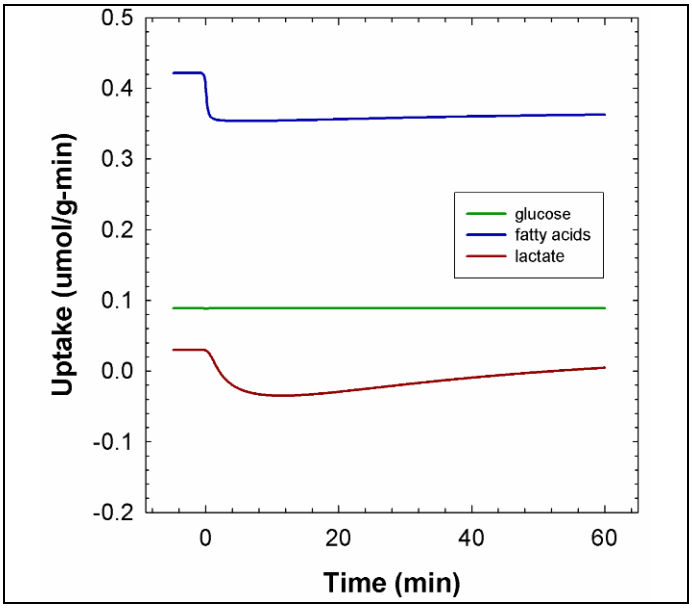


*Figure 5.20: Effect of GL, FA and LA uptake (bottom graph) to 30% ischemia.*

ATP and PC levels were also monitored in these *in vivo* experiments. Figure 5.21 shows both data and simulation of these fluctuations.

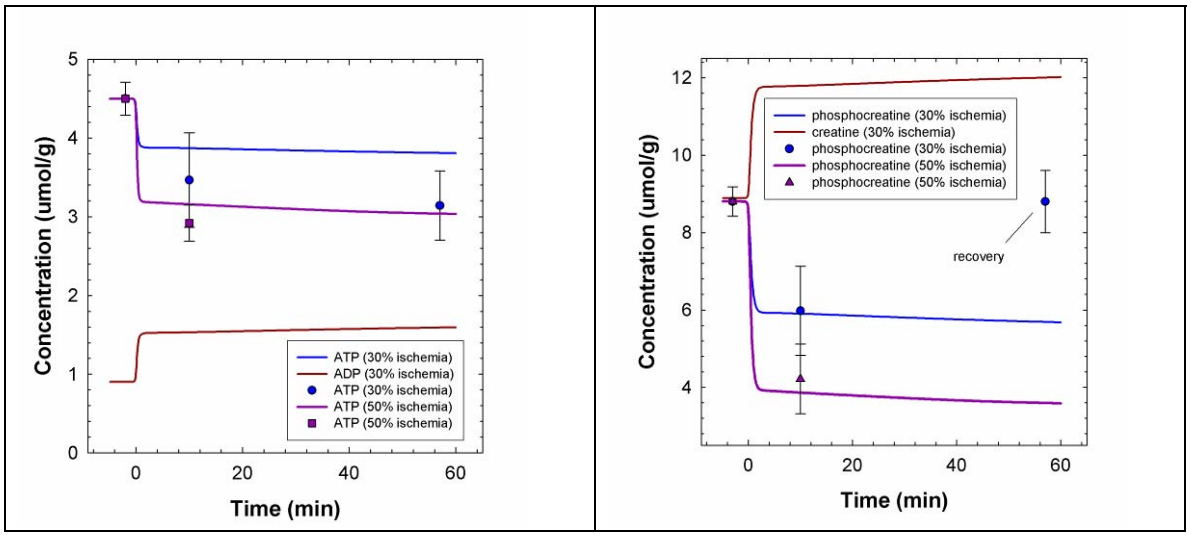


*Figure 5.21: ATP and PC evolutions compared. Experimental data points are plotted with simulation curves for 30% and 50% ischemia.*

Comparisons between experiment and our simulations are summarized in Table 5.3. Because the control metabolite concentrations differed slightly between experiment and simulation, all values were normalized with the control (initial) concentrations ($\overline{C}_j = C_j / C_{jo}$). ATP and PC data are mean values of subendocardium, midmyocardium and subepicardium levels.

*Table 5.3: Comparison of experiment to simulation during 1-hour ischemia.*

| Metabolite | 5-10 mins 30% ischemia | | 5 mins 50% ischemia | |
|---|---|---|---|---|
| | Experiment | Simulation | Experiment | Simulation |
| ATP | 0.70±0.26 | 0.83 | 0.65±0.10 | 0.67 |
| Phosphocreatine | 0.68±0.15 | 0.64 | 0.48±0.21 | 0.40 |
| Lactate | 2.26±1.1 | 2.14 | | |
| O2 consumption | 0.77±0.16 | 0.92 | | |

In these experiments, the authors have reported recovery of ATP, PC and other metabolite levels after 60 minutes of continued mild to moderate ischemia. Arai *et. al.* speculates that active down regulation could have decreased the demand for ATP thus putting the heart in a state of "partial hibernation". This recovery could be a result of intracellular pH improving on a similar time course to the myocardial lactate content. In this picture, the free energy available per ATP would have recovered towards preischemic levels. The authors also point out that pH alone cannot account for full recovery and further speculate the involvement of free phosphate (Pi), altered $Ca^{2+}$ transient size or altered myofibril-$Ca^{2+}$ interactions in the recovery process.

Yet another possible cause for recovery not pointed out by the authors is the influence of all other tissues and organs in the anesthetized animal model via venous return. Since a fully

coupled organism will differ from an isolated, heart-only model with constant arterial blood metabolite levels, a realistic comparison to experimental models has to be limited to the earliest effects of acute ischemia. That is, before the onset of possible compensatory effects by other parts of the organism including hormonal regulation. Thus, the comparison is limited to only the first 5 to 10 minutes, when the first measurements were taken. Nevertheless, because the model is coupled to the mechanical power output demands of the heart we can easily test Arai's proposition of reduced energy demand by asking how large a decrease in the power output could have led to a recovery of metabolites to preischemic levels. It was found that a 25% increase in the available free energy around the middle of the experiment would have been sufficient to return metabolite concentrations to preischemic levels after the onset of a 30% ischemia.

Figure 5.22 shows a few more results from the 30% ischemia simulation. It is known that in the heart about 60 to 90% of the acetyl-CoA comes from the breakdown of fatty acids (FA $\rightarrow$AC) with the remainder coming mostly from pyruvate breakdown (PY $\rightarrow$AC), both before and after ischemia. This was captured in our simulations. At rest, the FA to AC pathway represents 67% of the total AC production (Figure 5.232, left panel). After the onset of ischemia this decreases temporarily and then approaches the previous fraction after 1 hour of continued ischemia. This is also reflected in the fluctuations of NAD and NADH (Figure 5.232, right panel). Here, ischemia causes a decrease in the redox state. This result is consistent with a recent paper [Zhou, 2005] but contradicts an earlier paper [Salem, 2002] by the same group.

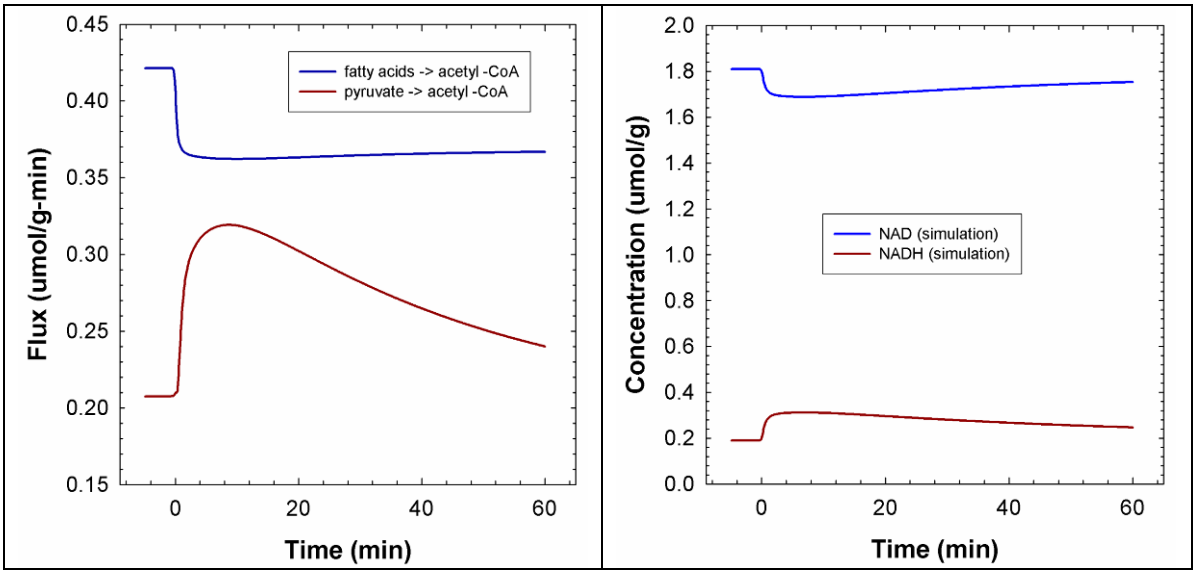


*Figure 5.22: Effects of 30% ischemia on AC production and redox state.*

The coupling to mechanical work, a unique feature of this model, deserves special attention. Figure 5.23 shows the effect of 50% ischemia on the various parameters controlling mechanical energy consumption.

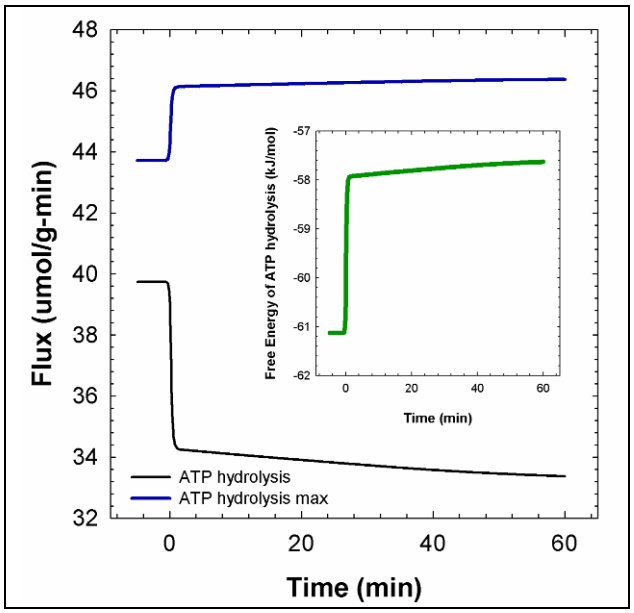


*Figure 5.23: Effect of 50% ischemia on ATP hydrolysis rate, max ATP hydro. rate and available free energy (inset).*

The graph shows that during ischemic conditions the maximum rate of ATP hydrolysis ($\lambda_{MAX}$) actually increases due to the smaller free energy available from the reaction. The rate of hydrolysis, on the other hand, decreases due to inadequate perfusion.

In conclusion, even thought our model falls within the (rather large) error bounds of experimental dog, pig and swine models, the mathematical model remains of qualitative precision only. This is because of the several shortcomings of the model including vastly simplified metabolic topology utilized in its construction and the limited experimental data available for model validation. However, the model is fairly robust and will give reasonable qualitative results under most physiological conditions.

Hypoxia Simulation

A hypoxia simulation was also performed during model validation (Figure 5.24). Even though these results were not compared against experiment at this point, they conform to expectation. Briefly, they resemble ischemia of a more severe intensity. Like ischemia, the heart switches to a net producer of lactate due to the limiting oxidative capacity of oxidative phosphorylation. Fatty acid, oxygen and carbon dioxide uptakes are all down-regulated to cope with the decreased oxidative potential of the cell.

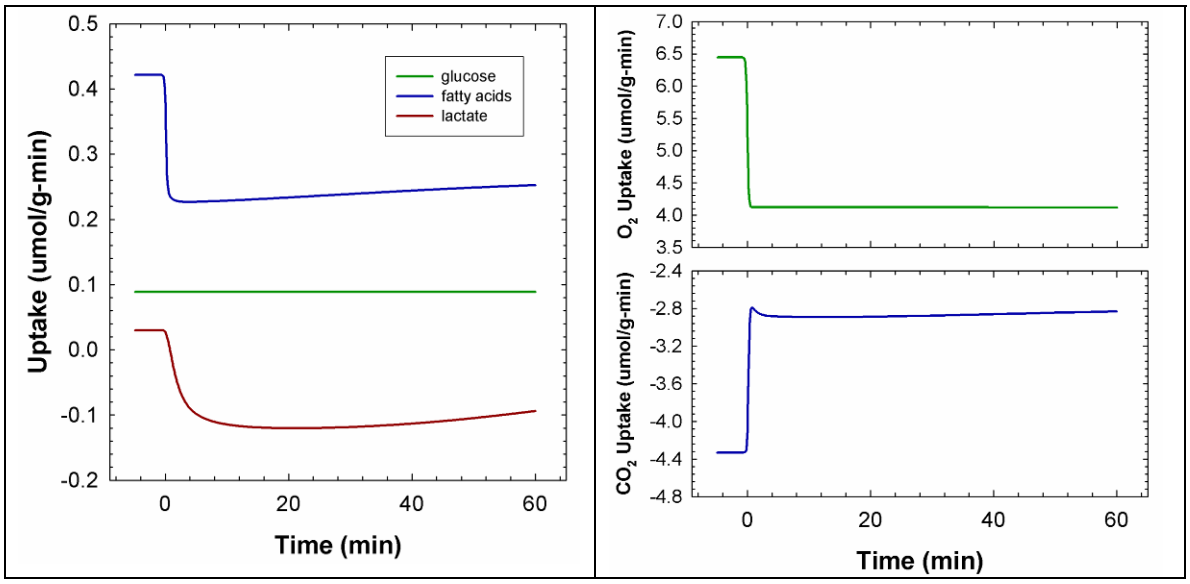


*Figure 5.24: Effects of 40% hypoxia on the uptake of several metabolites and blood gasses.*

**Model Stability**

Our model was able to display a well-behaved response (no oscillations) for step input changes of as fast as 0.1 minutes. To demonstrate stability we have simulated an extreme near total ischemia (99.9%) for 1 hour (Figure 5.25). Most physiological changes in the human body are relatively milder and slower changing, however. Thus it is expected that the current model remains stable after incorporation into the larger-scale human model.

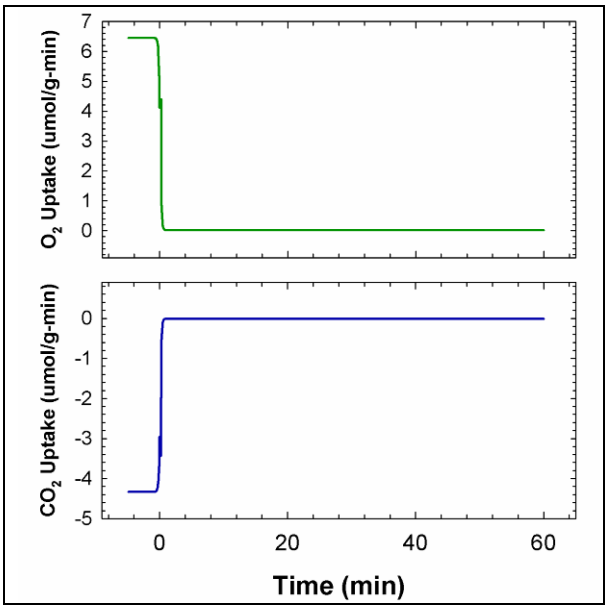


*Figure 5.25: 99.9% ischemia simulation.*

## 5.11 Perfusion of a Cell in an Organ and Cell Metabolism

A realistic spatio-temporal metabolism model was developed in CoBi. The CoBi metabolism model consists of a 3D spatially meshed model, using realistic single cell dimensions and an unstructured grid. The simulation was transient, and utilized CoBi's flow, membrane, species, and reaction modules. The geometry consisted of capillary blood flow around a circular cell, which included the cytosol, 20+ mitochondria, and an unmeshed nucleus. Membrane structures were present between the blood-cytosol and the cytosol-mitochondria interfaces. Present through the geometry were 18 species. In the blood flow, species were transported through both convective and passive transport. Throughout the cytosol and mitochondria species were transported via passive and active transport. Active transport was assumed to be a saturable two-step process where transporter sites in the membrane were bound to the molecule before being transported. This treatment also gave Michaelis-Menten kinetics for active transport. Passive membrane transport was governed through a conjugate gradient equation. In the mitochondria, there were 7 species reactions, while 17 species reactions were occurring in the cytosol. These reactions in conjunction with the transport of the species resulted in quasi-steady state conditions for the cell similar to those seen in the three-compartment model (Figure 5.26 and Figure 5.27).

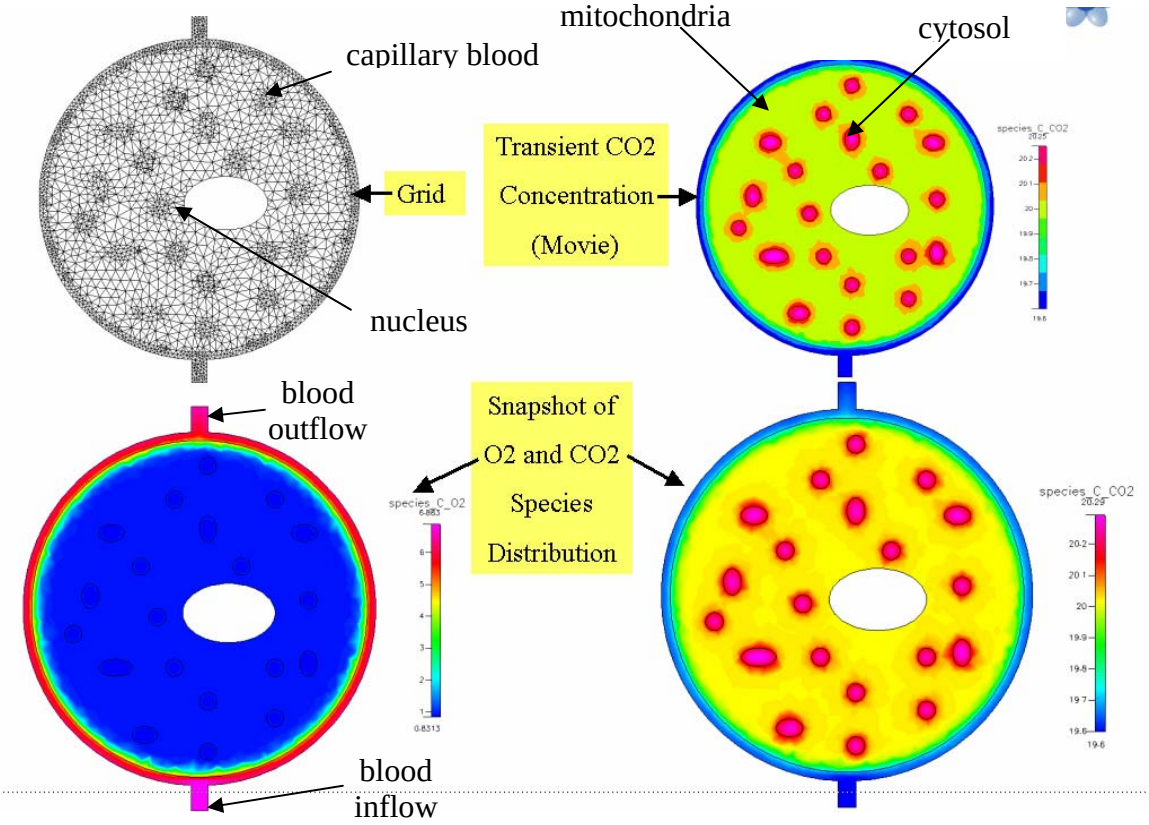


*Figure 5.26: Snapshots of the cell model. (Top Left) The unstructured mesh grid used for simulations. (Bottom Left) Oxygen distribution.(Top and Bottom Right) Carbon dioxide distributions. Capillary blood flow is shown circling both sides of the cell and entering from the bottom part of the figure. Species are transported in and out of the cell through the cell membrane and then into the mitochondria where energy is converted into ATP and $CO_2$.*

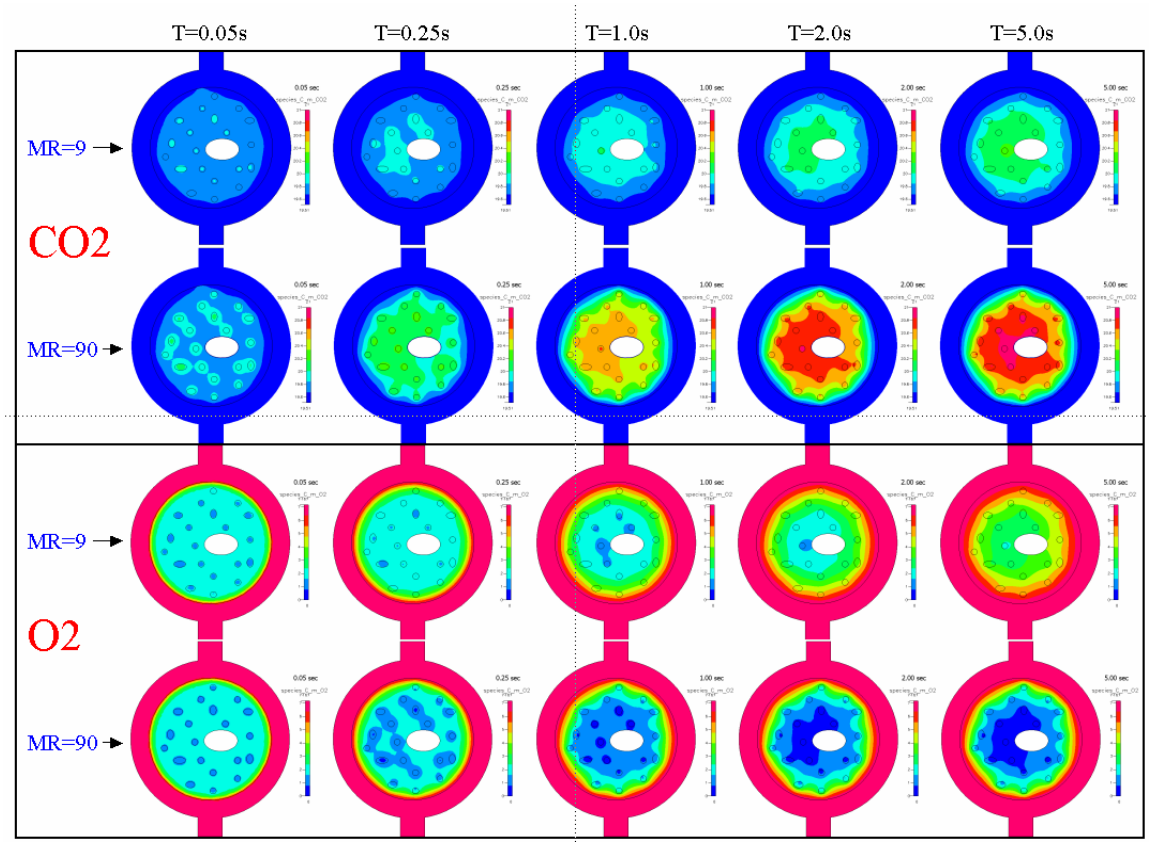


*Figure 5.27: A series-in-time showing the progression of metabolism in a cell. Top figures show $CO_2$ concentration evolution throughout the cell for two different metabolic rates (MR = 9 and 90). The time stamps are indicated at the top of the figure. Bottom figures show the $O_2$ distribution for the same simulation and time points. Notice the increased $O_2$ consumption and $CO_2$ generation when energy demands on the cell are increased 10-fold.*

# 6. CONCLUSIONS AND RECOMMENDATIONS

## 6.1 Summary and Conclusions

This report presents the results of a two-year project performed by CFD Research Corporation under the DARPA/IPTO BioCOMP Program. The BioCOMP Program objective was to develop advanced simulation framework called Simulation Program for Intra-Cellular Processes (Bio-SPICE), for comprehensive simulations of cell biology processes. The role of the Bio-SPICE framework is to enable the construction of sophisticated models of intracellular processes that can be used to predict and control the behavior of living cells.

Most of the cell biology models typically reported the open literature are formulated as single compartment (well stirred) reaction models. Our approach in this project was to formulate them as 1D, 2D and even 3D transient (spatiotemporal) models and to perform parametric simulations to assess model performance in the multi dimensional form. Spatiotemporal modeling of cell biology is performed on a numerical grid. In this project we have explored two ways to generate computational grids for biological cells: image based mesh generation, and meshing idealized geometries representative of biological ells e.g. sphere and rod. In this project we have used CFD-Micromesh software it for image processing, geometry construction, and for generation of 2D and quasi 3D (extruded 2D) meshes for simulation of cellular biophysics and biochemistry. In the CoBi software environment the mesh is either imported as a file if the geometry is complex or automatically generated in the JCoBi tool for simple geometric shapes such as square, cube, rod, sphere, ellipsoid, and bacteria–like shape.

A critical review of published spatiotemporal models describing biochemistry and biophysics of prokaryotic and eukaryotic cells was conducted. The objective was to select the models with important applications in military medicine. Several problems were selected for parametric simulations including:

- Cellular chemosensing
- Cell cycle biochemistry model
- Cell cycle and division model
- Polarization and oscillations during E Coli cell division
- Signaling pathways during cacterial chemotaxis
- Multivalent binding
- Neutrophil chemotaxis
- E Coli chemotaxis

The main objective of the BioCOMP Program was to develop a self-contained software framework solving partial differential equations governing flow, diffusion, and biochemistry applicable for spatiotemporal modeling of cell and organ biology problems. During a two year period CFDRC has developed CoBi to simulate complex cell and organ biology problems. The code was written in modern C++ programming language using state of the art numerical techniques for solving large systems of partial differential equations (PDEs) and CFDRC multiphysics modeling expertise. A graphical user interface (GUI) for CoBi, JCoBi, was written in Java language and interactive 3D graphics. CoBi has been designed to interact with the other

Bio-SPICE software tools using SBML as a standard interface. The prototype CoBi software developed in this project was delivered in source to DARPA (SRI Bio-SPICE site) in February 2005 and the final code along with the code documentation was delivered to AFRL/IFTC at the end of the project.

During this project CoBi code has been tested on several fluid flow, diffusion, and chemistry problems and results have been compared to CFD-ACE+ and to published benchmark solutions. The code showed very good accuracy and numerical robustness in solving 3D problems. In the current project some of the cell biology problems studied in our previous BioCOMP Program presented in Appendix A were reproduced.

The major achievement of this project was the development of a 3D volumetric modeling tool, CoBi, designed for spatiotemporal modeling of cell biology by coupling cell biophysics and biochemistry equations. A generalized biochemistry solver module for modeling cell signaling and metabolic pathways problems including extracellular, intracellular, and membrane bound biochemical reactions was developed. This report describes the mathematical formulation of cellular biophysics and biochemistry used in the code development, numerical methods for solving large scale systems of PDE equations, and CoBi software structure. The code has been applied to a number of cell biology problems. This report describes details of model description and presents simulation results for the flowing cell biology problems:

- *Bacillus Subtilis* Min protein dynamics
- Autocrine EGFR signaling
- Multi-cellular perfused tissue EGF signaling
- Cellular calcium oscillations
- Tissue calcium waves
- Cellular oxygen metabolism
- Morphogenesis of yeast cell
- Perfusion of a cell in an organ and cell metabolism

At the end of the project CFDRC has prepared CoBi documentation: JCoBi Users Manual and four CoBi tutorials and delivered to AFRL/IFTC, Rome NY, along with the CoBi source software. They are available to other DoD Laboratories.

It is felt that all of the major objectives of this project have been successfully accomplished. The CoBi code has been developed, validated, and demonstrated on several cell biology and organ physiology problems. The code has been used as the starting point for several DARPA and DoD projects. CFDRC is using CoBi as the enabling technology for projects related to military medicine, personnel protection, and bio defense.

The CoBi code delivered at the end of this project will be available to other US government organizations and to collaborating academic institutions without license fees. Technical support for the effective use of the CoBi code is available from CFDRC.

## 6.2 Future Developments and Recommendations

This project has established excellent foundations for future **computational medicine and biology projects (CMB)** at CFDRC for military and civilian medical applications. After two years of this project CoBi has matured to the point that it can be used for solving problems not only in cell biology but also organ biology and whole body (organism) physiology. During 2005-2006 CFDRC has invested significant IR&D resources in CoBi code development, integration, and testing. The code is being used as a starting point in several projects with DoD focused on biotechnology, nanotechnology, and military medicine. As a result several new capabilities are being implemented in CoBi including: flow in porous media, conjugate heat transfer, electrostatics, electrochemistry, stress/deformation and structures dynamics, moving body simulation, and. Some of the current projects that utilize the CoBi software capability and contribute to further development and applications are:

- AFRL/IFTC SBIR Phase II project on "Bio-CAD Tools for DNA Computing" adapting the CoBi code to simulate a DNA based bio computer, and a DNA based self assembly of nano devices for next generation of computers and sensors,
- DARPA/DSO BAA Surviving Blood Loss (SBL) in collaboration with University of Alabama Birmingham and US Army WRAIR on "Enhanced Survival following Trauma-Hemorrhage and Extended Period of Hypotension Using Hormonal and Metabolic Support". CFDRC is using CoBi to develop whole-body model of human cardiopulmonary circulation, respiration, metabolism and hemorrhage. In an ongoing project we are also developing rat and pig models to study novel pharmacological treatment and resuscitation strategies,
- DARPA/DSO SBIR Phase II on "Multiscale Modeling Tools for Blast Wave Traumatic Brain Injury". In this project CoBi is being adapted for modeling tissue biomechanics (stress/deformation) during shock wave impact and penetration through human lungs and brain,
- US Army Aeromedical Research Laboratory, Ft Rucker AL Phase II project on "Image/Model Based System for Optimized Helmet Design". Here CoBi is being adapted to simulate kinetic and blast impact on a human head with a protective helmet,
- AFRL/HEPA Wright Laboratories Dayton OH on "An Integrated Modeling Framework for Predictive Human Performance". In this project we will integrate CoBi software tools with bio-dynamics and anthropologic databases of human (aircraft pilot) body injury,
- US Army WRAIR Phase II STTR Project with UC Irvine on "Portable Near Infrared Detection of Blast Lung Injury" CFDRC is developing integrated hardware NIRS sensor and CoBi software for model based detection of lung injury,
- NIH phase II SBIR project with Vanderbilt University on "Multiscale Model of Tumor Angiogenesis". CoBi is being adopted for modeling tumor perfusion and role of anti angiogenesis drugs in optimized chemotherapy.

CFDRC is also involved in several commercial applications for civilian medicine and for model based development of novel medical instruments and sensors.

**REFERENCES**


- Araujo R.P., Petricoin E.F., Liotta L.A., (2005)"A mathematical model of combination therapy using the EGFR signaling network", BioSystems, V 80, 57–69, 2005
- Arkin A. McAdams H.M. (1998) "Simulation of Prokaryotic Genetic Circuits" Annu. Rev. Biophys. Biomol. Struct.. 27:199–224, 1998
- Binding, Trafficking, and Signaling Oxford University Press
- Bottino D. C. (2000)," Computer Simulations of Mechanical Coupling in a Deforming Domain Applications to Cell Motion", "IMA Volumes in Mathematics and its Applications, Frontiers in Applied Mathematics Series" Volume 121: Mathematical Models for Biological Pattern Formation. Philip K. Maini and Hans G. Othmer (eds.) Springer-Verlag, New York, 2000
- Bottino D., Mogilner A., Roberts T., Stewart M., and Oster G.(2002) "How Nematode Sperm Crawl" Journal of Cell Science 115, 367-384 (2002)
- Bray D. "Unanswered Questions of Bacterial Chemotaxis" http://www.zoo.cam.ac.uk/comp-cell/Questions.html
- Berg H. (2000) "Motile Behavior of Bacteria", *Physics Today*, 53(1), 24-29 (2000).
- Bray, D. (2001). "Cell Movements from Molecules to Motility", 2nd ed, Garland Publishing, New York 2001
- EGF-receptor system: a paradigm for systems biology", Trends in Cell Biology Vol.13 1 43-50, Jan. 2003.
- Eisenbach M. "Bacterial Chemotaxis", Nature Encyclopedia of Life Sciences, 2001 www.els.net
- Elowitz M.B. et all (1999) "Protein mobility in the cytoplasm of E Coli" J. Bact. V 181, 1, 197-203, Jan 1999
- Erickson H. (2001) "The FtsZ protofilament and attachment of ZipA -structural constraints on the FtsZ power stroke" Current Opinion in Cell Biology 13:55-60, 2001
- Fall C.P., Marland E.S., Wagner J.M., Tyson J.J. "Computational Cell Biology", Springer 2000
- Fink C.C., Slepchenko B., Moraru I.I., Watras J., Schaff J.C. Loew L.M. (2000)"An Image-Based Model of Calcium Waves in Differentiated Neuroblastoma Cells", Biophys J, Vol. 79, 1, 163-183, July 2000
- Gal Almory, Lewi Stone and Nir Ben-Tai, "Multi-State Regulation, a Key to Reliable Adaptive Biochemical Pathways," Biophysical Journalm 81, pp3016-3028, Dec., 2001.
- Garvey T.D. Lincoln P., Pedersen C.J. Martin D. and Johnson M. (2003)' BioSPICE: Access to the Most Current Computational Tools for Biologists", OMICS Journal of Integrative Biology V.7, 4, 2003
- H. C. Berg H.C "The Rotary Motor of Bacterial Flagella", Annul. Rev. Biochem. 2003. 72:19–54
- Hans Meinhardt H. de Boer P.A.J. (2001),"Pattern formation in Escherichia coli: A model for the
- Howard M., Rutenberg A.D., and de Vet S. (2001)"Dynamic Compartmentalization of Bacteria: Accurate Division in E. Coli", Phys. Rev. Lett., V87, 27, 278102-1-4, Dec. 2001.

- http://www.zoo.cam.ac.uk/comp-cell/Questions.html, Dennis Bray Cambridge U. 2002
- Huang K.C. Meir Y., and Wingreen N.S. (2003)", Dynamic structures in Escherichia coli: Spontaneous formation of MinE rings and MinD polar zones", PNAS, V100, 22, 12724–12728, 2003
- Jacobson, K., E. D. Sheets, and R. Simson. 1995. Revisiting the fluid mosaic model of membranes. Science. 268:1441–1442.
- Jenkins J. and Hood J. 2006. "Organophosphate Neural Protectants", CFDRC DoD Phase I SBIR with the US Army/MRMC 2005
- Kholodenko, B. N., O. V. Demin, G. Moehren, and J. B. Hoek (1999), "Quantification of short term signaling by the epidermal growth factor receptor", J. Biol. Chem. 274:30169–30181, 1999.
- Lauffenburger, D.A. and Linderman, J.J. (1993) Receptors: Models for
- Levchenko, A., Iglesias, P. A. (2002). Models of Eukaryotic Gradient Sensing: Application to Chemotaxis of Amoebae and Neutrophils. Biophys J 82: 50-63,
- Lodish H et all (2000) "Molecular Cell Biology", 4th ed., WH Freeman &Co, 2000
- Lutkenhaus J., S.G. Addinal "Bacterial Cell Division and the Z ring" (1997), Ann. Rev. Biochem, 66, 93-116, 1997
- Lutkenhaus J. (2002) "Dynamic proteins in bacteria", Current Opinion in Microbiology 2002, 5:548–552
- Maly I., Lee R.T. and Lauffenburger D. A. (2004)" A Model for Mechanotransduction in Cardiac Muscle: Effects of Extracellular Matrix Deformation on Autocrine Signaling" Annals of Biomedical Engineering, Vol. 32, 10, 1319–1335, Oct. 2004.
- Maly I.V., Willey H.S, and Lauffenburger D.A. (2004)", Self-Organization of Polarized Cell Signaling via Autocrine Circuits: Computational Model Analysis, Biophysical J. V. 86, 10–22, Jan. 2004
- McCool G.J., (2001) "Exploring Structure and Function of FtsZ, A Prokaryotic Cell Division Protein and Tubulin-Homologue", www.umass.edu/microbio/chime/pipe/ftsz/present/septum.htm.
- Meinhardt H. and Piet A.J. de Boer, (2001) "Pattern Formation in E-Coli : A Model for the Pole-to-Pole of Min Proteins and the Localization of the Division Site", PNAS, V.98, No., 25, Dec., 2001.
- Michal G. (1998), "Biochemical Pathways: An Atlas of Biochemistry and Molecular Biology", Gerhard Michal (Editor), Willey ,December 1998
- Mogilner A., Edelstein-Keshet, L.,(2002) "Regulation of Actin Dynamics in Rapidly Moving Cells: A Quantitative Analysis", Biophys. J., V83, 1237-58, Sept. 2002
- Narang A., Subramanian K.K., and Lauffenburger D.A. 2001), "A Mathematical Model for Chemoattractant Gradient Sensing Based on Receptor-Regulated Membrane Phospholipid Signaling Dynamics", Annals of Biomedical Engineering, Vol. 29, pp. 677–691, 2001
- Othmer HG and Hillen T.(2002), "Chemotaxis equations from the diffusion limit of transport equations", SIAM JAM, 62, 1222-1250, (2002)
- Perelson A., and Weisbuch G. (1997) "Immunology for Physicists", Reviews of Modern Physics, Vol. 69, No. 4, October 1997
- Perelson, A.S., DeLisi, C., Wiegel, F.W., (1984), "Cell Surface Dynamics; Concepts and Models", Marcel Dekker.

- Sarkar C.A. and LAuffenburger D.A. (2003), “Cell-Level Pharmacokinetic Model of Granulocyte Colony- Stimulating Factor: Implications for Ligand Lifetime and Potency in Vivo”, Mol Pharmacol 63, 1, 147–158, 2003
- Schaff J. L.M. Loew; (1999),“The Virtual Cell”, Pacific Symp. on Biocomputing 4:228-239 (1999), http://www.smi.stanford.edu/projects/helix/psb99/Schaff.pdf
- Shih Y-L., Le T., and Rothfield L. (2003)” Division site selection in Escherichia coli involves dynamic redistribution of Min proteins within coiled structures that extend between the two cell poles”, PNAS, V 100, 13, 7865–7870, June 24, 2003
- Singer S.L. and G. L. Nicolson, “The fluid mosaic model of the structure of cell membranes”, Science, 175(23):720–731, 1972.
- Slepchenko B.M., Schaff J.C, Macara I, and Loew L.M. (2003), “Quantitative Cell Biology with the Virtual Cell”, Trends in Cell Biology V.13, 11, 570-577, Nov. 2003
- Sulzer, B. and Perelson, A. S., (1996), “Equilibrium Binding of Multivalent Ligands to Cell: Effects of Cell and Receptor Density,” Mathematical Biosciences, Vol. 135, pp.147-185.
- Sveiczer, A., Csikasz-Nagy, A., Gyorffy, B., Tyson, J. and Novak, B., “Modeling the fission yeast cell cycle: Quantized cycle times in wee$^{1}$- cdc25D mutant cells,” PNAS, Vol. 97, July 2000, pp.7865-7870.
- Takahashi K. et all (2003), “E-Cell System Version 3: A Software Platform for Integrative Computational Biology” Genome Informatics 14: 294-295 (2003)
- Tomita M.,(2001) "Whole cell simulation: A grand challenge of the 21st century" Biotechnology, 19,6, 205-210, 2001
- Wang Z.J. R.F. Chen R.F., Hariharan N. Przekwas A.J. and Grove D (1999) “A 2N Tree Based Automated Viscous Cartesian Grid Methodology for Feature Capturing”, AIAA-99-3300, 1999
- Wiley H.S., Shvartsman S.Y., Lauffenburger D.A. (2003)” Computational modeling of the EGF-receptor system: a paradigm for systems biology”, Trends in Cell Biology V.13, 1, 43-50, Jan. 2003

# APPENDIX A

**Summary of CFDRC Subcontract Project with Lawrence Berkeley Laboratory under DARPA BAA BioCOMP Project on**

# An Experimental Test Suite for Development of the BioSPICE Kernel

**Lawrence Berkeley Laboratory Principal Investigator:**
**Dr. Adam Arkin**

**CFDRC Subcontract Number: 6513845**

## Background

CFD Research Corporation (CFDRC) has been involved in the DARPA/IPTO BAA 01-26 BioCOMP Program between January 2002 and April 2006. The objective of the DARPA BioCOMP Program was to develop a computational framework that enables the construction of sophisticated models of intracellular processes that can be used to predict and control the behavior of living cells. One of the program tracks was to develop Bio-SPICE modeling framework, which stands for the Simulation Program for Intra-Cellular Processes.

During the period of January 2002 to December 2003 CDRC was involved in the DARPA BioCOMP Program as a subcontractor to the Lawrence Berkeley Laboratory (LBL) team led by Dr. Adam Arkin. Dr. Philip Colella of LBL was the lead scientist in charge of spatial model development in the LBL Bio-SPICE Team. CFDRC's project task was first to formulate and explore a spatiotemporal (multidimensional) modeling approaches and then to implement and demonstrate it on cell and organ biology problems.

The LBL team was responsible for the development of an open source software tool, CHOMBO, for spatiotemporal modeling of cellular biology (http://seesar.lbl.gov/anag/chombo/index.html). CFDRC's task was to formulate fundamental mathematical models and their numerical solution procedures for solving spatiotemporal cell biology problems. The models were tested using the existing CFDRC software framework, CFD-ACE+ and CFD Micromesh. Successful models were presented to the LBL team for further implementation in the Bio-SPICE and CHOMBO framework. CFDRC was also in charge of the development of 3D cell membrane model that could be implemented in the CHOMBO code. This project, completed in December 2003, provided excellent starting point for the follow up project with DARPA/IPTO and the AFRL/IFTC Rome NY.

**Acknowledgments**

Dr. Adam Arkin, of the Lawrence Berkeley Laboratory, was our inspiration to the Bio-SPICE simulation concept. We would like to thank Adam for including CFDRC in his DARPA Bio-SPICE proposal and entrusting us with the development and exploration of the spatiotemporal computational biology field. Adam has helped us immensely in better addressing cell biology, in identifying challenging modeling examples, and in providing critical feedback to our work. Technical discussions with Drs. Phillip Colella, Peter Schwarz, and Joseph Grcar during the first project are greatly appreciated.

**Project Objectives**

The overall objective of the LBL-CFDRC team in the BioCOMP Program was to develop a software toolkit and modeling framework for multidimensional, spatiotemporal comprehensive modeling of cell biology. The objective of the CFDRC task was twofold:

a) Formulate and implement multidimensional cell biology models in CFD-ACE+ software and to perform parametric simulation and validation tests for selected spatiotemporal cell biology problems, and
b) Develop a generalized mathematical model of a cell membrane and implement it in a software module for integration in the spatiotemporal cell biology model developed by the LBL team.

Both objectives of that project have been successfully accomplished. CFDRC has demonstrated exciting simulation results for several challenging cell biology problems such as cellular chemosensing, chemotaxis and cell division. C++ software tools for 3D modeling of cell membrane biology has been developed, documented, tested, and delivered in open source form to the LBL Bio-SPICE team. This Appendix presents summary of results of that project.

**Project Approach**

During this project, 01/2002 – 12/2003, CFDRC has formulated fundamental mathematical models and their numerical solution procedures for solving spatiotemporal cell biology problems. The models were tested using the well-established CFDRC software framework, CFD-ACE+. Successful models were presented to the LBL team for further implementation in the Bio-SPICE and CHOMBO framework. Most of the models were formulated based on models published literature. Typically such models were formulated as 0D or 1D problems. Our approach was to reformulate these published models as 2D and even 3D transient problems and to perform parametric simulations to assess model performance in the multi dimensional form. C++ software tools for 3D modeling of cell membrane biology have been developed, documented, tested, and delivered in open source form to the LBL Bio-SPICE team. The results of this project provided solid foundation for the follow up project directed by the Air Force Research Laboratory AFRL/IFTC.

During that period CFDRC BioSPICE team has been involved in:

- Technical discussion with BioSPICE PI and team members,
- Literature review on biophysics, biochemistry and modeling of *Bacillus Subtilis* sporulation and chemotaxis of bacterial and immune cells
- Automated geometry and mesh generation for realistic cell shapes,
- Formulation of mathematical models for cell membrane, membrane receptors, cell transport of macromolecules in cytoplasm, chemosensing, chemotaxis and others
- Development of core functions for 0D/1D/2D/3D cell biophysics processes

The following sections present summary of results obtained during the course of the CFDRC project with LBL under the DARPA BioCOMP Program.

***Generation of Computational Meshes Spatiotemporal Models of Cell Biology***

Spatiotemporal modeling is typically performed on a numerical grid (also called mesh) forming set 3D control volumes or finite elements. The generation of the computational grid for complex geometries, such as 3D biological cell, is a challenging problem. In this project, we have explored two ways to generate computational grids for biological cells: image based mesh generation, and meshing idealized geometries representative of biological ells e.g. sphere and rod. Early in the Bio-SPICE project, CFDRC has adapted CFD-Micromesh software for the application in automated image processing, geometry construction, and for generation of 2D and quasi 3D (extruded 2D) meshes for simulation of cellular biophysics and biochemistry. Figure A.1 presents example results in terms of original cell image, unstructured tetra mesh, adaptive binary tree mesh, and multi block structure mesh for a typical shape of the *Bacillus Subtilis* cell during germination process. Note the cell membrane capturing capability and formation of septum.

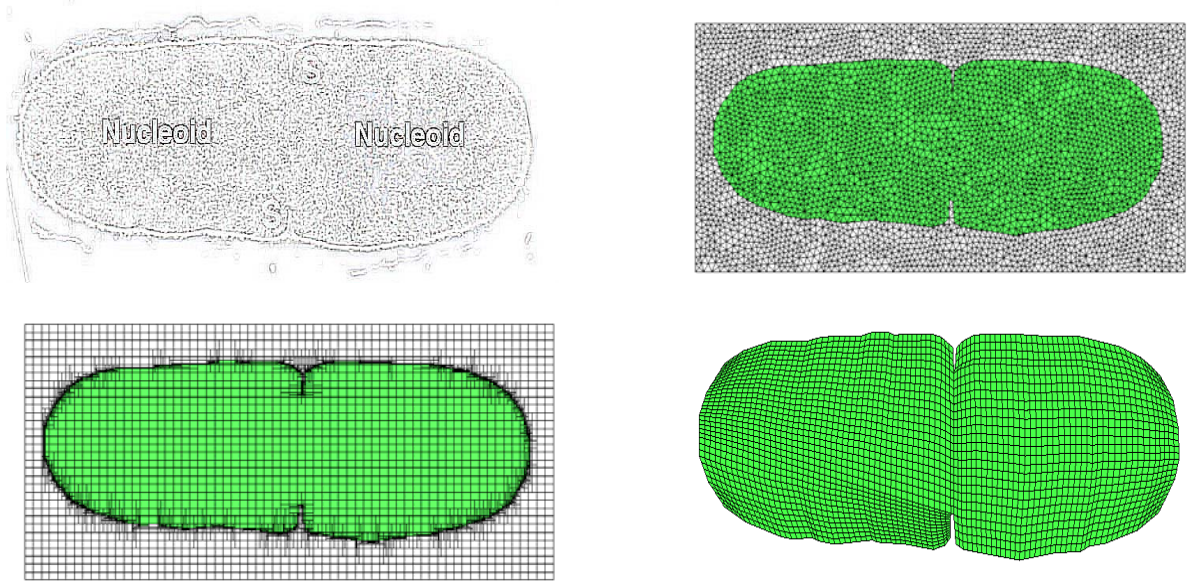


*Figure A.1: Bacillus Subtilis geometry and computational mesh during germination cell cycle division. Image and mesh examples obtained with CFD-Micromesh*

CFD-Micromesh has been also used to generate mammalian cells with embedded nucleus. Geometric/Mesh models should preserve topological information about membranes and

organelles so that separate equations (e.g. for signaling or sensing receptors or membrane deformation) can be solved. Figure A.2 shows the image-based computational mesh with volume conditions for the nucleus, cytoplasm, and plasma/nuclear membranes.

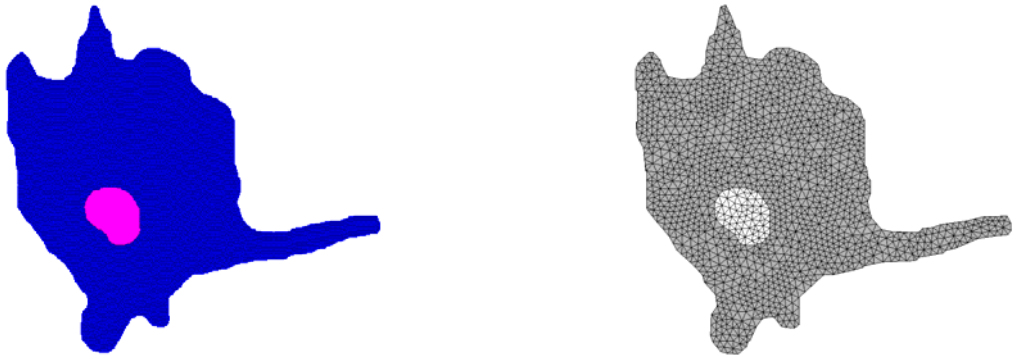

*Figure A.2: CFD-Micromesh generated geometrical image and computational mesh for and immune cell with a complex plasma membrane and an example organelle (nucleus).*

***Model of Membrane Geometry***

The membrane software module was developed by CFDRC and was delivered in mid March 2003 to UCB/LBL in the source form. The membrane module was written in C++ using object-oriented programming with a very powerful database for geometry, mesh, solution fields, properties, and boundary/volume conditions. It combines comprehensive surface constrained diffusion models with simple reaction kinetics. It is anticipated that the kinetics module will be replaced with a much more advanced reaction kinetics module from the Bio-SPICE LBL team. This team will take the lead in integrating the membrane module with the LBL CHOMBO main code. CFDRC has performed initial tests as described in the Results section.

It has been decided that the initial version of the membrane module will be driven from an input text file; the grid will be read from a file with the CFDRC MFG format, and output in the FAST format. The FAST format (developed at NASA Ames) is an "aerospace" standard format for visualization of unstructured grids and data fields. The input data should include: mesh information, boundary and initial conditions, and solution controls.

The membrane module code delivered to LBL consists of the following modules:
- In-core database with all variables, properties, mesh, solution
- I/O routines
- Main driver (not needed when linked with LBL solver)
- Interface APIs to LBL code
- Mesh and geometry initialization module
- Physical data initialization
- Mesh movement module
- Flux calculassions module (diffusive, advective)
- Simple chemical kinetics source terms evaluation module (including linearization)
- Matrix assembly

- Linear equation solvers

**Cellular Chemosensing**

Cellular chemosensing is a typical spatiotemporal cell biology problem. It involves diffusion of a chemoattractant in 3D extracellular matrix, cell membrane binding kinetics, and transport of receptors along membrane surface toward the chemoattractant gradient - all coupled to an intracellular signaling network. Figure A.3 presents an example chemosensing problem proposed by Prof. Lauffenburger team at MIT (Narang et all 2001) with multi step compartmentalized chemical kinetics of PIP3 signaling in cytoplasm and in endoplasmic reticulum (ER), migration of membrane receptors, and cell polarization.

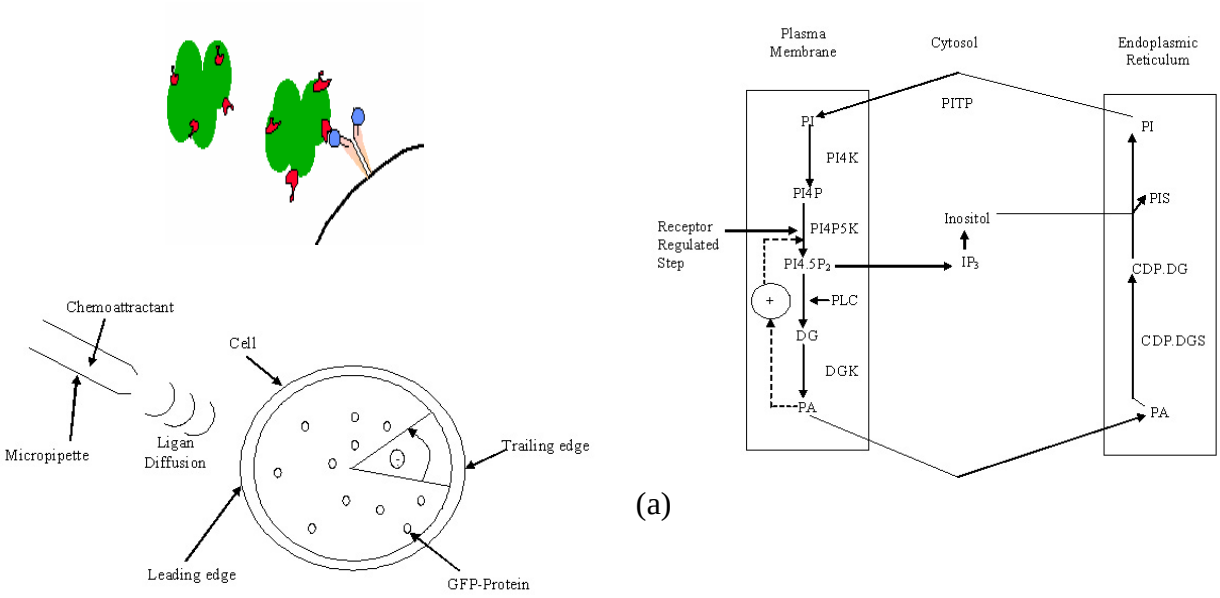


*Figure A.3: Conceptual model of ligand-receptor binding at the cell membrane. Schematics of chemosensing experiment, and biochemical intracellular IP3 signaling model, Narang 2001.*

In this simulation the chemoattractant (ligand) is released at a point away from the cell, diffuses to the cell membrane, and stimulates membrane bound receptors. The receptors respond by diffusing to the ligand causing receptor crowding in that zone. We solve for ligand diffusion in the extracellular space, for diffusion and crowding of membrane bound receptors, and for the intracellular signaling pathway as sown in Figure A.3 above. The cellular membrane has been constructed using the existing membrane model with membrane equations solved only for the membrane fixed and surface diffusing receptors.

The cell-membrane model includes: 3D external matrix chemoattractant diffusion, binding to membrane receptors, receptor diffusion along membrane, biochemical reaction on membrane, in cytosol, and in external matrix. In the original paper by Narang and Lauffenburger the model was solved as one dimensional problem (along the membrane equator). In the present study we model as 2D coupling extracellular, membrane, and intracellular space.

Figure A.4 and Figure A.5 present example simulation results for the cellular chemosensing problem. Some of the variables used in the figures below are:

- $r_{10}$ : Active Receptors,
- $\pi$ : Membrane Phosphoinositides.
- $\pi_S$ : Phosphoinositides in ER,
- $\iota$ : Cytosolic Inositol and Phosphates

Figure A.4 presents transient response of membrane active receptors, $r_{10}$, and membrane phosphoinositides, $\pi$, to an increase of uniform chemoattractant concentration for two levels of stimulation: stimulus value = 1 and 10. Note that stronger stimulation solicits more intensive response (red lines). Figure A.5 presents time snapshots of membrane phosphoinositides concentration $\pi$ during the stimulation.

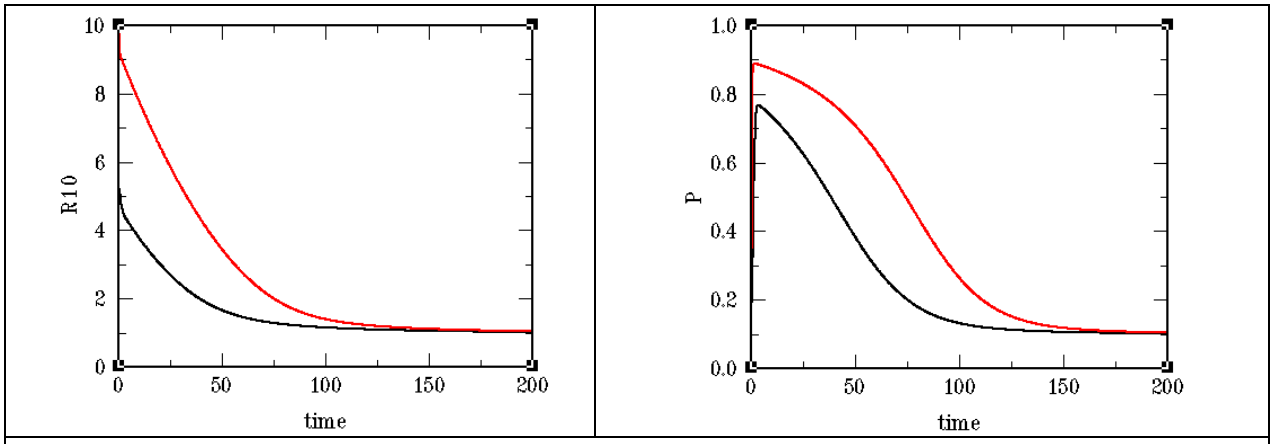


*Figure A.4: Transient response to an increase of uniform chemoattractant concentration for two values of chemoattractant stimuli.*

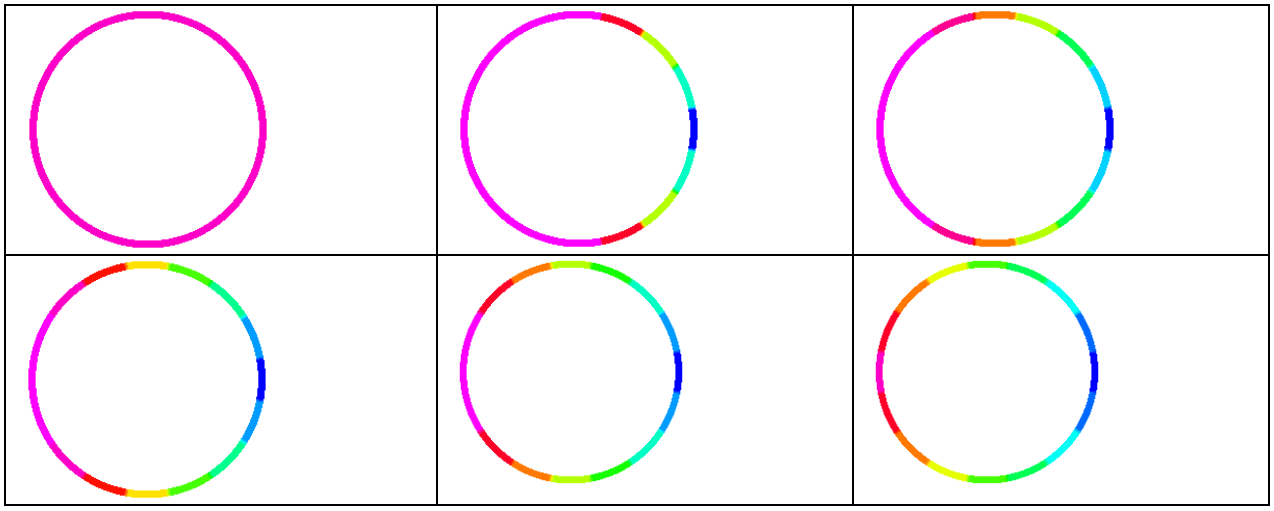

*Figure A.5: Membrane phosphoinositides concentration $\pi$, as a function of cell response time. Top left initial conditions, bottom right final equilibrium state.*

**Cell Cycle Biochemistry Model**

During the second year of the BioCOMP Program CFDRC and LBL discussed best methods for coupling the Bio-SPICE biochemistry problems described with ODEs and multidimensional cell biophysics described with PDEs. To evaluate computational algorithms needed for that coupling CFDRC has stared an effort to link simple metabolic pathways (ODEs) with multidimensional cell morphology and geometry (PDEs). We have chosen Yeast cell cycle model as a test case and ACE+ Multiphysics as the simulation software.

The usual form for the cell cycle models is identification of relevant CDKs, catalytic agents and other enzymes, and their effects on various stages in the cell cycle, such as G1 phase, S phase and so on. The models involve rate expressions for change in the level of these chemical agents, in the form of ODEs, which are interdependent via concentration dependent rate constants. We have incorporated a robust, coupled ODE solver in ACE+ for the modeling of cell cycle, expressed in the rate expression form. As an example, we simulated the fission yeast cell cycle developed by A. Sveiczer, John Tyson and others [Sveiczer 2001]. The model includes eleven ordinary differential equations and several rate functions.

We simulated the 'wild' type cell cycle as well as several mutant cycles involving changes in the rate constant expressions in some of the key CDKs. Figure A.6 below shows the calculated concentration-time variation of several of the CDKs and other relevant enzymes during the cell cycle of the wild type fission yeast cells. These compare well with the results from the original reference [Sveiczer 2001].

Table below presents the cell cycle model, in terms of the rate equations (Sveiczer 2001):

*Table A.1: Cell Cycle Model*

$$\frac{d}{dt}Rum1 = k_s - k_6'\cdot Rum1 - k_{1'}\cdot(MPF_a + \alpha_1\cdot SK\cdot mass)\cdot Rum1 + (k_{1P}' + k_{1P}\cdot PP)\cdot Rum1P - k_J\cdot MPF\cdot Rum1 + k_{JR}\cdot CR + k_{2c}\cdot CR$$

$$\frac{d}{dt}Rum1P = k_{1'}\cdot(MPF_a + \alpha_1\cdot SK\cdot mass)\cdot Rum1 - (k_{1P}' + k_{1P}\cdot PP)\cdot Rum1P - (k_6' + k_6)\cdot Rum1P + k_J\cdot MPF\cdot Rum1P + k_{JR}\cdot CRP + k_{2c}\cdot CRP$$

$$\frac{d}{dt}CR = k_J\cdot MPF\cdot Rum1 - k_{JR}\cdot CR - k_{2c}\cdot CR - k_6'\cdot CR - k_{1'}\cdot(MPF_a + \alpha_1\cdot SK\cdot mass)\cdot CR + (k_{1P}' + k_{1P}\cdot PP)\cdot CRP$$

$$\frac{d}{dt}CRP = k_{1'}\cdot(MPF_a + \alpha_1\cdot SK\cdot mass)\cdot CR - (k_{1P}' + k_{1P}\cdot PP)\cdot CRP + k_J\cdot MPF\cdot Rum1P - k_{JR}\cdot CRP - k_{2c}\cdot CRP - (k_6' + k_6)\cdot CRP$$

$$\frac{d}{dt}MPF = k_1\cdot mass - k_2\cdot MPF - k_{Wee}\cdot MPF + k_{C25}\cdot preMPF - k_J\cdot MPF\cdot(Rum1 + Rum1P) + k_{JR}\cdot(CR + CRP) + k_6'\cdot CR + (k_6' + k_6)\cdot CRP$$

$$\frac{d}{dt}preMPF = k_{Wee}\cdot MPF - k_{C25}\cdot preMPF - k_2\cdot preMPF$$

$$\frac{d}{dt}Ste9 = (k_{Ste9R}' + k_{Ste9R}\cdot PP)\cdot\frac{1 - Ste9}{J_{Ste9R} + 1 - Ste9} - k_{Ste9}\cdot(MPF_a + SK\cdot mass)\cdot\frac{Ste9}{J_{Ste9} + Ste9}$$

$$\frac{d}{dt}Mik1 = (k_1' + k_{MR}' + k_{MR}\cdot PP)\cdot\frac{1 - Mik1}{J_{MikR} + 1 - Mik1} - k_M\cdot MPF_a\cdot\frac{Mik1}{J_{Mik} + Mik1}$$

$$\frac{d}{dt}Wee1 = (k_{WR}' + k_{WR}\cdot PP)\cdot\frac{1 - Wee1}{J_{WeeR} + 1 - Wee1} - k_W\cdot MPF_a\cdot\frac{Wee1}{J_{Wee} + Wee1},\quad \frac{d}{dt}Cdc25 = k_{25}'\cdot MPF_a\cdot\frac{1 - Cdc25}{J_{25} + 1 - Cdc25} - (k_5' + k_{25R}' + k_{25R}\cdot PP)\cdot\frac{Cdc25}{J_{25R} + Cdc25}$$

$$\frac{d}{dt}Slp1 = k_{ai}\cdot MPF_a - k_{ad}\cdot Slp1,\quad \frac{d}{dt}Slp1_a = (k_{ai}' + k_{ai}\cdot MPF_a)\cdot(Slp1 - Slp1_a) - k_{ai}\cdot Slp1_a - k_{ad}\cdot Slp1_a,\quad \frac{d}{dt}Inh = k_3 - k_7\cdot Inh\cdot PP + k_{IR}\cdot PI - k_4\cdot Inh$$

$$\frac{d}{dt}PI = k_7\cdot Inh\cdot PP - k_{IR}\cdot PI - k_4\cdot PI,\quad \frac{d}{dt}mass = \mu\cdot mass,\quad \frac{d}{dt}R_{DNA} = \frac{K}{1 + Y\cdot MPF_a}$$

Rate functions

$k_2 = V_2' + V_2\cdot Ste9$, $k_{2c} = V_{2c}' + V_{2c}\cdot Ste9$, $k_{Wee} = V_{Wee}'\cdot Wee1 + V_{Wee}'(1 - Wee1) + V_{Mik}\cdot Mik1 + V_{Mik}'(1 - Mik1)$, $k_{C25} = V_{25}'\cdot Cdc25 + V_{25}''(1 - Cdc25) + V_{Pyp}\cdot Pyp3$, $k_4 = V_4' + V_4''\cdot Slp1_a$

Auxiliary functions†

$MPF_a = MPF + \alpha\cdot preMPF$, $PP = 1 - PI$

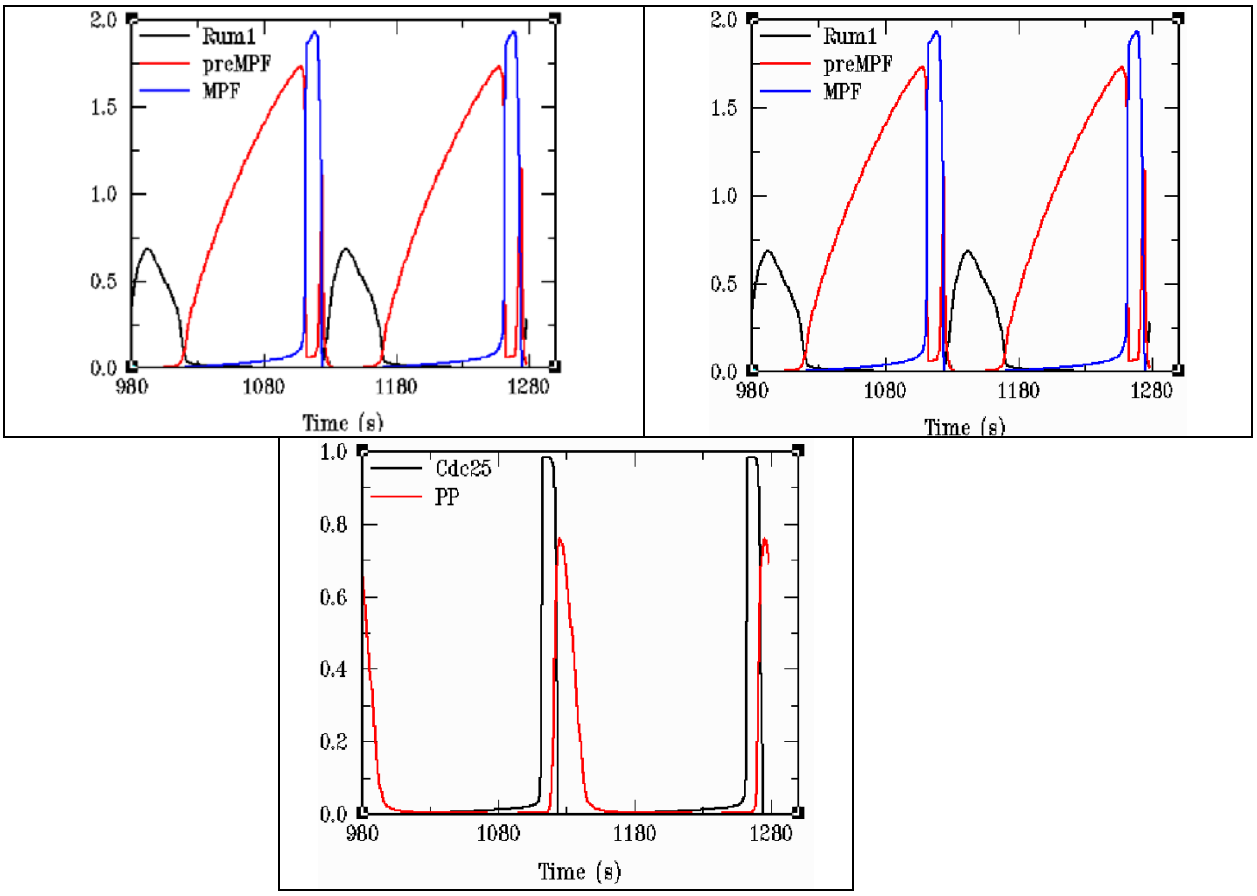


*Figure A.6: CFDRC simulation results for time-variation of various chemical species in the yeast cell cycle model*

**Multidimensional Modeling of Bacterial Sporulation Biophysics**

The common accepted model to understand the cell division process is focusing on the behaviors of **Min** proteins and Z-rings inside cell and along cell membrane [Meinhardt 2001, Howard 2001]. According to this pole-to-pole model, the proteins, MinC, MinD and MinE, etc. inside the cell oscillate from one side to another. The MinE protein forms in the center of the cell along the membrane at the beginning of oscillation. Once MinE forms it will chase the MinC/D proteins staying on the one pole of cell. Mean time ions inside cell form one Z-ring, Ftsz ring, along cell membrane. They shrink toward the center point of cell. MinC/D will be pressed to diffuse into other pole of cell slowly. When MinE reaches the pole, it disappears while MinC/D located on the other side of cell and FtsZ ring divides the cell into two identical daughter cells. This process will continue to both daughter cells.
Figure *A.7*a below shows the cell structure, mins proteins and FtsZ ring and
Figure *A.7*b shows the formation and motion of FtsZ ring [Lutkenhaus 1997, Erickson 2001].

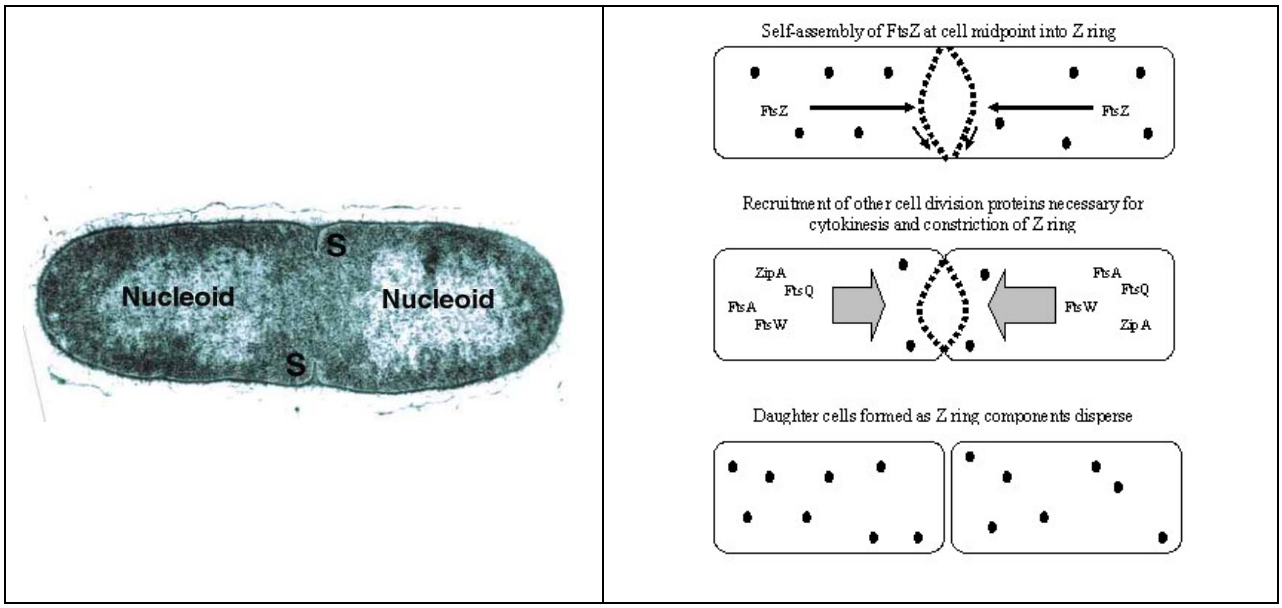


*Figure A.7: Image of bacterial bell early in the sporulation event and an oscillatory behavior of Min proteins and formation FtsZ ring, [Lutkenhaus 1997, Erickson 2001].*

.

During the first year of the BioCOMP Program CFDRC has implemented a 2D model of bacterial sporulation. We followed the 1D approach recently proposed for FtsZ ring formation and sporulation for *E Coli* [Howard 2001]. In the model description below the "Mins" proteins bounded by membrane are denoted by *D, E* and *F* while the "Mins' proteins of free form are denoted by *d, e,* and *f.* The letters *D (d), E (e)* and *F (f)* mean MinD, MinE and FtsZ respectively. The transportations of those three species are governed by the following reaction-diffusion equations in multi dimension form:

$$\frac{\partial F}{\partial t} = \rho_F f \frac{F^2 + \sigma_F}{1 + \kappa_F F^2} - \mu_F F - \mu_{DF} DF + \frac{\partial}{\partial x_i} \Gamma_F \frac{\partial F}{\partial x_i} \tag{A.1}$$

$$\frac{\partial f}{\partial t} = \sigma_f - \rho_F f \frac{F^2 + \sigma_F}{1 + \kappa_F F^2} - \mu_f f + \frac{\partial}{\partial x_i} \Gamma_f \frac{\partial f}{\partial x_i} \tag{A.2}$$

$$\frac{\partial D}{\partial t} = \rho_D d(D^2 + \sigma_D) - \mu_D D - \mu_{DE} DE + \frac{\partial}{\partial x_i} \Gamma_D \frac{\partial D}{\partial x_i} \tag{A.3}$$

$$\frac{\partial d}{\partial t} = \sigma_d - \rho_D d(D^2 + \sigma_D) - \mu_d d + \frac{\partial}{\partial x_i} \Gamma_d \frac{\partial d}{\partial x_i} \tag{A.4}$$

$$\frac{\partial E}{\partial t} = \rho_E e \frac{D}{1 + \kappa_{DE} D^2} \frac{E^2 + \sigma_E}{1 + \kappa_E E^2} - \mu_E E + \frac{\partial}{\partial x_i} \Gamma_E \frac{\partial E}{\partial x_i} \tag{A.5}$$

$$\frac{\partial e}{\partial t} = \sigma_e - \rho_E e \frac{D}{1 + \kappa_{DE} D^2} \frac{E^2 + \sigma_E}{1 + \kappa_E E^2} - \mu_e e + \frac{\partial}{\partial x_i} \Gamma_e \frac{\partial e}{\partial x_i} \tag{A.6}$$

Where, $\rho$ is catalytic production rate, $\sigma$ is constant production rate, $\kappa$ is saturation and mutual interference, $\mu$ is decay rate, $\Gamma$ is diffusion coefficient. The index denotes the corresponding species. The distributions of proteins will be given by solving equations A.1 to A.6. The cell division process will be solved by geometry deformation approach. Figure A.8 presents conceptual representation of *Bacillus Subtilis* cell division process and a 2D computational mesh used for parametric simulations.

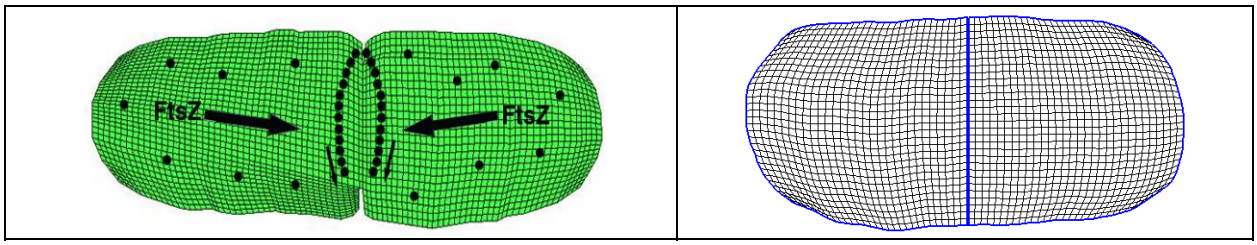


*Figure A.8: E-Coli cell geometry and mesh.*

In order to avoid the singularity of geometry during the cell deformation, we create a very tiny flat region in the center of cell where FtsZ ring will stay and shrink. The initial protein locations are shown below. Figure A.9 shows the oscillation history of MinD protein and cell deformation. At the final stage the septum is completely closed.

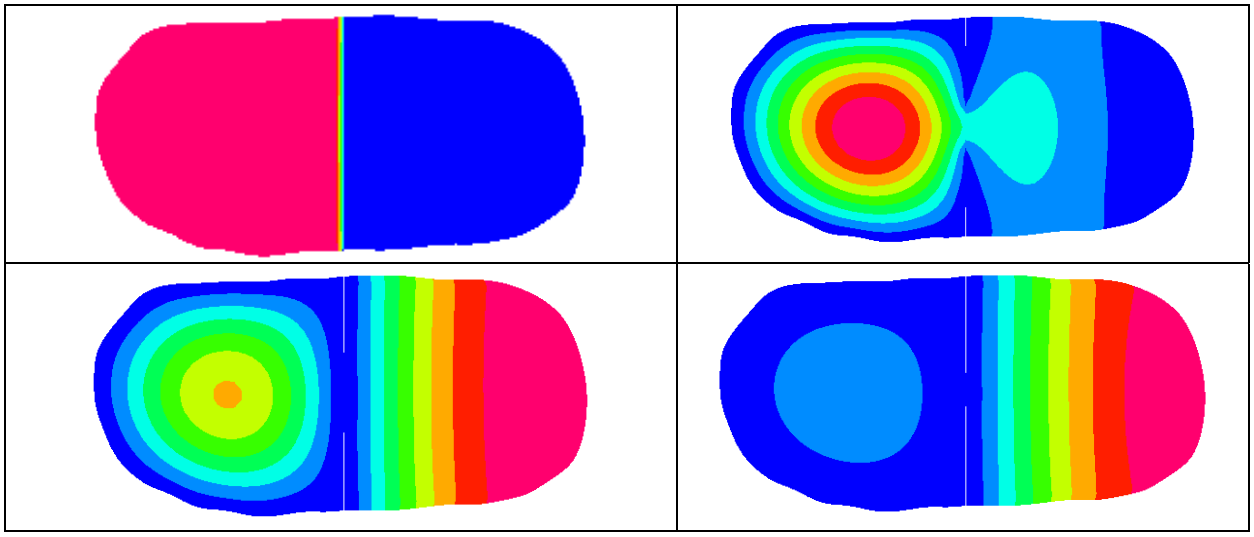

*Figure A.9: Predicted concentration oscillation history of MinD protein and cell deformation.*

**Polarization and Oscillations during E Coli Cell Division**

Bacterial cell division is driven by the formation of a contractile FtsZ protein ring at the cell division site. Proper placement of the FtsZ , a special ring formed at the cell midpoint between segregating daughter chromosomes, is mediated by two mechanisms, 1) nucleoid occlusion, and 2) MinC, Mind, MinE protein system spatiotemporal oscillation. In *E. coli* during each oscillation period MinD accumulates in the cell membrane in a ‘‘polar zone’’ at one end of the

cell. This polar zone then shrinks toward the end of the cell as a new accumulation forms at the opposite pole. MinC follows the same pattern as MinD, and the two proteins form complexes on the membrane. In contrast, MinE forms a ring at the boundary of the MinD polar zone with some MinE dispersed throughout the polar zone. The MinE ring moves toward the end of the cell as the MinD polar zone shrinks. Figure A.10 presents the life cycle and division of E. coli.

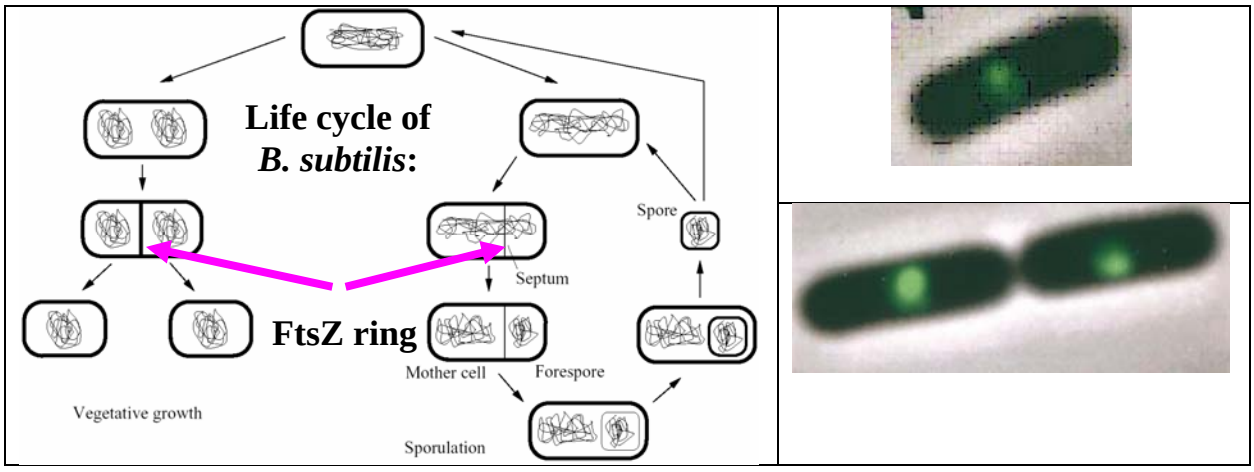


*Figure A.10: Schematic and a microcopy image illustration of life cycle and division of E. coli.*

Three models of the Min protein oscillations have been recently proposed: Howard (2001), Meinhardt (2001), and Huang (2003). All of these models successfully generate oscillations, but none can be meaningfully compared with *in vivo* observations.

**Meinhardt (2001) model** used six 1D diffusion-reaction equations for MinC, D, E at the membrane and Minc, d, e, in the cytoplasm. The model requires newly synthesized protein to form both the MinD polar zones and MinE ring, because the proteins disappear (are degraded) from the simulation on dissociation from the membrane. This is not fully confirmed in experiments. That model also arbitrarily assumes that MinE attaches preferentially to an intermediate concentration of MinD.

**The model of Howard (2001)** produces oscillations only if MinE is driven onto the membrane by cytoplasmic MinD, despite evidence that MinE is recruited to the membrane-by-membrane-associated MinD. In addition the model predicts oscillations that have the opposite dependence of frequency on MinD concentration than is observed, and MinD forms a medial band that moves toward the end of the cell, contrary to the experimental observation that MinD forms directly as a polar zone.

**In Hwang (2003) model** the oscillations are driven by hydrolysis of ATP: (1) MinD binds ATP and the complex binds to the membrane; (2) MinE binds to the MinD:ATP, induces ATP hydrolysis, and all constituents are released from the membrane; (3) MinD:ADP releases ADP, completing the cycle. This is the only model using cell bioenergetics of ATP.

The equation system used in the Meinhardt de Boer (2001) model is presented in table below.

Note that the membrane bound proteins are: Min*D*, *E* and *FitsZ* and the free intracellular proteins are Min*d*, *e* and *f*.

*Table A.2: Equation system used in the Meinhardt de Boer (2001) Model.*

| | |
|---|---|
| **FitsZ** | $\frac{\partial F}{\partial t} = \nabla(\Gamma_F \nabla F) + \rho_F f \frac{F^2 + \sigma_F}{1 + \kappa_F F^2} - \mu_F F - \mu_{DF} DF$ |
| **FitsZ** | $\frac{\partial f}{\partial t} = \nabla(\Gamma_f \nabla f) + \sigma_f - \rho_F f \frac{F^2 + \sigma_F}{1 + \kappa_F F^2} - \mu_f f$ |
| **MinD** | $\frac{\partial D}{\partial t} = \nabla(\Gamma_D \nabla D) + \rho_D d(D^2 + \sigma_D) - \mu_D D - \mu_{DE} DE$ |
| **MinD** | $\frac{\partial d}{\partial t} = \nabla(\Gamma_d \nabla d) + \sigma_d - \rho_D d(D^2 + \sigma_D) - \mu_d d$ |
| **MinE** | $\frac{\partial E}{\partial t} = \nabla(\Gamma_E \nabla E) + \rho_E e \frac{D}{1 + \kappa_{DE} D^2} \cdot \frac{E^2 + \sigma_E}{1 + \kappa_E E^2} - \mu_E E$ |
| **MinE** | $\frac{\partial e}{\partial t} = \nabla(\Gamma_e \nabla e) + \sigma_e - \rho_E e \frac{D}{1 + \kappa_{DE} D^2} \cdot \frac{E^2 + \sigma_E}{1 + \kappa_E E^2} - \mu_e e$ |

Where ρ is catalytic production rate, σ is constant production rate, κ is saturation and mutual interference, and μ is decay rate. The nonlinear kinetics of binding cytoplasmic proteins to the membrane, and an order of magnitude larger cytoplasmic diffusion compared to membrane diffusion result in the spatial oscillations of Min proteins.

The model proposed by Howard (2001) uses only four coupled reaction diffusion equations describing respectively the concentrations of proteins MinD in the cytoplasm, Mind on the membrane, MinE in the cytoplasm and Mine on the membrane. The model does not have explicit conservation equation for FitsZ. Table below presents the equation system for the Howard model.

*Table A.3: Equation system for the Howard Model.*

| | | |
|---|---|---|
| **MinD binding MinE to membrane MinD recruits MinE to membrane** | $\frac{\partial D}{\partial t} = \Gamma_D \nabla^2 D - \frac{\sigma_1 D}{1 + \sigma'_1 e} + \sigma_2 e \cdot d$ | **MinD expels MinE Into cytoplasm** |
| | $\frac{dd}{dt} = \frac{\sigma_1 D}{1 + \sigma'_1 e} - \sigma_2 e \cdot d$ | |
| | $\frac{\partial E}{\partial t} = \Gamma_E \nabla^2 E - \sigma_3 D \cdot E + \frac{\sigma_4 e}{1 + \sigma'_4 D}$ | |
| | $\frac{de}{dt} = \sigma_3 D \cdot E - \frac{\sigma_4 e}{1 + \sigma'_4 D}$ | |

The model proposed by Huang (2003) is also using only MinD and MinE proteins but it includes the ATP hydrolysis driven membrane binding kinetic mechanism. The specific interactions of the Huang model are shown schematically in Figure A.11. The oscillations are driven by a cycle in which MinD:ATP complex first associates with the membrane, preferentially where other MinD:ATP is located. MinE then attaches to the MinD:ATP, activates ATP hydrolysis, and MinE and MinD:ADP reenter the cytoplasm in a 1:1 ratio. The equations describing the time evolution of MinD and MinE concentrations in a cylindrical cell are shown in Figure A.11.

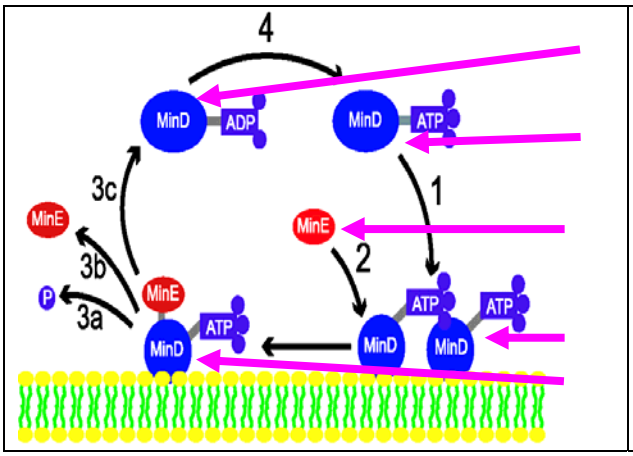


$$\frac{\partial D:ADP}{\partial t} = \Gamma_D \nabla^2 D:ADP - k_4 D:ADP + k_{3c}{}^m de$$

$$\frac{\partial D:ATP}{\partial t} = \Gamma_D \nabla^2 D:ATP - k_4 D:ADP - [k_1{}^m + k_1{}^{'m}(d+de)]\cdot$$

$$\frac{\partial E}{\partial t} = \Gamma_E \nabla^2 E + k_{3b} de - k_2{}^m d \cdot E$$

$$\frac{\partial d}{\partial t} = -k_2 dE + [k_1{}^m + k_1{}^{'m}(d+de)]\cdot D:ATP$$

$$\frac{\partial de}{\partial t} = -k_3{}^m de + k_2{}^m d \cdot E$$

*Figure A.11: Schematic and a microcopy image illustration of life cycle and division of E. coli. Shown are equations A.7 thru A.10, Huang 2003.*

During this project we have used both CFD-ACE+ and the Membrane Model software (later also repeated with CoBi tools) to test all three models and we have reproduced their behavior. The 3D model was used to assess the scalability of the code and to explore potential anomalous and interesting behavior of the models for 3D bacterial cell geometries.

Figure A.12 presents example simulations results for *E. Coli* polar oscillations of Min proteins obtained for 1D and for 3D cell geometries. The model was setup as a transient reaction-diffusion problem with coupled equation systems for cytoplasmic and membrane bound Min proteins. As shown in Figure A.12 our model properly predicted unstable oscillations of MinE and MinE proteins and focusing of FtsZ protein near the center of the cell, septum formation site. When the model was run in 3D configuration with a rod like bacterium we have noticed an interesting pattern of not only axial instabilities but also circumferential instabilities as well. Figure A.12 b presents an FtsZ protein concentration on the bacterial membrane.

Notice that the code properly predicts maximum concentration in the middle of the cells but it also shows that FtsZ is initially preferentially focusing at a point on the membrane. We observe that the focus point is circumferentially moving on the membrane surface. This has not been reported in the literature before.

The results obtained with the Membrane Model software have later been successfully reproduced with the CoBi code. CoBi has the potential to predict experimentally observed formation of spiral arrays of Min proteins on the inner side of the cell membrane.

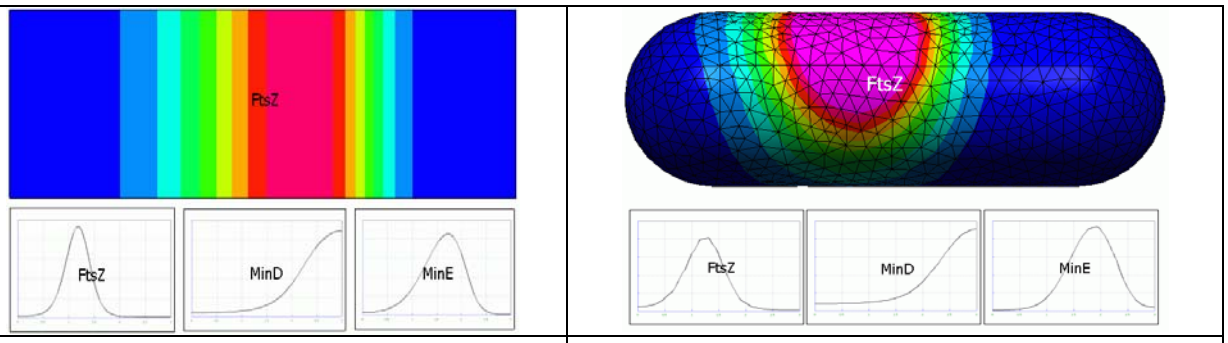


| 1D Solution (PNAS 2001) | 3D Solution (CFDRC 2004) |
|---|---|

*Figure A.12: 1D and 3D simulation results for the bacterial oscillations of Min proteins during bacterial division. Results obtained with the membrane model (later reproduced with the CoBi code).*

One of the major challenges in computational spatial cell biology is the solution- and time-dependent geometry of the dividing cell. We decided to demonstrate the CoBi code on modeling an idealized problem involving cell division, transient diffusion of membrane receptors and simple external ligand cell receptor binding kinetics. Figure A.13 presents two time instants of the membrane geometry and unstructured deforming mesh just prior to division initiation and at the cell separation instance. Note that during the division process surface receptors diffuse between two parts of the membrane. Figure A.14 presents selected snapshots of the membrane receptor concentration color maps during the cell division.

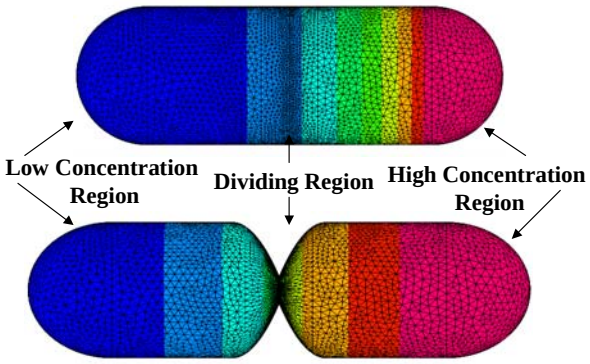


*Figure A.13: Bacterial cell division simulation with the membrane model of the Bio-SPICE cell biology framework.*

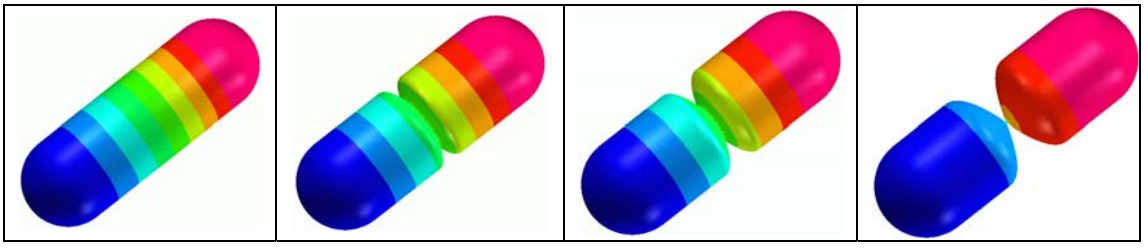

*Figure A.14: Transient distributions of membrane receptors during bacterial cell division.*

**Bacterial Chemosensing and Chemotaxis**

During this project CFDRC and LBL selected bacterial chemotaxis as the most challenging example of spatiotemporal cell biology. Figure A.15 schematically illustrates E. Coli chemotaxis signaling pathways and their spatial intracellular locations. Mathematical modeling of bacterial chemotaxis would need to integrate several biophysical and biochemical phenomena such as: signaling pathways, energetics, intracellular diffusion, molecular motor chemo-mechanics, and flagella propulsion and bacteria dynamics in bio films with spatial chemoattractant gradients. Following is the description of the salient features of the model and simulation results of model components.

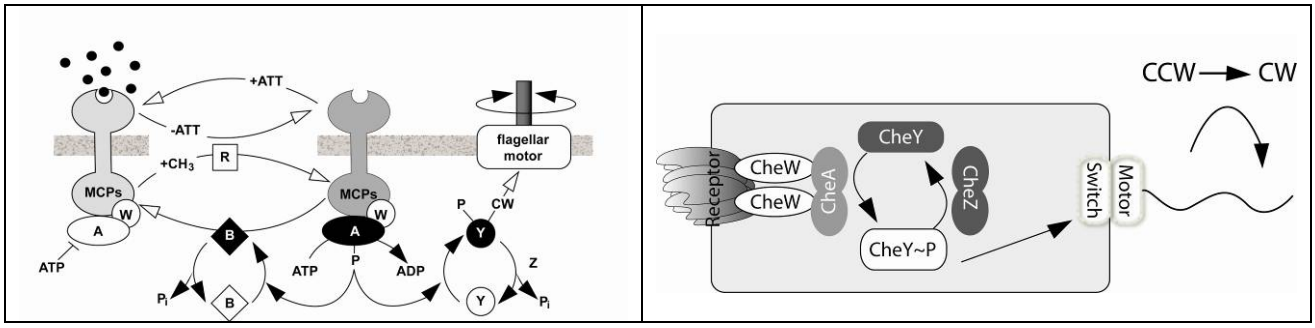


*Figure A.15: Schematic of signaling pathways for E Coli chemotaxis. [Eisenbach 2001, Spiro 1997].*

The bacterial motion is driven by the rapid rotation of helical flagellar filaments that protrude from the cell wall. Flagellum rotation is driven by a motor located in the cell wall at the aft side of the cell. The motors are powered by the chemo-mechanical reactions and resultant flux of ions (H+, Na+) across the plasma membrane. In an isotropic environment a bacterium swims about in a random walk produced by alternating episodes of

- **Runs**, counterclockwise (**CCW**) rotation of the flagellum and motor, and
- **Tumbles**, clockwise (**CW**) flagellar rotation.

In a field of chemoattractant gradient, the cell uses multiple transmembrane chemoreceptors (e.g. methyl-accepting chemotaxis proteins –MCPs) to bind ligands on the periplasmic side. Binding events stimulate cascades of cytoplasmic signaling reactions, which create functionalized chemicals that extend the duration of runs (duration of CCWs) that happen to carry it in favorable directions.

The cytoplasmic signaling cascade is initiated close to the MCPs where several proteins (CheA, CheY, CheZ) are activated by methylation and phosphorylation events, some of which (CheY) move to the aft part of the cell to communicate with the flagellar motors via a phosphorelay sequence. Figure A.15 (above) illustrates potential mechanisms of chemotactic signaling in E. coli. Detailed discussions of the mechanism and mathematical model have been published [Spiro 1997].

During the BioCOMP Program we have modeled two signaling pathways for E coli proposed by:

- {**SPO**} Spiro, Parkinson, and Othmer, PNAS July, 1997, and
- {**ASBT**} Almogy, Stone, and Ben-Tal, Biophysical J., Dec. 2001.

We have extended the ASBT model to multidimensional form by implementing diffusive flux of CheY and CheYP within the bacterial cytoplasmic space. We present comparison of ODE and PDE models.

SPO Model

The signaling mechanism of the SPO model is illustrated in Figure A.15 (above) and schematically in Figure A.16. The corresponding reaction mechanism is summarized in the table below:

*Table A.4: SPO model reaction mechanism.*

| Description | Reaction Labels | Kinetics and rate labels |
|---|---|---|
| Methylation<br>Michaelis-Menten kinetics | $r_1 \ldots, r_4$ | $T_2 + R \underset{k_{1b}}{\overset{k_{1a}}{\Leftrightarrow}} T_2R \xrightarrow{k_{1c}} T_3 + R$ |
| First-order kinetics | $r_1 \ldots, r_4$ | $T_2 + R \xrightarrow{k_{-1}} T_2 + B_p$ |
| Demethylation | $r_{-1} \ldots, r_{-4}$ | $T_3 + B_p \xrightarrow{k_{-1}} T_2 + B_p$ |
| Ligand binding | $r_5, r_6, r_7; r_{-5}, r_{-6}, r_{-7}$ | $T_2\_L \underset{k_{-5}}{\overset{k_5}{\Leftrightarrow}} LT_2$ |
| Autophosphorylation | $r_8, \ldots, r_{13}$ | $T_2 \xrightarrow{k_8} T_{2p}$ |
| Phosphotransfer | $r_t$ | $T_{2p} + B \xrightarrow{k_b} T_2B_p$<br>$T_{2p} + Y \xrightarrow{k_y} T_2 + Y_p$ |
| Dephosphorylation | | $B_p \xrightarrow{k_{-b}} B$<br>$Y_p + Z \xrightarrow{k_{-y}} Y + Z$ |

Here T2, T3, T4 represent methylated states of the Tar chemoreceptors, abbreviations A,B,R,Z are used to denote Che proteins, and subscript p denotes phosphorylated state. In addition there are Tar receptor ligation reactions on the periplasmic side. Figure A.16 presents complete schematic of the reaction system. L is the external stimulus to which the system must adapt.

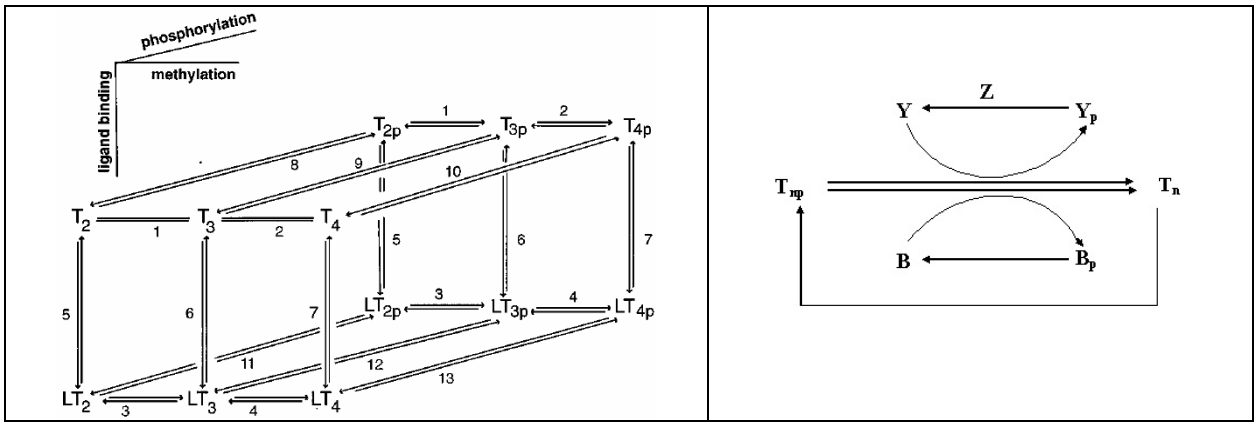


*Figure A.16: Ligand-binding, phosphorylation, and methylation reactions of the Tar–CheA–CheW complex, and detail of the phosphotransfer reactions, Spiro 1997.*

The dependent variables to be solved by the differential equations are:
T2,T3,T4, LT2,LT3,LT4, T2P,T3P,T4P, LT2P,LT3P,LT4P, YP, and BP.

Example species conservation equations are:

$$\frac{dT_2}{dt} = \underbrace{-Lk_5T_2 + k_{-5}LT_2}_{\text{Ligand binding/release}} - \underbrace{k_8T}_{\text{Phosphorylation}} + \underbrace{k_yT_{2p}\left(Y_c - Y_p\right) + k_bT_{2p}\left(B_c - B_p\right)}_{\text{Phosphotransfer}}$$
$$- \underbrace{k_{1c}R\frac{T_2}{k_{1b}/k_{1a}+T}}_{\text{methylation}} + \underbrace{B_pk_{-1}T_3}_{\text{Demethylation}} \qquad \text{(A.11)}$$

We write the equations for $\text{CheY}_\text{p}$ and $\text{CheB}_\text{p}$ as

$$\frac{dY_p}{dt} = k_yT_p\left(Y_c - Y_p\right) - k_{-y}ZY_p \qquad \text{(A.12)}$$

$$\frac{dB_p}{dt} = k_bT_p\left(B_c - B_p\right) - k_{-b}B_p \qquad \text{(A.13)}$$

where TP is the level of total phosphorylated receptor complex:

$$T_p \equiv T_{2p} + LT_{2p} + T_{3p} + LT_{3p} + T_{4p} + LT_{4p} \qquad \text{(A.14)}$$

We have made use of the conserved quantities

$$T_c \equiv T_2 + LT_2 + T_3 + LT_3 + T_4 + LT_4 + T_{2p} + LT_{2p} + T_{3p} + LT_{3p} + T_{4p} + LT_{4p} \qquad \text{(A.15)}$$

$$Y_c \equiv Y + Y_p \qquad (5.17) \qquad \text{and} \qquad B_c \equiv B + B_p \qquad \text{(A.16)}$$

Note that CheY and CheYP are the two key species that diffuse through the cytoplasm from the sensing (chemoreceptor) side of the bacteria to the aft (motored) side.

ASBT Model

This model has been formulated and demonstrated by in:
Gal Almory, Lewi Stone and Nir Ben-Tai, "Multi-State Regulation, a Key to Reliable Adaptive Biochemical Pathways", Biophysical Journal 81, pp3016-3028, Dec., 2001.

The Chemotaxis signaling mechanism of the ASBT model is:

$$\begin{aligned}
&\mathrm{Re}ceptor(active) + CheY \xrightarrow{k_1} CheY_p + \mathrm{Re}ceptor(active)\\
&CheZ + CheY_p + CheZ(active) \xrightarrow{e} 2CheZ(active) + CheY_p\\
&CheZ(active) \xrightarrow{f} CheZ\\
&CheZ(active) + CheY_p \xrightarrow{b\cdot k} CheY + p + CheZ(active)\\
&CheAs(free) + CheZ(free) \xrightarrow{c} \{CheAs - CheZ\}\\
&\{CheAs - CheZ\} \xleftarrow{d} CheAs(free) + CheZ(free)\\
&\{CheAs - CheZ\} + CheY_p \xrightarrow{b} CheY + p + \{CheAs - CheZ\}
\end{aligned}$$

The rates equation for $\mathrm{CheY_p}$, $\{\mathrm{CheAs-CheZ}\}$ and $\mathrm{CheZ(active)}$ are as follows:

$$\begin{aligned}
\frac{d(CheY_p)}{dt} &= A(CheY_{total} - CheY_p) - b\cdot CheY_p[\{CheAs - CheZ\} + k\cdot CheZ_{active}]\\
\frac{d(CheAs - CheZ)}{dt} &= c[\frac{A}{k_1} - \{CheAs - CheZ\}]\cdot[CheZ_{total} - \{CheAs - CheZ\}] - d\{CheAs - CheZ\}\\
\frac{d(CheZ_{active})}{dt} &= e(CheZ_{active} + \varepsilon)CheY_p(CheZ_{free} - CheZ_{active}) - f\cdot CheZ_{active}
\end{aligned}$$

Where, A, b etc. are model constants.

We simulate transport of $\mathrm{CheY_p}$ from production site to reduction site in the following diffusion-reaction process:

$$\frac{\partial(CheYp)}{\partial t} = \frac{\partial}{\partial x} D \frac{\partial(CheY_p)}{\partial x} + \dot{R} \qquad \text{(A.17)}$$

Where, D is the diffusivity, $\dot{\mathrm{R}}$ is reaction rate at production site and reduction site respectively. Figure A.17 schematically illustrates spatially polarized locations of the production and consumption of $\mathrm{CheY_p}$ and the central part of the cell where CheYp diffuses through cytoplasm.

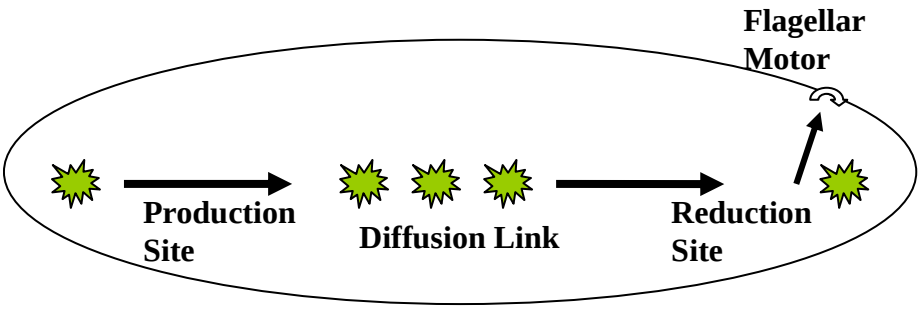


*Figure A.17: Bacterial chemotaxis signal transduction pathway including diffusive transport.*

At the production site, the governing equation for $CheY_p$ is

$$\frac{\partial(CheY_p)}{\partial t} = \frac{\partial}{\partial x} D \frac{\partial(CheY_p)}{\partial x} + A(CheY_{total} - CheY_p) \tag{A.18}$$

$$\dot{R}_1 = A(CheY_{total} - CheY_p) \tag{A.19}$$

At the diffusion link, the governing equation for $CheY_p$ is

$$\frac{\partial(CheY_p)}{\partial t} = \frac{\partial}{\partial x} D \frac{\partial(CheY_p)}{\partial x} \tag{A.20}$$

$$\dot{R}_2 = 0 \tag{A.21}$$

At the reduction site the governing equation for $CheY_p$ is

$$\frac{\partial(CheY_p)}{\partial t} = \frac{\partial}{\partial x} D \frac{\partial(CheY_p)}{\partial x} - b \cdot CheY_p[\{CheAs - CheZ\} + k \cdot CheZ_{active}] \tag{A.22}$$

Let vector Y(3) denote the current (new) concentration of $CheY_p$ at the site 1, 2, and 3. Where the number 1, 2, and 3 means production site, diffusion link and reduction site. With the finite volume(or finite difference) method, we have the matrix for $CheY_p$ :

$$AY = Y^o + dt \cdot \dot{R} \qquad \text{where} \qquad A = \begin{bmatrix} 1+dtD & -dtD & 0 \\ -dtD & 1+2dtD & -dtD \\ 0 & -dtD & 1+dtD \end{bmatrix} \tag{A.23}$$

$Y^o$ is the is the concentration of previous time step and R is the reaction rate defined as:

$$Y^o = \begin{bmatrix} Y^o(1) \\ Y^o(2) \\ Y^o(3) \end{bmatrix} \qquad \dot{R} = \begin{bmatrix} \dot{R}_1 \\ \dot{R}_2 \\ \dot{R}_3 \end{bmatrix} \tag{A.24}$$

D is diffusivity and dt is the time interval.

We have solved the above matrix equation using two approaches:

- Full 1-dimensional model using mesh do represent diffusive fluxes, and
- Three Compartment model by converting diffusive fluxes form PDE form to ODE form for 3 points along the length of bacterium.

In the limiting case the PDE with 3 grid cells should give identical results as the multi compartment ODE model;

Figure A.18 shows the time history of $CheY_p$ at different sites. Figure A.19 shows the comparison between ODE solution of equation (2) and diffusion-reaction equations. We can see that the production site and reduction site clearly make difference. The diffusion-reaction equation should be more accurate to handle the transduction pathways.

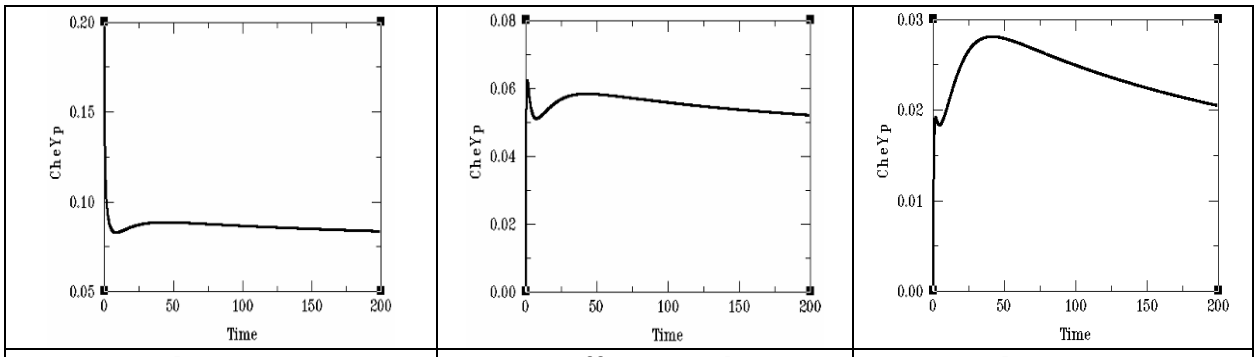


| Production Site | Diffusion Link | Reduction Site |
|---|---|---|

*Figure A.18: Time history of the concentration of $CheY_p$ at three sites along the E Coli body.*

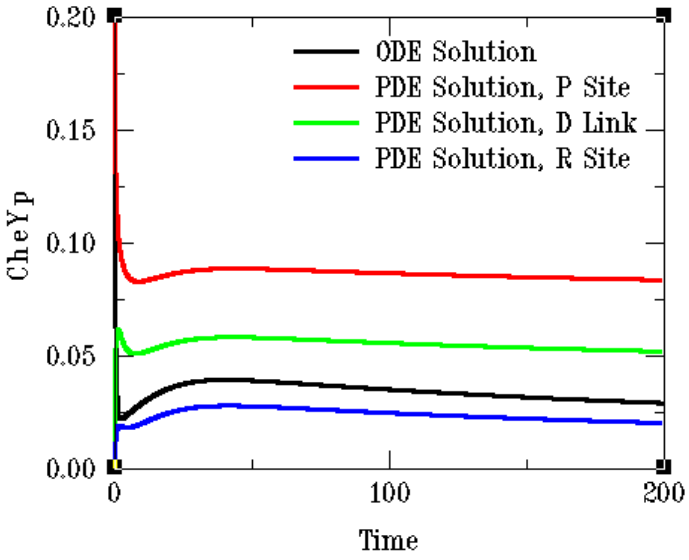


*Figure A.19: Comparison between ODE solution and diffusion-reaction solution.*

Figure A.20 shows the time snapshots of the $CheY_p$ diffusion process.

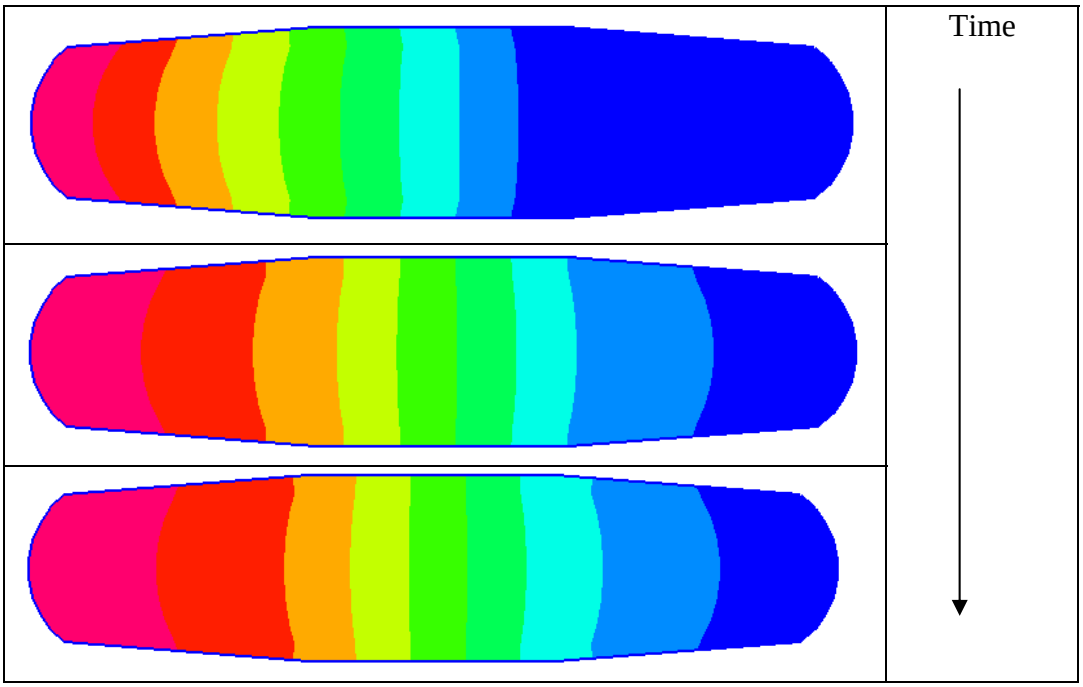


*Figure A.20: Distribution of* $CheY_p$ *within thee coli cytoplasm during the transduction process.*

It should be pointed out since we do not know the rate constants and diffusivity of $CheY_p$, therefore the solutions shown here is need to be verified. What we do is to propose a concept to simulate the process in transduction pathway.

**Three Dimensional Integrated Model of E Coli Chemotaxis**

CFDRC under the DARPA BioCOMP Program has demonstrated a 3D bacterial chemotaxis model within CFD-ACE+ framework. The model combines chemosensing, intracellular signaling, chemo-mechanics of molecular motors, switching mechanism, hydromechanics of flagellar beating, and the dynamics of bacterial body due to propulsive and viscous drag forces and moments.

The flagellar filament, a thin, helical tube, joins the flagellar basal body via a hollow, flexible hook, which acts as a universal joint [Berg 2000]. The hook is connected to the rod, a straight tube that forms the driveshaft. Three rings surround the rotating rod: MS ring in the cytoplasmic membrane, P ring in the peptidoglycan layer, and the L ring in the outer membrane.

Each of the six or so motors on the surface of an E. coli is a cylindrical structure about 50 nm in diameter, is powered by the transmembrane proton motive force, and rotates at more than 100 revolutions per second. It consists of over 40 different kinds of proteins of which MotA and MotB make up a proton channel through the cytoplasmic membrane. The motor-switch complex embedded in the MS ring consists of three proteins FliG, FliM, and FliN that constitute the directional motor switch formed in a characteristic bell-shape structure known as the cytoplasmic

C-ring. The switching is controlled by the concentration of the small diffusible cytosolic protein CheY_P, which binds to FliM.

Flagellar motors of *E. coli* are powered by protons flowing from the periplasm into the cytoplasm down an electrochemical gradient, through the discrete channels (approx 8) in the clearance between stationary Mot and rotating Fli complexes. We understand the structure and function of the flagellar motor but not very much about the details of how it works, or how it accomplishes abrupt switching from forward (CCW) to reverse (CW) rotation.

In molecular and cellular biology compact elegant mathematical models are rare. Theories and models are described in a narrative language based on laboratory observations. A detailed multidimensional mathematical model of cellular chemotaxis, including molecular pathways and biophysical dynamics does not exist. Recent advances in molecular and structural cell biology as well as remarkable interest in computational biology, resulted in series of exiting reports demonstrating successful component models of cell biology. Most outstanding progress has been achieved in computational cellular biochemistry where cell metabolism is described by large systems of ODEs. Some of them, related to *E. Coli* chemotaxis are identified below.

To our knowledge this is the first attempt to integrate the models of biochemical signaling pathways, metabolic pathways, molecular motor functionality, flagella rotation, with the compete bacterial body hydrodynamics. Moving parts of the molecular proton motor are submicroscopic and immersed in a viscous medium (water or lipid), so the Reynolds number is very small and viscous dissipation effects should be included along with electrostatic interactions, protein conformational changes, and proton binding kinetic events as it cascades down in the channel from the periplasm to the cytoplasm.

Computational modeling of bacterial propulsion has been investigated half a century ago by Sir. Geoffrey Taylor in "The Action of Waving Cylindrical Tails in Propelling Microscopic Organisms" Proc Royal Soc. Vol 211, pp 225-239, Feb 1952. Since then several semianalytical models have been presented, not much better than original Taylor's work. Recently Japanese bio-nano consortium, ERATO, led by Prof Keiichi Nanda have presented first 2D axisymmetric model of motile bacterium with a single flagellum using full Navier-Stokes equestrians and moving deforming grid (personal communication between Dr. A. Przekwas CFDRC and Professor Keichi Namba 2005, also http://www.nanonet.go.jp/english/mailmag/2004/011a.html.

During the second year of the BioCOMP Program CFDRC has integrated a complete E Coli chemotaxis model coupling signaling pathways, flagella motors, beating and rotating flagella, and bacterial swimming in a 3D fluid. The present model involves overset mesh for bacterial body, molecular motor and switching sub-models, flagella rotation and large displacement during CCW-CW switch.

We have performed several simulations, created animations, and observed bacterial runs and tumbles. Figure A.21 presents the model definition and example simulation results for a bacterium with a single flagellum and with four flagella. Figure A.22 presents computational simulation results for bacterial micro-hydrodynamics, pressure maps and vorticity isosurfaces at selected time instants during the bacterial run-tumble motion.

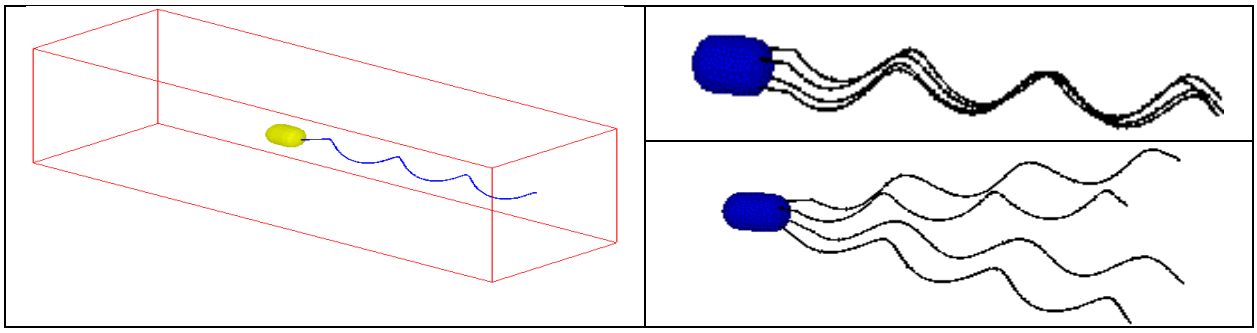

*Figure A.21: Computational model of Motile Bacterium with rotating flagella using full Navier Stokes equations micro-hydrodynamic model and an overset mesh.*

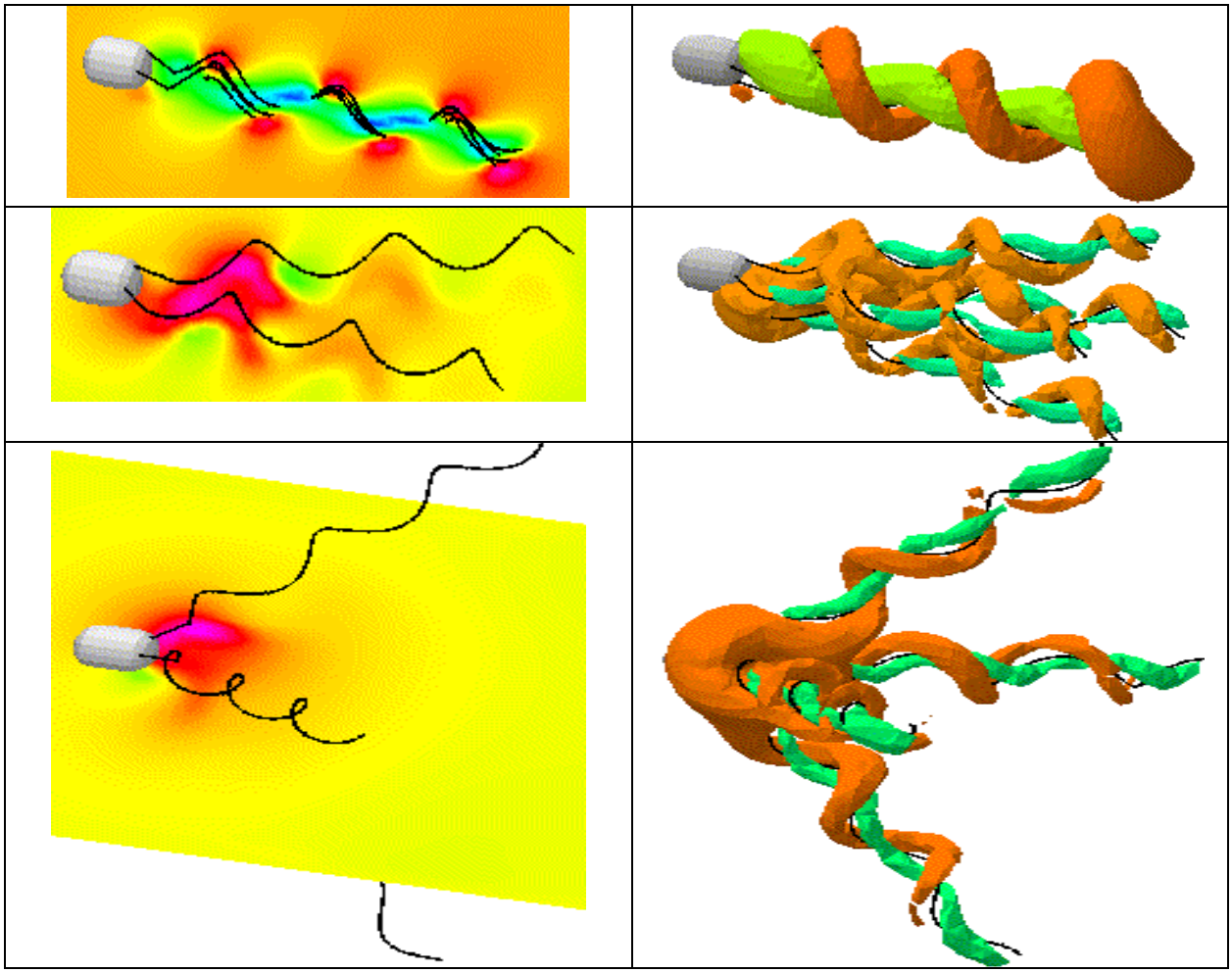

*Figure A.22: Computational simulation results for bacterial micro-hydrodynamics. Pressure maps and vorticity isosurfaces at selected time instants during run-tumble motion.*

**Multivalent Binding**

Interaction of cells with other cells, bacterial membrane attachment, virus endocytosis, and cell interaction with functionalized substratum involves multivalent binding (MVB). Figure A.23 schematically illustrates the concept of multivalent ligands (6 and 12 valent) binding to single and bivalnet receptors on cell or substrate wall.

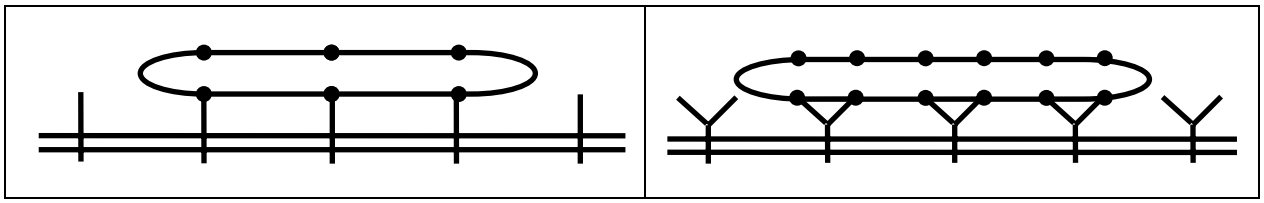

*Figure A.23: A 6 valent ligand binding through 3 sites to single valence cell membrane receptor, and single multivalent ligand bound to bivalent cell membrane receptor (e.g. Ab).*

Multivalent Ligand-Receptor (L-R) binding can be mathematically represented as n-th order chemical kinetics (Laufenburger 1993; Perelson, 1994). Figure A.24 presents the MVB modeling concept for a simple bivalent ligand and for a cell. Note that the binding becomes stronger with more sites attached. Biological; cells (bacteria, immune cells) are using this mechanism for strong attachment to substrates in the flowing media.

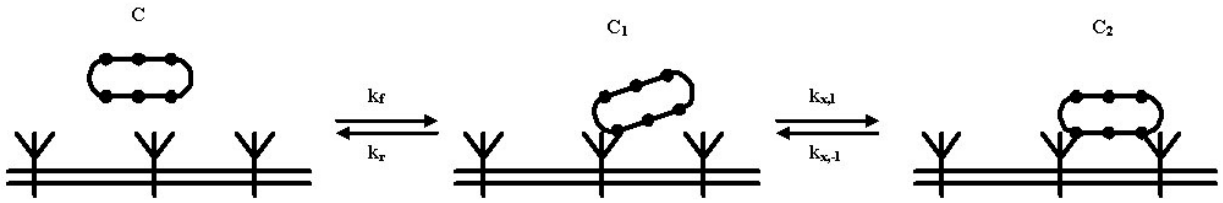


*Figure A.24: Chemical kinetics model of a binding of a globular multivalent ligand (or a cell) to trivalent surface receptors*

To date MVB events have been modeled in ODE framework using n-order kinetics. Until this project only monovalent ligand-receptor (L-R) binding model was available in CFD-ACE+. In this project we have impenitent MVT in both ODE and PDE framework. It will be demonstrated on cell-cell and cell-surface attachment.

When a multivalent ligand of valence 'n' binds to a cell surface, it can attach to the surface at i = 1,…n sites. This different configuration is called as 'molecule bound state'. Let $X_n(i)$ be the concentration of the bound state in which a ligand of valence n is bound to a cell surface receptor at the $i^{th}$ binding site. The general equation that governs the binding reaction rate is given as (Sulzer, 1996; Perelson, 1998):

$$\dot{X}_n(i) = (n-i+1)k_i R X_n(i-1) + (i+1)k_{-(i+1)} X_n(i+1) - \{ik_{-i} + (n-i)k_{i+1}R\}X_n(i), \quad 1 \le i < n-1$$

$$\dot{X}_n(n) = k_n R X_n(n-1) - nk_{-n} X_n(n), \quad i = n$$

Where $k_i$, $k_{-i}$ are the forward and backward (or association and dissociation) rates, and R is the number of receptor sites on the cell surface. Both the total number of receptor sites, $R_T$, and total number of ligands, $X_{nT}$, are conserved. The constraint restrictions on the above equation are:

$$R_T = R + \sum_{i=1}^{n} iX_n(i)$$

$$X_{nT} = X_n(0) + \alpha B \sum_{i=1}^{n} X_n(i)$$

where B is number of cells per unit volume.

If we define the various concentrations as :
Volume concentration : mol/L,
Cell concentration : $(mL)^{-1}$ ,
Surface concentration : $cm^{-2}$,
then

$$\alpha = 10^3 A / N_A \ cm^2 \ mol.$$

where A is the cell mean surface area in $cm^2$, $N_A$ the Avogadro's number, $N_A = 6.023 \times 10^{23} / mol$. Using these definitions, $R_T$ is receptor density per $cm^2$. For a cell with radius of 3.5 μm, the surface area A is $1.5*10^{-6}$ $cm^2$, and the value of $\alpha \approx 2.5 \times 10^{-27}$.

We further define cross-linking affinity, $K_i = \frac{k_i}{k_{-i}}, i > 1$, binding affinity $K = K_1 = \frac{k_1}{k_{-1}}$, and dimensionless cross-linking affinity $\kappa_x = K_x R_T$.

We simulated a test case given by Sulzer (1996) involving binding between an 8-valent ligand and receptors, both for steady state and transient cases. We performed simulations for different values of the key parameters $k_x$ and B, where $k_x$ refer to the cross-linking affinity of the $i^{th}$ valence. For the present calculations, all $k_x$ for all valences were assumed to be the same. Figure A.25 shows the calculated binding states, where i is valence (on the abscissa), and $X_8(i)$ is the binding surface density for valence I (on the ordinate). Results for a range of values of $k_x$ are plotted in Figure A.25; the remaining parameters in these calculations are outlined in the figure caption. We can see that the binding density strongly depends on the parameter $k_x$. This is natural, since $k_x$ is the ratio of forward and backward association and dissociation rates.

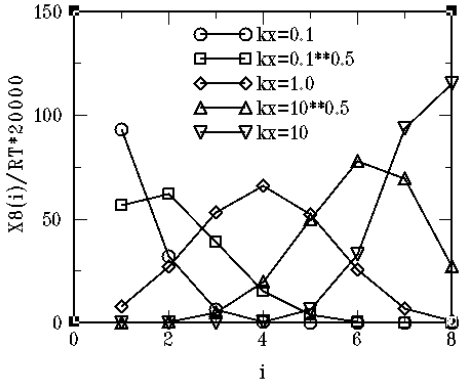


*Figure A.25: Distribution of bound states in the excess receptor regime with different* $\kappa_x$.
*Parameters:* $K = 10^8 M^{-1}, S_T \equiv nX_{nT} = 10^{-10}, R_T = 10^{10} cm^{-2}, \alpha = 10^{-26} cm^2 mol, B = 10^7 / mL.$.

Figure A.26a and Figure A.26b show the transient solutions for two of the cases shown in Figure A.25. The transient results are thus consistent with the steady results shown above for large times. For small cross-linking affinity coefficients, (e.g. 0.1), concentrations of the single bond are highest, while the 8-bond concentrations are highest when the affinity coefficient ratio is large. For the middle-range values of the affinity coefficients, the peak concentrations are at the mid-range of the bond numbers, in the present case at 4-valence, with the single- and 8-bond concentrations both very low.

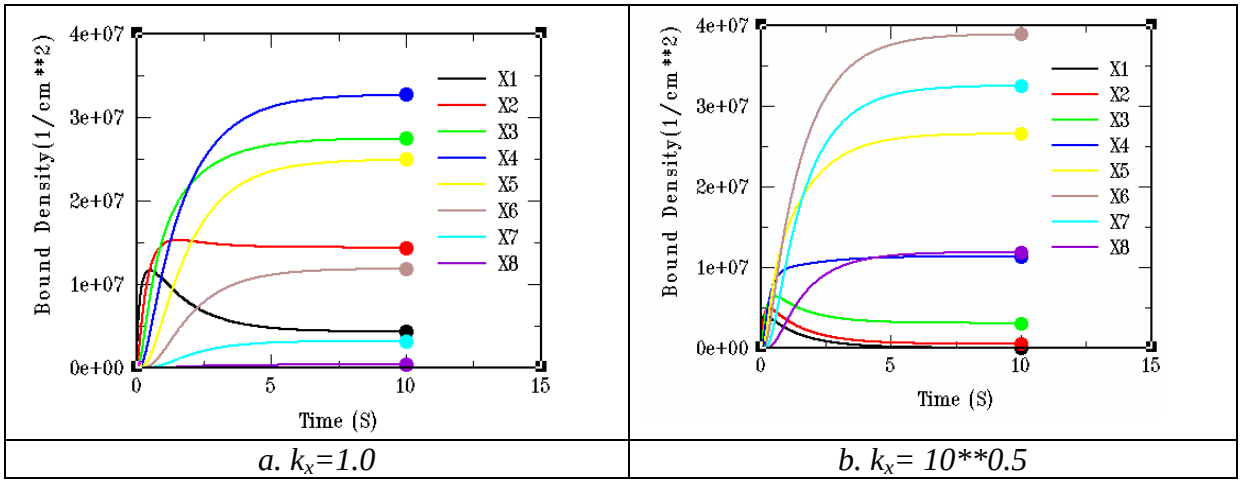


*a. $k_x$=1.0* | *b. $k_x$= 10**0.5*

*Figure A.26: Time history of binding density for each state at two different $k_x$ values. Circles are steady state solutions.*

A methodology for modeling of multivalent binding (MVB) described above was implemented in a biochemistry module (in CFD-ACE+). This methodology is based on solutions of ordinary differential equations (ODEs) that describe the rates of change of concentrations of different chemical species. We have also coupled the MVB calculations with the particle transport model to calculate binding forces on cells as they attach to surfaces and cells using MVB of surface receptors.

# APPENDIX B

## Input Data for Selected Computational Cell and Tissue Biology Test Cases Performed with the CoBi Code and Presented in Chapter 5 of this Report.

This Appendix presents annotated input files , *.SIM, for test cases computed with the CoBi code and described and discussed in Section 5 of this report. Whenever possible, schematics of the test cases are also provided for ready reference and easier interpretation of the input files. After completed simulations, CoBi creates an output file for visualization of the solution results. The output file is created in the **vtk** format (www.**vtk**.org/pdf/file-**format**s.pdf ). The vtk file can be viewed using **VisIt** visualization tools developed by the Lawrence Livermore National Laboratory (www.llnl.gov/**visit**/), or other visualization software.

The line numbers, 01, 02, … shown in the input files for examples below are not needed in the *.SIM file used by the CoBi code. Here they are used only to annotate and explain individual commands of the *.SIM file.

**Diffusion Problem on Planar Square Thin Film -**

```
01      thickness 0.01
02      iteration 10

03      module share
04        vc Membrane const_dens 1

05      module species f1
06        sweeps 500
07        relaxation 0.1
08        vc Membrane const_diff 0.1
09        bc Left fix_value 0.0
10        bc Right fix_value 1.0
11        bc Top fix_flux 0.0
12        bc Bottom fix_flux 0.0
13        bc Membrane_outside fix_flux 0
14        bc Membrane_inside fix_flux 0
```

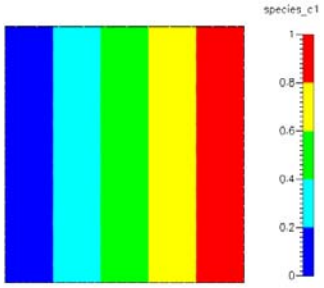


In the input file keyword *thickness* is the membrane thickness. Keyword *iteration* is the number of iterations for the steady state case or each time step. Keyword *transient* is used to set the number of time steps, size of a time step and output frequency. Keyword *module* is used to specify input data for the module. Keyword *share* means that input for shared data, such as density.

Keyword *vc* is used to specify a volume condition followed by a volume name, constant density, and the value. Keyword *species* is used for input of species module. Keyword *sweeps* is used to specify the maximum number of sweeps for the species. Keyword *relaxation* is used to input linear relaxation between a previous value and a new value. The next line *vc* sets the constant diffusivity for volume Membrane. Keyword *bc* means the input for boundary condition followed by boundary name, boundary condition type (fixed value/fixed flux).
Line 01 sets membrane thickness to 0.01;
Line 02 sets number of sub-iteration to 10;
Line 03 declares the start of share module;
Line 04 sets density to 1 for membrane;
Line 05 declares the start of species f1 equation;
Line 06 sets number of iterations for linear equation solver;
Line 07 sets relaxation factor for f1 to 0.1;
Line 08 sets the volume condition (vc) of species diffusivity to 0.1 for membrane;
Line 09-10 set fix concentration 0 on the Left and 1on the Right Boundaries;
Line 11-12 set zero gradient concentration on bottom/bottom surfaces;
Line 13-14 set no flux boundary condition to membrane inside/outside surfaces;

**Diffusion on a Spherical Cell Membrane**

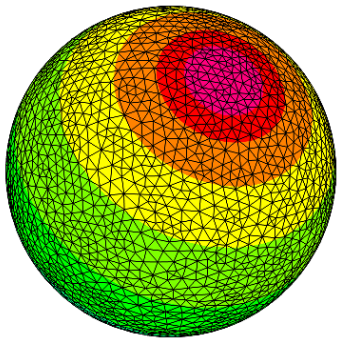

```
01      thickness 0.01
02      iteration 10

03      module share
04       vc Membrane const_dens 1
05       vc Top const_dens 1
06       vc Bottom const_dens 1

07      module species c1
08        vc Membrane const_diff 10
09        vc Top const_diff 10
10        vc Bottom const_diff 10
11        bc Membrane_outside fix_flux 0.0
12        bc Top_outside fix_value 1.0
13        bc Top_inside  fix_value 1.0
14        bc Bottom_outside fix_value 0.0
15        bc Bottom_inside  fix_value 0.0

16      module species c2
17        vc Membrane const_diff 1
18        vc Top const_diff 1
19        vc Bottom const_diff 1
20        bc Membrane_outside fix_flux 0.0
21        bc Top_outside fix_value 0.0
22        bc Top_inside  fix_value 0.0
23        bc Bottom_outside fix_value 1.0
```

```
24      bc Bottom_inside  fix_value 1.0
```

In the file, keyword *"thickness"* is the membrane thickness. Keyword "*iteration"* is the number of estimated iterations to solve a steady state case or for each time step for the transient problem. Keyword "*transient"* is used to set the number of time steps, size of a time step and output frequency. Keyword "*module"* is used to specify input data for the module. Keyword "*share"* means input for shared data, such as density.

Keyword "*vc*" is used to specify a volume condition followed by volume name, constant density and the value.
Keyword "*species*" is used for input of species module.
Keyword "*sweeps*" is used to specify the maximum number of sweeps for the species. Keyword "*relaxation*" is used to input linear relaxation between the previous value and a new value.
The next line "*vc"* sets the constant diffusivity for volume Membrane.
Keyword "*bc*" means the input for boundary condition followed by boundary name, boundary condition type (fixed value/fixed flux).

Line 01 sets membrane thickness to 0.01;
Line 02 sets number of sub-iteration to 10;
Line 03 declares the start of share module;
Line 04-06 set density to 1 for membrane, top and bottom of membrane regions;
Line 07 declares the start of species c1 equation;
Line 08-10 set diffusivity to 1 for the membrane, top and bottom of membrane regions;
Line 11 sets no flux boundary condition to membrane outside surface;
Line 12-13 set fix concentration 1 to top inside and top outside surfaces;
Line 14-15 set fix concentration 0 to bottom inside and bottom outside surface;

Line 16-24 repeat procedure of Line 07-15 for species c2, but the concentration values are set to the values opposite to c1.

**Diffusion-Reaction of a Flat Membrane**

```
01      thickness 1.00
02      iteration 10
03      transient 100 0.01 10

04      module share
05        vc Membrane const_dens 1

06      module species test_f1
07        sweeps 500
08        relaxation 0.1
09        vc Membrane const_diff 0.1
10        bc Left fix_value 0.0
11        bc Right fix_value 1.0
```

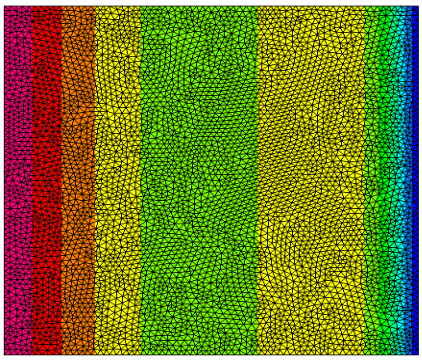

```
12        bc Top fix_flux 0.0
13        bc Bottom fix_flux 0.0
14        bc Membrane_outside fix_flux 0
15        bc Membrane_inside fix_flux 0

16      module species test_f2
17        vc Membrane const_diff 0.1
18        bc Left fix_value 1.0
19        bc Right fix_value 0.0
20        bc Top fix_flux 0.0
21        bc Bottom fix_flux 0.0
22        bc Membrane_outside fix_flux 0
23        bc Membrane_inside fix_flux 0
```

Line 01 sets membrane thickness to 0.01;
Line 02 sets number of sub-iteration to 10;
Line 03 sets number of time steps, time step size and output frequency;
Line 04 declares the start of share module;
Line 05 sets density to 1 for membrane;
Line 06 declares the start of species _f1 equation;
Line 07 sets number of sweeps for the linear solver;
Line 08 sets relaxation for _f1 to 0.1;
Line 09 sets species diffusivity to 0.1 for the membrane;
Line 10-11 set fix concentration to 0 for left boundary and to 1 for right boundary;
Line 12-13 set no flux boundary condition to top and bottom boundaries;
Line 14-15 set no flux boundary condition to outside and inside membrane boundaries;

Line 16-23 repeat procedure of Line06-15 for species _f2, but the concentration values are set to the values opposite to _f1.

**Multicellular Perfused Tissue EGF Signaling**

```
001     iteration 3
002     transient 100 800 1

003     DTF

004     membrane MEM 2e-9 Cell_Gap

005     module share
006       vc Cell const_dens 1000
007       vc Gap  const_dens 1000
008       vc MEM_Cell_Gap const_dens 1000
009       vc MEM_Cell_Gap reaction SignalModel1_Mem euler
010       vc Cell reaction SignalModel1_Vol euler
```

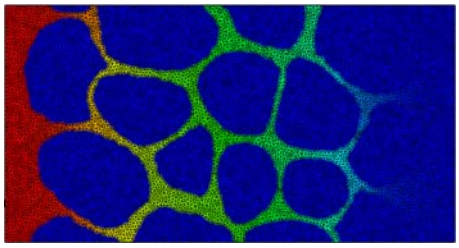

```
011  module flow f
012    sweeps 30 30
013    diagrelaxation .5 .5 .5
014    relaxation 0 0 0 0.2
015    vc Cell const_diff 0.
016    vc Gap  const_diff 1.57e-3
017    vc MEM_Cell_Gap const_diff 0.
018    bc Gap_Inlet  fix_velocity 0.001 0 0
019    bc Gap_Outlet fix_pressure 0.0
020    bc Cell symmetry
021    bc Gap  symmetry
022    bc MEM_Cell_Gap_Gap  fix_velocity 0 0 0
023    bc MEM_side_boundary symmetry

024  module species L
025    sweeps 80
026    vc Cell const_diff 0.
027    vc Gap  const_diff 1.e-16
028    vc MEM_Cell_Gap const_diff 1.e-16
029    bc Gap_Inlet  fix_value 1.e-9
030    bc Gap_Outlet fix_value 0.
031    bc Cell fix_flux 0
032    bc Gap  fix_flux 0
033    bc MEM_Cell_Gap_Cell cg_wall
034    bc MEM_Cell_Gap_Gap  cg_wall
035    bc MEM_side_boundary fix_flux 0

036  module species Li
037    sweeps 80
038    vc Cell const_diff 1.e-16
039    vc Gap  const_diff 0.
040    vc MEM_Cell_Gap const_diff 1.e-16
041    bc Gap_Inlet  fix_value 0.
042    bc Gap_Outlet fix_value 0.
043    bc Cell fix_flux 0
044    bc Gap  fix_flux 0
045    bc MEM_Cell_Gap_Cell cg_wall
046    bc MEM_Cell_Gap_Gap  cg_wall
047    bc MEM_side_boundary fix_flux 0

048  module species Rs
049    sweeps 80
050    vc Cell const_diff 0.
051    vc Gap  const_diff 0.
052    vc MEM_Cell_Gap const_diff 1.e-16
053    bc Gap_Inlet  fix_value 0.
```

```
054     bc Gap_Outlet fix_value 0.
055     bc Cell fix_flux 0
056     bc Gap  fix_flux 0
057     bc MEM_Cell_Gap_Cell cg_wall
058     bc MEM_Cell_Gap_Gap  cg_wall
059     bc MEM_side_boundary fix_flux 0
060     init MEM_Cell_Gap fix_value_bbox 0.05 -2 -2 -2 2 2 2

061   module species Cs
062     sweeps 80
063     vc Cell const_diff 0.
064     vc Gap  const_diff 0.
065     vc MEM_Cell_Gap const_diff 1.e-16
066     bc Gap_Inlet  fix_value 0.
067     bc Gap_Outlet fix_value 0.
068     bc Cell fix_flux 0
069     bc Gap  fix_flux 0
070     bc MEM_Cell_Gap_Cell cg_wall
071     bc MEM_Cell_Gap_Gap  cg_wall
072     bc MEM_side_boundary fix_flux 0
073   module species Ri
074     sweeps 80
075     vc Cell const_diff 1.e-16
076     vc Gap  const_diff 0.
077     vc MEM_Cell_Gap const_diff 1.e-16
078     bc Gap_Inlet  fix_value 0.
079     bc Gap_Outlet fix_value 0.
080     bc Cell fix_flux 0
081     bc Gap  fix_flux 0
082     bc MEM_Cell_Gap_Cell cg_wall
083     bc MEM_Cell_Gap_Gap  cg_wall
084     bc MEM_side_boundary fix_flux 0
085     init MEM_Cell_Gap fix_value_bbox 1.68e-7 -2 -2 -2 2 2 2

086   module species Ci
087     sweeps 80
088     vc Cell const_diff 1.e-16
089     vc Gap  const_diff 0.
090     vc MEM_Cell_Gap const_diff 1.e-16
091     bc Gap_Inlet  fix_value 0.
092     bc Gap_Outlet fix_value 0.
093     bc Cell fix_flux 0
094     bc Gap  fix_flux 0
095     bc MEM_Cell_Gap_Cell cg_wall
096     bc MEM_Cell_Gap_Gap  cg_wall
097     bc MEM_side_boundary fix_flux 0
```

Line 01 sets number of sub-iteration to 3;
Line 02 set number of time steps to 100, time step to 800 and output frequency to 1 time step;
Line 03 sets input file as DTF format (DTF is CFDRC database format);
Line 04 creates membranes between cell and gaps and sets membrane thickness to 2e-9 meter;
Line 05 declares the start of share module;
Line 06-08 set density to 1000 for cells, gaps between cells and membrane
Line 09 sets reaction to membrane signaling model for membrane and implicit Euler method for ODE solver;
Line 10 sets reaction to cell signaling model for cells and implicit Euler method for ODE solver;

Line 11 declares the start of flow module;
Line 12 sets number of sweeps to 30 for both momentum and continuity equations;
Line 13 sets inertia relaxations to 0.5 for momentum equations in x, y, z directions;
Line 14 sets relaxations to 0.2 for pressure equation and 0 to momentum equations;
Line 15-17 set viscosity to 1.57e-3 for gaps in between cells and 0 for inside cells and membranes(means no flow);
Line 18 sets fixed velocity to 0.001 in x direction for boundary Gap_Inlet;
Line 19 sets fixed pressure boundary condition to 0 for boundary Gap_Outlet;
Line 20-21 set top and bottom of cells to symmetrical boundaries;
Line 22 set non-slip wall condition for outside wall of membranes;
Line 23 sets symmetry boundary for rest of boundaries;
Line 24 declares the start of species Ligand equation;
Line 25 sets number of sweeps to 80 for linear equation solver;
Line 26-28 set species diffusivity to 0 for inside cell and 1e-16 for gaps in between cells and membrane;
Line 29-30 set Ligand concentration to 1e-9 at inlet and 0 at outlet;
Line 31-32 set no flux boundaries at top and bottom of cells;
Line 33-34 set permeable wall for membrane inside and outside wall;
Line 35 sets no flux boundary for rest of boundaries;

Line 36-97 repeat procedure of Line24-35 for species Li, Rs, Cs, Ri, Ci, but the diffusivities and boundary conditions are set to the different values.

**Morphogenesis of Yeast Cell**

iteration 5
transient 11500 0.01 50

DTF
movingGrid

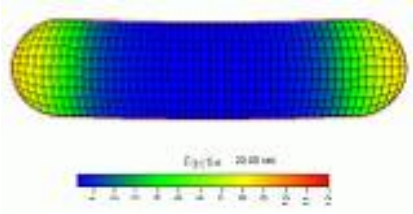

reaction Yeast_Morphogenesis_Model
  method euler
  abs_tolerance 1.e-1
  rel_tolerance 1.e-1

```
  t = mod(time,150)
  ks = t < 115 ? 0.2 : 0.1
  kd = 0.05
  k31 = t<115 ? 6. : 0.
  k32 = t<115 ? 8. : 0.
  k4  = 5.
  ksu = t < 115 ? 0.05 : 0.025
  kdu = 0.05

  v1 = (k31+k32*Fu*Ffactin*Ffactin)*Fgactin
  v2 = k4*Ffactin
  Ffactin' = -kd*Ffactin + v1 - v2
  Fgactin' = ks - kd*Fgactin - v1 + v2
  Fu' = ksu - kdu*Fu

reaction Yeast_Morphogenesis_Model_Mid
  method euler
  abs_tolerance 5.e-1
  rel_tolerance 5.e-1

  t = mod(time,150)
  ks = t < 115 ? 0.2 : 0.1
  kd = 0.05
  k31 = t<115 ? 6. : t>125 ? 50. : 0.
  k32 = t<115 ? 8. : 0.
  k4  = 5.
  ksu = t < 115 ? 0.05 : 0.025
  kdu = 0.05

  v1 = (k31+k32*Fu*Ffactin*Ffactin)*Fgactin
  v2 = k4*Ffactin

  Ffactin' = -kd*Ffactin + v1 - v2
  Fgactin' = ks - kd*Fgactin - v1 + v2
  Fu' = ksu - kdu*Fu

module share
  vc VC const_dens 1
  vc VC reaction Yeast_Morphogenesis_Model

module species Ffactin
  sweeps 30
  vc VC const_diff 1.
  bc BC fix_flux 0
  init VC fix_value 0.0
```

module species Fgactin
  sweeps 30
  vc VC const_diff 120
  bc BC fix_flux 0
  init VC fix_value 0.0

module species Fu
  sweeps 30
  vc VC const_diff 0.5
  bc BC fix_flux 0
  init VC fix_value 0.0

**Rate Equations**

1. $$\phi_{GL\to GP} = \lambda_{MAX,GL\to GP}\frac{1/PS}{1/PS_o + 1/PS}C_{GL}$$

2. $$\phi_{GY\to GP} = \lambda_{MAX,GY\to GP}\frac{1}{1+\frac{PS_o}{PS}+\left(\frac{CS_o}{CS}\right)^2}C_{GY}$$

3. $$\phi_{GP\to PY} = \lambda_{MAX,GP\to PY}\frac{1}{1+\frac{PS_o}{PS}+\left(\frac{1/RS_o}{1/RS}\right)^2}C_{GP}$$

4. $$\phi_{GP\to GY} = \lambda_{MAX,GP\to GY}\frac{1}{1+\frac{1/PS_o}{1/PS}+\left(\frac{1/CS_o}{1/CS}\right)^2}C_{GP}$$

5. $$\phi_{PY\to AC} = \lambda_{MAX,PY\to AC}\frac{1}{1+\frac{1/AF_o}{1/AF}+\frac{1/RS_o}{1/RS}}C_{PY}$$

6. $$\phi_{PY\to LA} = \lambda_{MAX,PY\to LA}\frac{RS}{RS_o + RS}C_{PY}$$

7. $$\phi_{AC\to CO_2} = \lambda_{MAX,AC\to CO_2}\frac{1}{1+\frac{PS_o}{PS}+\frac{1/RS_o}{1/RS}}C_{AC}$$

8. $$\phi_{FA\to AC} = \lambda_{MAX,FA\to AC} \frac{1}{1+\frac{1/AF_o}{1/AF}+\frac{1/PS_o}{1/PS}+\frac{1/RS_o}{1/RS}} C_{FA}$$

9. $$\phi_{FA\to TG} = \lambda_{MAX,FA\to TG} \frac{1/PS}{1/PS_o+1/PS} C_{FA}$$

10. $$\phi_{O_2\to H_2O} = \lambda_{MAX,O_2\to H_2O} \frac{1}{1+\frac{PS_o}{PS}+\frac{RS_o}{RS}} C_{O_2}$$

11. $$\phi_{PC\to CR} = \lambda_{MAX,PC\to CR} \frac{PS}{PS_o+PS} C_{PC}$$

12. $$\phi_{CR\to PC} = \lambda_{MAX,CR\to PC} \frac{1/PS}{1/PS_o+1/PS} C_{CR}$$

13. $$\phi_{TG\to FA} = \lambda_{MAX,TG\to FA} C_{TG}$$

14. $$\phi_{LA\to PY} = \lambda_{MAX,LA\to PY} \frac{1/RS}{1/RS_o+1/RS} C_{LA}$$

15. $$\phi_{CoApool\to FC} = \lambda_{MAX,CoApool\to FC} \frac{1}{1+\frac{1/RS_o}{1/RS}+\frac{1/FC_o}{1/FC}} C_{CoApool}$$

16. $$\phi_{AC\to CoApool} = \lambda_{MAX,AC\to CoApool} \frac{1}{1+\frac{1/RS_o}{1/RS}+\frac{1/FC_o}{1/FC}} C_{AC}$$

17. $$\phi_{ATP\to ADP} = \frac{\dot{W}}{-\beta\Delta G_{ATP\to ADP}\cdot M} \frac{1/PS}{K_{ATP\to ADP}+1/PS}$$